FINAL REPORT

ANALYSIS OF SURFACE LEACHING PROCESSES IN VITRIFIED HIGH-LEVEL NUCLEAR WASTES USING IN-SITU RAMAN IMAGING AND ATOMISTIC MODELING

U. S. Department of Energy
Office of Science

Grant Number DE-FG07-96ER45616

Joseph H. Simmons
Principal Investigator
University of Florida*
Gainesville, FL 32611

Current Address:
Professor and Head
Department of Materials Science & Engineering
University of Arizona
Tucson, AZ 85721
simmonsj@u.arizona.edu

TABLE OF CONTENTS

page

1 EXECUTIVE SUMMARY.....1

2 BACKGROUND.....4

Chemical Identification..... 4
Optical Measurements..... 5
Optical Response of Insulators..... 8
Vibrational Theory..... 9
Determination of Dielectric Properties from Optical Measurements..... 11
Kramers-Kronig relations..... 12
Dispersion Analysis..... 13
Conclusion..... 15

3 REFLECTIVITY OF ALKALI SILICATE GLASSES DURING LEACHING.....16

Introduction..... 16
Experiment..... 18
Glass Preparation..... 18
Sample Preparation..... 18
Measurements..... 18
Experimental Procedure..... 19
Results..... 19
Theory and Analysis..... 22
Kramers-Kronig analysis..... 23
Classic Dispersion Analysis..... 25
Gaussian Dispersion Analysis..... 25
Analysis..... 27

Conclusions and Future Work 41

4 EFFECTS OF ROUGHNESS ON REFLECTIVITY 43

Introduction and Background 43
Experiment 44
Sample Preparation 44
Optical Measurements 45
AFM and Profilometry 46
Results 46
Discussion of Results 49
Theory 50
Definitions of Roughness 50
Reflectance vs. Surface Roughness 51
Conclusions 56

5 LIQUID ATTENUATED TOTAL REFLECTANCE 57

Introduction 57
Background 57
ATR liquid cell 58
Analysis of ATR spectra 60
Quantitative Optical Analysis 65
Beer's Law 66
Quantitative Dispersion Analysis 67
Experiments 68
Chemical Preparation 68
The Attenuated Total Reflectance Liquid Cell 68
Experimental Procedure 68
Results 69
Discussion of Results 75
Analysis by GDA 81
Estimation of error 89
Conclusions and Future Work 90

6 OPTICAL PROPERTIES OF $Te_2As_3Se_5$ 91

Introduction 91
Experiment 91
Results 92
Discussion of Results and Analysis 94
Conclusions 100

7 FIBER OPTIC CHEMICAL SENSING PROBE 101

Introduction 101
Background 101

Current Methods of Remote Chemical Analysis 101
Current Analysis Techniques 103
Experiment 105
The Fiber Probe 105
Chemical Preparation 106
Measurements 107
Results 108
Discussion of Results and Analysis 112
Theory 114
Introduction 114
Theory Applicable to Fiber Optic Probe 114
Theoretical Predictions 119
Introduction 119
Model 120
Calculations 122
Conclusions and Future Work 127

APPENDIX COMPUTER PROGRAMS USED FOR DATA ANALYSIS 129

Module Atrtest: 129
Module CalculateOscillator 130
Module fiberfunctions 131
Module FiberTest 134
Module Filefunctions 135
Module KKreflectanalysis 141
Module Kktheta 142
Module LevenburgMarquardt 143
Module MixxedATR 147
Module Opticalfunctions 148
Module Runfitonparamfile 157
Module Roughness 158
Module RunATRFIT 159

LIST OF REFERENCES 161

EXECUTIVE SUMMARY

The in-situ analysis of surface conditions of vitrified nuclear wastes can provide an important check of the burial status of these radioactive objects without risk of radiation exposure. This check could be conducted over time and be used to monitor conditions in a storage site. The major degradation process of concern is clearly the chemical corrosion of the glass that contains the waste materials. Since, glass compositions for waste vitrification have been developed to resist chemical corrosion, the appearance of any evidence of corrosion, if any, may not appear for a long period of time. Therefore, we have examined, in this grant, the possibility of developing optical testing techniques for in-situ monitoring of the chemical corrosion of vitrified waste glasses under storage conditions. Since chemical corrosion of glasses begins by surface reaction processes, we have restricted our studies to test methods that analyze the glass surface. Finally, optical methods we chosen in order to have the tests remain non-destructive tests and allow remote monitoring.

There are 2 methods for optical analysis of glass surfaces. These are: Raman spectroscopy and reflection infrared absorption. Raman spectroscopy has the advantage of being insensitive to an immersion medium, so that the surface of the material can be under water during the analysis, without affecting the measurements. Infrared reflection analysis is affected by the presence of a medium, ie., the signal is absorbed by the medium. Thus Raman measurements can be conducted truly in-situ, while infrared reflection measurements require either wiping/drying the surface prior to the measurement, or placing the source and detector of the signal in close proximity to the surface and using subtraction methods for removing the water signal.

With these pre-conditions, it was initially decided to try Raman spectroscopy as the most promising method for testing the surface condition of glasses undergoing chemical corrosion. In the first year of the project, we conducted extensive tests of simple glass compositions to determine the changes in Raman signals from the glass surfaces undergoing chemical corrosion reactions. The results were mixed. We found that if the glasses were not resistant to chemical corrosion, the Raman method was indeed very useful in identifying chemical changes in the glass surface during corrosion. However, if the glass exhibited good resistance to corrosion, the modified surface layer was so thin that Raman scattering was relatively insensitive to the chemical processes associated with corrosion.

We determined that under normal Raman scattering conditions, the penetration of the incident light into the material sampled a deep region of the glass below the surface, thus attenuating the changes occurring in the first 100 nm of the material – depths typical of corrosion in durable glasses. The use of confocal optics in the collection of the Raman scattered signal can reduce the depth of the sampled volume to about a micron, but this depth is still too large and makes the Raman measurement less useful. At that point, we decided to investigate infrared reflection spectroscopy. It was determined that absorption of infrared light in the glass should limit the depth of penetration into the bulk and away

from the surface. This result was borne out and the infrared signal is limited to about a depth of 100 nm as shown in this report. The absorption of visible light in typical waste glass samples is not as severe. Thus Raman scattering using visible light cannot receive the same benefit.

At that point in the study, we turned our attention to the use of infrared reflection spectroscopy to determine chemical corrosion processes in glass by surface analysis. Incidentally, before leaving the issue of Raman scattering, it is important to note that since the end of the research grant and after my move from the University of Florida to the University of Arizona, I have acquired and developed instrumentation for improving the sensitivity of Raman scattering to a thin surface layer. These methods are currently in use in my lab for examining the surface of biological and cellular materials. They include the use of near field optical microscopy (NSOM) and the use of two photon Raman scattering. The latter could very well provide a means of applying Raman scattering to the studies of chemical corrosion of glasses.

In the infrared reflection studies, we noted that many investigators have conducted FTIR (fast Fourier infrared) measurements of glass surfaces during corrosion. However the results were always qualitative due to the many absorption peaks produced and the shift in frequency of the peaks observed. Theoretically, such shifts are difficult to understand, since once a chemical species is formed, its absorption properties remain constant and change very little with changes in concentration. Some change may be expected from the Ligand field due to a change in the environment. But the changes observed are far to large to result from this cause. This calculation prompted us to investigate the analysis of reflected infrared absorption. We discovered that all previously reported reflection measurements are analyzed incorrectly and that it is this false analysis that leads to shifts in observed absorption peaks.

In the second year of the project, we derived the functions needed for a correct analysis of reflection absorption data. We discovered that the software available with FTIR instruments for analyzing reflection data is also incorrect. Our calculations led to the development of novel equations and novel software for optical reflection analysis. When used with IR reflection data the results are consistent with known theories of optical reflectivity and molecular absorption processes.

The remaining period in the second year and third years were used to investigate the surface corrosion behavior of model silicate glasses for extension to nuclear waste glasses. A test methodology was developed and applied to both model and simulated nuclear waste glasses. The developed methodology is consistent with the known theory of optical propagation in dielectric media and uses the Kramers-Kronig formalism. The results show that indeed it is possible to study the corrosion of glass by analysis of the glass surface using reflection FTIR measurements and the newly developed “dispersion analysis method.” The data presented in this report show how this analysis can be used to monitor the corrosion behavior of vitrified waste glasses over extended periods of storage.

The “dispersion analysis” developed demonstrates that glasses undergoing chemical corrosion exhibit absorption peaks that originate both from the pristine glass composition and from the chemical corrosion products. These absorption peaks are generally Gaussian in shape and both the peak positions and peak shapes remain unchanged during the corrosion process, going from the onset of corrosion to the case of severe attack. Thus, once these peaks are measured and identified, they can be catalogued and used in different glasses with similar composition. Using, this method, we were able to follow surface changes in glasses undergoing corrosion, and to obtain a **quantitative** measure of the change in composition of the glass surface. This test was conducted on a family of silicate glasses, including simulated waste glasses. The method and results are discussed below.

As for the original purpose of this work, we have demonstrated that the newly developed “dispersion analysis” of reflection data has the characteristics needed to conduct in-situ, real time analysis of corrosion processes in stored nuclear waste glasses. The major problem of the effect of water immersion can be solved by proper subtraction from the obtained spectra. These results have been presented at several EMSP meetings and there are several investigators associated with Tank Focus Area studies who have made plans to adopt the results presented here.

The program graduated 2 MS students and 2 PhD students. One of the PhD graduates has since extended this work to the in-situ real-time analysis of chemical processes in a variety of liquids (milk, grape juice, etc.) in which the absorption processes change with fermentation of the liquid. The results are reported in Chapters 5, 6 and 7.*

(Most of this work is presented in a PhD thesis: Steven A. MacDonald, “Analysis of Non-Crystalline Materials with Optical Measurements by Dispersion Analysis”, PhD Thesis, University of Florida, 2000.)

CHAPTER 2
BACKGROUND

Chemical Identification

All methods of chemical identification and detection rely upon the measurement of a physical property and comparing that measured physical property with previously measured standard, and considered accurate, properties of a species (an element, an ion, or a molecule). The types of different analytical techniques are numerous and varied with the possibility for many overlaps in detection and identification depending on the sample and sampling requirements. Some methods can determine quantitative information, concentrations, while other methods can only identify the inclusion or exclusion, within the detection limits of the technique, of a particular species.

With today's technology, the ability to quantitatively identify the components is easily accomplished by a number of different means. They range from separation by distillation and identification by measuring and comparing the boiling points to standards all the way to mass spectrometry. The complete identification of a sample becomes more difficult when restrictions are placed upon the resources available. The different techniques each have specific sample requirements, often consuming the material, requiring large, costly apparatus and can take considerable time to perform[1, 2].

Additionally, many of the classical chemical analysis techniques are not possible for in-situ analysis

Optical methods are often the choice for non-destructive characterization, in-situ, and/or for remote characterization. Light, or an electromagnetic wave, typically does not damage or change the material and can often be impinged on a sample and a signal measured remotely. Electromagnetic waves vary with energy ($h\nu$), in units of eV, according to their wavelength (λ) in units of nm, as

$$h\nu = \frac{1242}{l} \tag{1}$$

and as such have a continuous range of energies theoretically from zero to infinity. Different wavelengths of light will interact differently with a particular material and as such a wavelength range that interacts in a measurable manner, and that will allow for identification, can be selected. This dissertation is mainly concerned with the infrared part of the spectrum from 2.5 μm to 25 μm where many organic and inorganic materials exhibit polarization in their optical response. Another common unit used in spectroscopy, analogous to wavelength, is the wavenumber, units cm^{-1}, and is inversely related to wavelength (in μm) by:

$$cm^{-1} = \frac{10000}{l} . \tag{2}$$

Wavenumbers will be used primarily in this dissertation.

Optical Measurements

The most common techniques used for infrared (IR) spectroscopy are transmission relative to air, and reflection relative to a silver mirror (>99% reflective in

the IR), yielding T(ω) and R(ω), respectively, with omega, ω, units of cm^{-1}. For any sample, the light impinging on the sample, $I_0(\omega)$, is either reflected from the sample's surface, absorbed by the sample or transmitted through the sample such that

$$I_0(w) = I_0(w)\big(R(w) + A(w) + T(w)\big). \tag{3}$$

Though both R(ω) and T(ω) are measurable, they are not intrinsic properties of the material, but rather extrinsic properties, and depend not only on the intrinsic optical properties of the material, but also on the sample thickness (x) and measurement geometry . The absorbed component, A(ω), is also extrinsic, but can not be measured directly and must be calculated based on R(ω) and T(ω) and Equation 3.

In cases of samples with an absorption large enough to prohibit transmission through the sample, only R(ω) can be measured. In this case, the reflectance for normal incidence is

$$R(w) = \frac{(n_i(w) - n_t(w))^2}{(n_i(w) + n_t(w))^2} \ , \tag{4}$$

with n_i being the complex index of refraction for the incident material, i.e. the sample, and n_t being the complex index of refraction of the medium that the light is being transmitted through, usually air. R(ω) as defined in Equation 4, is also known as the single surface reflectance. In cases where the sample does transmit some portion of the incident light, the following equations for transmission and reflectance at normal incidence apply as they take into account multiple reflections at the sample's surfaces:

$$T_{total}(w, x) = \frac{(1 - R(w))^2 \exp(-a(w)x)}{1 - R(w)^2 \exp(-2a(w)x)} \tag{5}$$

and

$$R_{total}(w,x) = R(w)(1 + T(w,x)\exp(-a(w)x)), \tag{6}$$

where α(ω) is referred to as the absorption coefficient, or also as the attenuation coefficient, defined as

$$a(w) = 4pk(w)w \tag{7}$$

with κ(ω), the imaginary component of the complex index of refraction. For a beam of light traveling in an absorbing medium, the light is attenuated as follows:

$$I(w,x) = I(w,x=0)\exp(-a(w)x) \tag{8}$$

Equations 5 and 6 take into account multiple reflections but do not consider interference of the incident beam with reflected beams and therefore are not used for thin films. Equation 8 takes into account only the attenuation as the light travels and not attenuation due to reflections. The inverse of α(ω) is the referred as to depth of penetration and is the distance into the sample that the intensity has diminished to 1/e of its original intensity.

Assuming that the thickness of the sample is known, Equations 5 and 6 can be solved for the intrinsic optical properties[3]. Though the determination of the intrinsic optical properties is possible it can be rather involved, and does require both T(ω) and R(ω) to be measured accurately. Nazarewics[3], due to the nature of these calculations, offers an abac chart for graphically solving Equations 5 and 6. Instead of measuring both T(ω) and R(ω) and solving the equations for the intrinsic optical properties, approximations are often made.

Absorbance, A(ω), is often expressed by the Optical Density (OD) calculated from T(ω) by

$$A(w,x) \cong OD \equiv \log_{10}\left(\frac{1}{T(w,x)}\right), \tag{9}$$

which with the approximation of

$$T(w,x) = \exp(-a(w)x), \tag{10}$$

leads to

$$A(w,x) = 2.303\, a(w)x. \tag{11}$$

The assumption made for these approximations is that the reflections on both surfaces are negligible and that the only loss of intensity is from absorption. If the reflection coefficients are not very large the approximation may be close, but is not valid for samples with non-negligible reflection coefficients.

Optical Response of Insulators

The materials that are of interest in this dissertation are insulators. A material is considered an insulator if the band-gap of the material is greater than 5 eV. The insulator response to an electromagnetic wave of greater energy than the band gap is to promote, by photo-excitation, an electron out of the bonding states to the conduction band. The insulator response to electromagnetic waves less than the band gap is polarization of either the electron cloud around each ion in the material or to polarize dipolar molecules.

The frequency of the electromagnetic wave is important in the polarization process. Polarization of either the dipolar molecule, or of the electron cloud and ion, takes time for the material to react to the alternating force of the electromagnetic wave and to polarize. If the wave period is shorter than the time for the polarization process, the forces on the electron cloud reverse before the species can react, and thus do not cause material polarization. If the time to respond is less than the period of the electromagnetic wave the material will polarize and can stay in phase with the electromagnetic wave. When the time to respond to the force is approximately the same as the period, the polarization is nearly complete when the forces change; thus a constant re-arrangement of the molecule or electron cloud leads to maximum energy losses and absorption of the electromagnetic wave.

Vibrational Theory

As the electromagnetic wave of light interacts with a sample, the electric field alternately attracts/repels the electron clouds/nucleus of the atoms in the molecule. This interaction causes polarization of the molecules. The continuously changing polarization, or vibration, will be infrared-active if the dipole moment is changed during the vibration.

The polarizability, P*(ω), is a frequency dependent complex quantity, which is directly related to the chemical bond structure of the material. A simple damped harmonic oscillator is the classic (Lorentz) model for the polarization, leading to:

$$P^*(\omega) = \frac{e^2}{m_e \varepsilon_0} \frac{1}{(\omega_0^2 - \omega^2) - i\Gamma\omega} \tag{12}$$

e is the electronic charge, m_e is the electronic mass , ε_0 is the vacuum permittivity, ω_0 is the resonant wave number, and Γ is the damping constant. If the local electric field is approximately equal to the applied electric field, the complex dielectric function is related to the complex polarizability by:

$$\varepsilon^*(\omega) = 1 + NP^*(\omega) \tag{13}$$

with N being the number of molecules. With N_j molecules contributing to the macroscopic optical properties, the summation leads to:

$$\varepsilon^*(\omega) = 1 + \frac{e^2}{m_e \varepsilon_0} \sum_j \frac{N_j}{(\omega_{0j}^2 - \omega^2) - i\Gamma_j \omega} . \tag{14}$$

The complex dielectric function $\varepsilon^*(\omega)$ is related to the index of refraction by:

$$\varepsilon^*(\omega) = n^*(\omega)^2 \tag{15}$$

with the following equations being applicable

$$\varepsilon^*(\omega) = \varepsilon_1(\omega) + i\varepsilon_2(\omega) \tag{16}$$

$$n^*(\omega) = n(\omega) + i\kappa(\omega) \tag{17}$$

related by

$$\varepsilon_1(\omega) = n(\omega)^2 - \kappa(\omega)^2 \tag{18}$$

$$\varepsilon_2(\omega) = 2n(\omega)\kappa(\omega) \tag{19}$$

and conversely

$$n(w) = \left\{ \frac{1}{2} \left(\sqrt{e_1^2(w) + e_2^2(w)} + e_1(w) \right) \right\}^{1/2} \tag{20}$$

$$k(w) = \left\{ \frac{1}{2} \left(\sqrt{e_1^2(w) + e_2^2(w)} - e_1(w) \right) \right\}^{1/2} . \tag{21}$$

As can be seen from the above equations, the polarization, and due to the linear relationship with, the dielectric function, are fundamental properties from which the complex index of refraction can be calculated. Also it should be noted that the optical properties are a function of the number of molecules and that the contribution of a single molecule to the overall optical properties is only additive in either the dielectric function or the polarizability function and not in the index of refraction.

Determination of Dielectric Properties from Optical Measurements

When making optical measurements it is often easy to think of the measurement as the end result and the material fully characterized by R(ω) or T(ω). As detailed above, the extrinsic measurements are based on intrinsic optical properties, which can be expressed by n and k, or conversely the real and imaginary parts of the dielectric function, as a function of wavelength. From these fundamental underlying properties all the external measurable properties can be calculated for any given geometry.

To obtain the fundamental underlying optical properties, a number of different analysis techniques have been developed. Some require measuring multiple extrinsic properties, such as both T(ω) and R(ω) as described above, or complex mathematical treatments of just one extrinsic property using causal relationships such as Kramers-Kronig or Dispersion Analysis.

Kramers-Kronig relations

The real and imaginary components of a function that relate to a physical process are not independent. The Kramers-Kronig transforms, also known as Hilbert transforms, relate the real and imaginary parts of any complex function that represent a physical process.

The complex index of refraction is such a complex function. The Kramers-Kronig transforms for n, and k are:

$$n(w) = 1 + \frac{2}{p} \mathrm{P} \int_0^\infty \frac{w' k(w')}{(w')^2 - w^2} \partial(w') \,, \tag{22}$$

$$k(w) = 1 + \frac{2}{p} \mathrm{P} \int_0^\infty \frac{w' n(w')}{w^2 - (w')^2} \partial(w') \,, \tag{23}$$

where P is the principle value.

Equation 4 above, for normal reflectivity, does not consider the phase change (the imaginary component) of the electromagnetic wave upon reflection. To consider the phase change, Equation 4 can be rewritten by the following:

$$R(w) = r(w) r^*(w) \,, \tag{24}$$

with

$$r(w) = \frac{n_i(w) - n_t(w)}{n_i(w) + n_t(w)} e^{ij} \quad , \tag{25}$$

with (r) representing the ratio of the amplitudes of the reflected electric field to the incident electric field, (r*) being the complex conjugate of (r), and $f(w)$ the phase change

upon reflection. The only difference between Equation 4 and Equations 24 and 25 is the addition of the phase change component, the complex part.

If both the phase change and relative intensity are known, n and k can be calculated by the Fresnel equations:

$$n(w) = \frac{1 - R(w)}{1 + R(w) - 2\sqrt{R(w)}\cos f(w)} \tag{26}$$

$$k(w) = \frac{2\sqrt{R(w)}\sin f(w)}{1 + R(w) - 2\sqrt{R(w)}\cos f(w)} \tag{27}$$

Due to the ease of measuring R(ω) compared to the difficulty of measuring the phase change, it is common to measure only the reflectivity spectrum. The use the Kramer Kronig relation below[4] is used to calculate the phase shift $f(w)$ from reflectivity:

$$f(w) = \frac{w}{p}\int_0^\infty \frac{\ln R(w') - \ln R(w)}{w^2 - w'^2} dw' \tag{28}$$

and with both the phase shift and the reflectivity, Equations 26 and 27 are used to calculate n, k and Equations 20 and 21 for the dielectric functions. The Kramers- Kronig transforms can be used on any of the complex optical functions, but it is most common to use Equation 28, as reflectivity is easily measured.

Dispersion Analysis

Another technique used to determine the optical properties of materials from optical measurements is Dispersion Analysis. With Dispersion Analysis, an oscillator model is developed with appropriate resonances (amplitude or oscillator strength, a central vibrational wavenumber, and damping constant or width) in the dielectric function

and values of reflectivity, or any other measurement, are calculated. The parameters for the model are adjusted to fit the measured data.

Classic Dispersion Analysis (CDA) makes use of a simple damped harmonic oscillator model for the complex dielectric function:

$$e^*(w) = e_\infty + \sum_j \frac{N_j}{(w_j^2 - w^2) - i\Gamma_j w} \tag{29}$$

where ε_∞ is the contribution to the real part of the dielectric function from higher frequency polarization, N_j is the product of the oscillator strength and number of oscillators, w_j the frequency, and G_j is the oscillator damping factor. The damping term results in a Lorentzian imaginary dielectric function (homogeneous line broadening). This method of dispersion analysis is fairly easy to employ due to the fact that both the real and imaginary parts of the dielectric function have analytical solutions and are ergodic with:

$$e_1(w) = e_\infty + \sum_j N_j \frac{w_j^2 - w^2}{(w_j^2 - w^2)^2 + \Gamma_j^2 w^2} \tag{30}$$

$$e_2(w) = \sum_j N_j \frac{\Gamma_j w}{(w_j^2 - w^2)^2 + \Gamma_j^2 w^2} \tag{31}$$

and thus it is only necessary to input three parameters per oscillator, sum over all frequencies and calculate the measured property. The oscillator parameters are adjusted until a satisfactory fit with the measured spectrum is achieved.

Kramers-Kronig and CDA are often used to try to relate measured data with the underlying optical properties. Dispersion analysis can be more flexible than Kramers-

Kronig as it can be applied to a more complicated geometry, but does assume a model for the polarization. Kramers-Kronig analysis is purely mathematical and a model is not assumed, but it needs the entire spectrum theoretically from zero to infinity. Omissions or truncations of the spectrum can introduce significant errors.

CHAPTER 3
REFLECTIVITY OF ALKALI SILICATE GLASSES DURING LEACHING

Introduction

The time-dependent changes in composition and structure occurring on the surface of a material are critical to the identification of the mechanisms of the reaction of the material with its environment. Numerous techniques have been used to analyze these changes, including methods that give the composition averaged over a fixed or adjustable surface layer and methods that give composition profiles into the material. These include a variety of beam analysis methods that can be considered as essentially destructive, since they require removal of the sample from solution and subsequent irreversible treatment of the surface. Such treatments include deposition of coatings for Scanning Electron Microscopy (SEM), replication for Transmission Electron Microscopy (TEM), exposure to a high vacuum for X-ray Photo-electron Spectroscopy (XPS) and Auger Electron Spectroscopy (AES), or bombardment with an energetic ion beam for Rutherford Backscattering Spectroscopy (RBS) and Secondary Ion Mass Spectroscopy (SIMS)[5-14].

Non-destructive methods are mostly optical and include backscattered Raman Spectroscopy and Infrared Reflection Spectroscopy. Both are sensitive to changes in structure and composition. Raman spectroscopy is the most attractive since it can be conducted in–situ on a sample submerged in a transparent liquid. Raman methods, however, probe too deeply into transparent targets and are not useful for the study of the

corrosion behavior of glass surfaces. Fourier Transform Infrared (FTIR) reflection spectroscopy is very sensitive to surface changes. It requires removal of the sample from the corrosion bath, but no surface treatment. Because of the high absorption for infrared wavelength radiation by most materials, including oxide glasses, the penetration depth can be less than 0.1 μm in the wave number range from 400 to 1500 cm^{-1}. Consequently infrared spectroscopy is sensitive only to the composition of a thin surface layer and has been popular in the study of the corrosion of glasses [10, 15-19]. This approach does not yield composition profile information; however, its non-destructive capability makes it very useful for time dependent studies on the same sample.

Investigators have observed changes in the FTIR reflection spectra of glasses during the leaching process that consist of complex changes in the intensity and *position* of the reflection maxima. However, these shifts in peak position have frustrated attempts to derive quantitative information from the measured reflection spectra.

There have been attempts to quantify reflectance measurements on glasses by using Ergodic Analysis. This is usually based either on a Kramers-Kronig analysis of the measured data or on dispersion analysis. In the first approach, the Kramers-Kronig relation is applied directly to the reflectance data to calculate the phase change (f) on reflection as shown in Chapter 2. Subsequently, the index of refraction (n) and absorption (k) can be calculated from f. The real and imaginary parts of the dielectric constant are then calculated from n and k and are examined as a function of exposure time. In the dispersion analysis approach, an oscillator model, classical dispersion analysis or a variation, is developed with appropriate resonances in the dielectric constant and these are transformed to reflectivity to fit the measured data [20-24]. Other methods

have been used that involve fitting the reflectivity data directly or using vague descriptive comments about the reflectivity peaks to infer some underlying structure [15, 16, 18, 23] These methods are only qualitative and lack information about the underlying processes.

Experiment

Glass Preparation

Glasses of 20% by mole Na_2O-80% SiO_2 and 20% by mole Li_2O-80% SiO_2 were prepared using reagent grade Na_2CO_3, SiO_2 and Li_2CO_3. The glasses were melted in a platinum crucible at 1400 °C in a Deltec high temperature furnace. After being allowed to homogenize at this temperature for 24 hours, the glasses were poured into graphite molds, forming 2.54 cm diameter rods. The glass rods were annealed for 1.5 hours at 500°C in a Thermolyne box furnace. After annealing, the glass rods were placed in a Blue-M drying oven for storage.

Sample Preparation

Samples were cut and polished to parallel sided half disks, 2.54 cm in diameter by 0.2 cm thick. The samples were wet polished on both sides with 600-grit silicon carbide paper until scratches were not visible by eye. Before the start of the tests, a final dry polish was performed with 600 grit silicon carbide paper to remove any corrosion layers formed during or after the wet polish.

Measurements

FTIR reflection measurements were conducted on the dry samples before corrosion. The FTIR measurements were made with a FTIR using a near normal reflectance stage and throughout the analysis normal incidence was assumed thus removing any polarization dependencies. A silver mirror was used as a standard reference

for all FTIR reflection measurements. The spectral range of the spectrometer used is 400 to 4000 cm^{-1}, though the data is often truncated for display.

Experimental Procedure

Corrosion was carried out in a Teflon vessel containing enough de-ionized (DI) water to obtain a surface to volume ratio of 0.1 cm^{-1}. Inside the corrosion vessel, the samples were placed on Teflon mesh stages in order for the water to have access to the entire surface area. FTIR reflection measurements were made at various times during the corrosion process. For each measurement, the sample was removed from the water bath, patted dry, rinsed with methanol and allowed to air dry before the reflection measurements were made. The sample was then returned to the same corrosion bath, placed same side down. All reflection measurements were made on the side of the sample that was not in contact with the Teflon mesh. In addition to the sodium and lithium samples, reflection measurements were made on a clean and dry sample of silica glass. The silica reflection spectrum was used as a test spectrum and used for peak assignments. The silica sample measurements were with both an FTIR and a grating IR spectrometer in order to obtain reflectivity measurements to 100 cm^{-1}. The spectra were then spliced together at 600 cm^{-1} to give the final spectrum.

Results

Figure 3.1 shows the measured reflectance spectrum for silica. There exists a peak at 400 cm^{-1}which is not shown as distinctly in other works. In Galeener's paper there is a slight change in curvature in the same region [24] and it is thought that the peak is not false. Figures 3.2 and 3.3 show the reflectance spectra corresponding to different submersion times for the 20% Na_2O-80% SiO_2 and 20% Li_2O-80% SiO_2 glasses

respectively. The data shown is spectrally truncated and submersion times are omitted from these Figures, for clarity. The reflectance of the uncorroded sodium sample has maxima near 1100, 1000, 780, and 480 cm^{-1}, while that of the uncorroded lithium sample has maxima near 1100, 950, 780 and 480 cm^{-1}. As the samples corrode, the maxima appear to shift in both position and intensity. Since the reflectivity is a function of both *n* and ***k***, and since both optical properties depend on the surface composition, it is necessary to examine both functions in order to study the behavior of the material during corrosion.

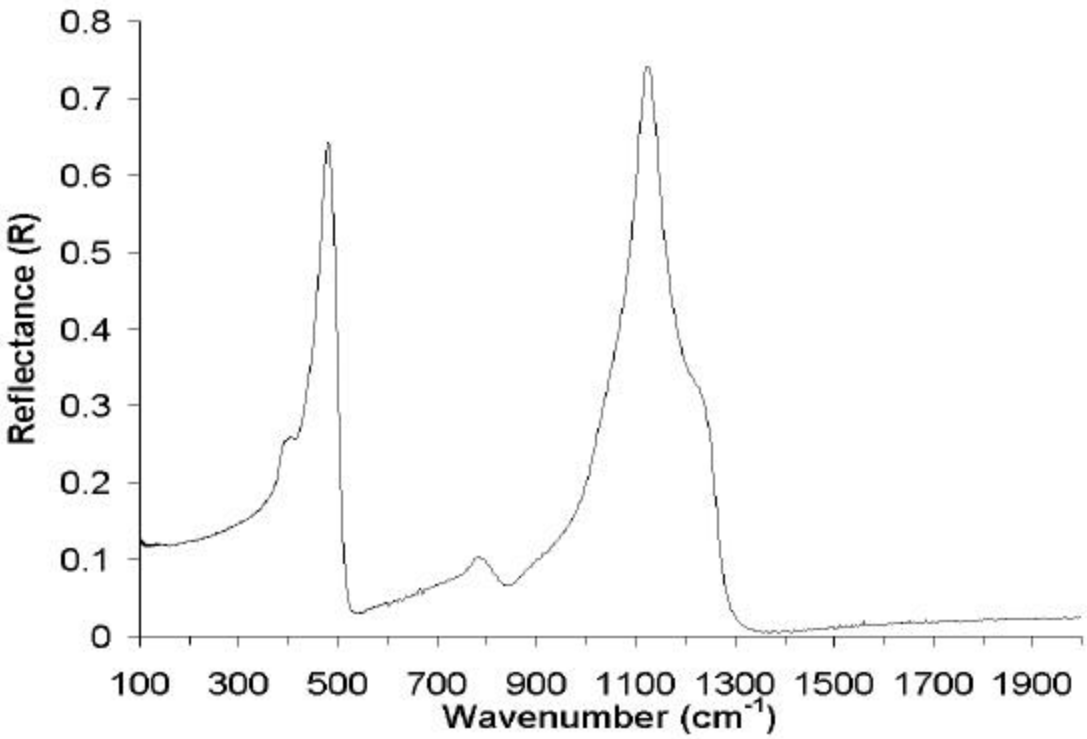

Figure 3.1 Measured FTIR reflectance of silica glass.

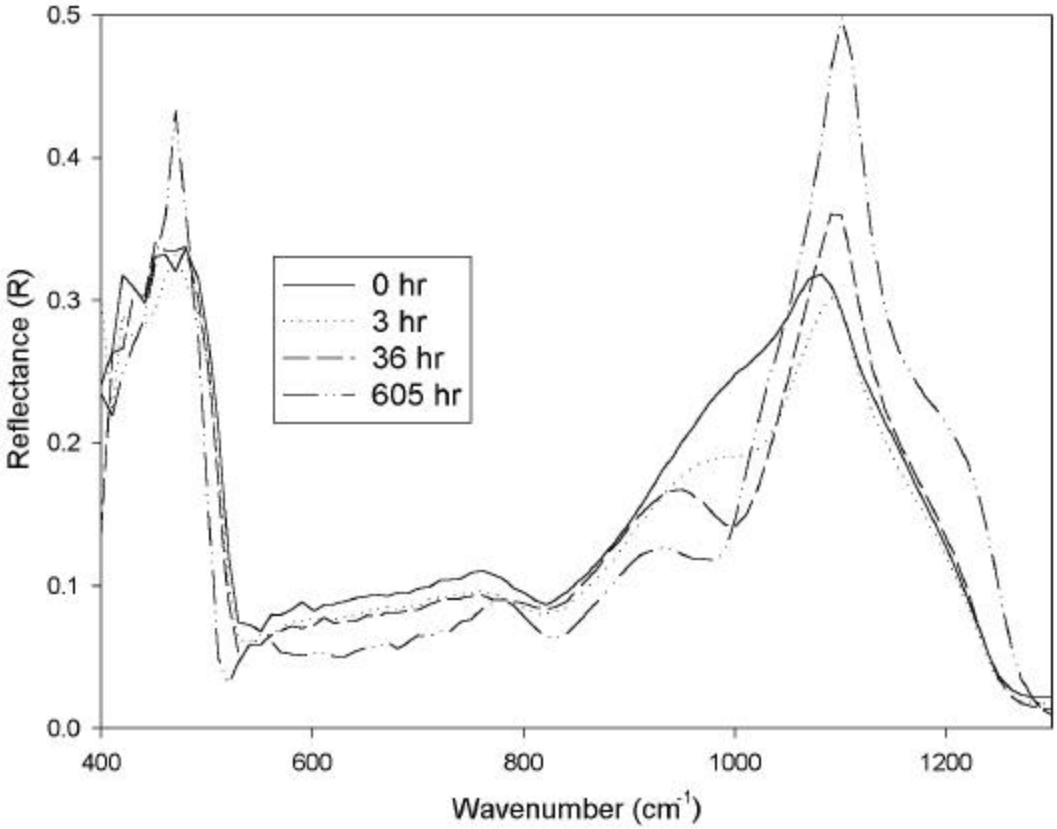

Figure 3.2 FTIR reflectance data for 20%Na_2O -- 80% SiO_2 glass for various exposure times using the static leach test at a temperature, T= 25 °C and with S/V=0.1 cm^{-1}.

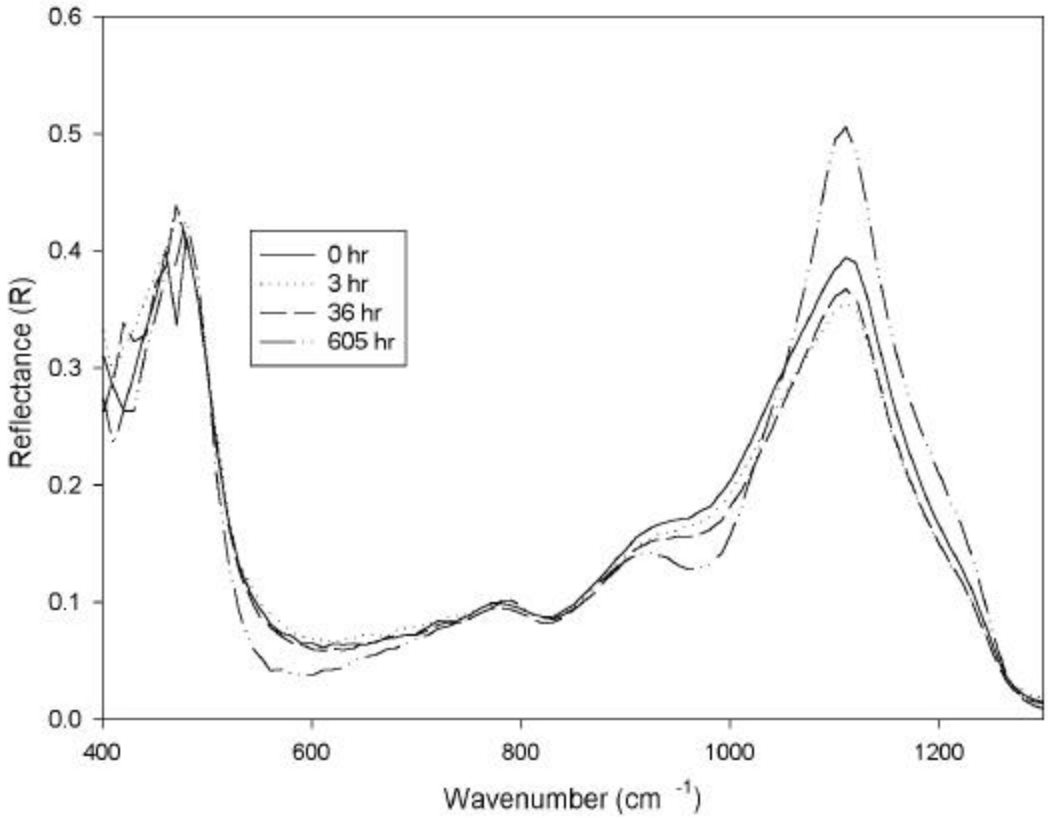

Figure 3.3 FTIR reflectance data for 20%Li_2O -- 80% SiO_2 phase-separated glass, for various exposure times using the static leach test at a temperature, T= 25 °C and with S/V=0.1 cm^{-1}.

Theory and Analysis

Since a comparison of the results of different submersion times involves an examination of the changes in either number or type of vibrational species, a proper analysis must address the imaginary part of the dielectric function and not the reflectance. Determination of the dielectric function from the reflectivity can be accomplished by either Kramers-Kronig or dispersion analysis techniques as discussed in Chapter 2.

Kramers-Kronig analysis

For Kramers-Kronig analysis of the reflectivity, a large part of the spectrum is needed and any unmeasured parts must be approximated with some function [4]. Problems with this method arise because the unmeasured portion of the spectrum often has a large effect on the calculated values of f. There are ways to deal with this error, however the solutions tend to work only for a limited set of experimental conditions [25]. In addition, because of the integral nature of the functions, any measurement uncertainty is greatly magnified. Both problems combine to produce large errors in the calculated values of the spectrum. The reflectivity spectrum of silica was analyzed with this method and Figure 3.4 shows the resulting imaginary dielectric function.

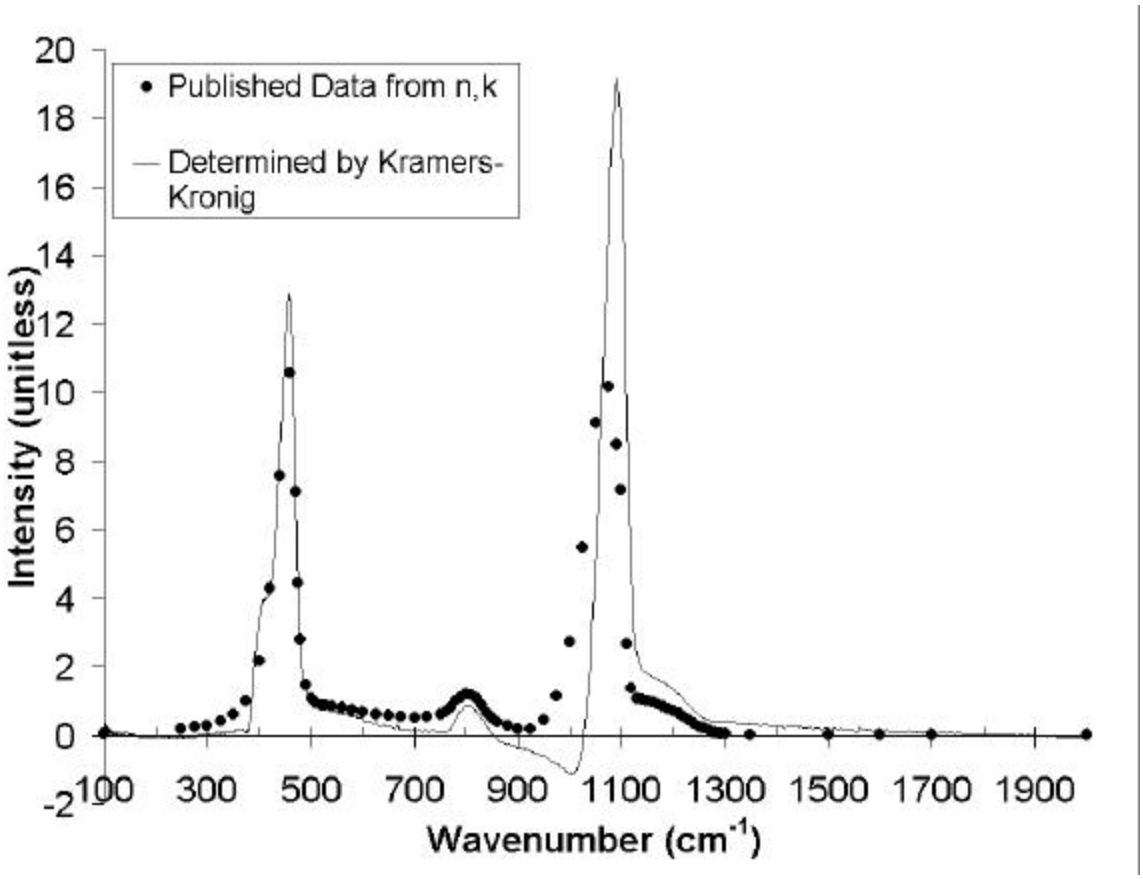

Figure 3.4 Comparison of imaginary dielectric functions of silica glass, as calculated from the Kramers-Kronig analysis of the reflection data as in [4], and compared to published data from n and κ measurements[26].

Data below 100 and above 4000 cm-1 were not estimated and the display was truncated. For comparison, the imaginary dielectric function calculated from published values of *n* and ***k*** [26] is also shown. Although the shape and trends match the published data, the negative values of the imaginary dielectric function calculated from the Kramers-Kronig transform of the reflection data are not possible and cause problems with subsequent calculations and interpretations. Similar results occurred with the spectra from the leached samples. These regions of negative imaginary dielectric function are clearly unsatisfactory for a quantitative examination of the changes in the number and

types of vibrational species, and thus this technique was abandoned in favor of the dispersion analysis.

Classic Dispersion Analysis

Dispersion Analysis is implemented by developing an appropriate model for the dielectric function and calculating the optical properties from this model. The model parameters are determined by fitting the calculated reflectivity to the experimentally measured reflectivity. Although a limited data set can still be problematic, if a proper model is developed, dispersion analysis is not as sensitive as Kramers-Kronig to unmeasured regions of the spectrum. In fact, the model can be used to approximate the unknown portions of the spectrum. In general, as long as all strong resonances are within the measured region, dispersion analysis will yield accurate results.

The reflection spectra for silica, and sodium and lithium silicate glasses were fitted by classic dispersion analysis using Equations 29, 30 and 31 presented in Chapter 2. In this case, the results were unsatisfactory, because the quality of the fit was poor even when many peaks (8 oscillators between 800 and 1400 cm^{-1}) were used to approximate the data.

Gaussian Dispersion Analysis

The classical dispersion analysis method is appropriate for crystalline systems in which the local environment is the same for all oscillators of a certain type. In glasses and other amorphous materials, the local environment is not uniform. The variation in local environments leads to inhomogeneous broadening of the resonance line-widths. Efimov and Makarova [21] proposed a thorough treatment of the broadening. In his model, the absorption bands are treated as a Gaussian distribution of homogeneously broadened Lorentzian oscillators. This model requires five adjustable parameters per

oscillator peak and is mathematically unwieldy to use for complex reflection spectra where there are many oscillator frequencies. An approximation can be made when the inhomogeneous broadening is much larger than the homogeneous linewidth. In this case, the absorption bands can be approximated by simple Gaussian distributions. This approximation reduces the number of adjustable parameters to three per oscillator peak and greatly simplifies the calculation of optical properties. We refer to this technique as Gaussian Dispersion Analysis (GDA). The basis of GDA is the expression of the imaginary dielectric constant as a sum of Gaussian terms, each corresponding to separate oscillations in the phonon density of states:

$$\varepsilon_2(\omega) = \sum_j A_j \exp\left(-\frac{1}{2}\left[\frac{(\omega - \omega_{0j})}{\Delta\omega_j}\right]^2\right) \tag{32}$$

where the subscript j refers to the jth resonance mode, ω_{0j} is the center frequency of the resonance, $\Delta\omega_j$ is the standard deviation of the mode and A_j is the amplitude. However, unlike the classical dispersion analysis, the expression for the real component of the dielectric function is complicated. The latter is calculated from the imaginary component by use of the Kramers-Kronig relation:

$$\varepsilon_1(\omega) = \varepsilon_\infty + \frac{2}{\pi}\int_0^\infty \frac{\omega'\varepsilon_2(\omega')}{\omega'^2 - \omega^2} d\omega' \tag{33}$$

This application of the Kramers-Kronig calculation does not have the same inherent drawback as the direct analysis of the reflection data, since the model can represent ε_2 over the entire spectrum. The numerical integration of Equation 33 can be carried out to adequate precision on a personal computer. This model was employed to

determine the dielectric function of the experimentally measured reflectivity spectra. An analytical expression for the Kramers-Kronig integral was derived which greatly simplifies the calculations and has the form:

$$e_1(w) = e_\infty - i\sum_{j=1}^{n} A_j \cdot erf\left(\frac{i\sqrt{2}}{2}\frac{w_{0j} - w}{\Delta w_j}\right) \cdot e^{-\frac{1}{2}\left(\frac{w - w_{0j}}{\Delta w_j}\right)^2} - A_j \cdot erf\left(\frac{i\sqrt{2}}{2}\frac{w_{0j} + w}{\Delta w_j}\right) \cdot e^{-\frac{1}{2}\left(\frac{w + w_{0j}}{\Delta w_j}\right)^2} \quad (34)$$

Analysis

The silica reflectivity data was fitted to determine the locations of the silicon-oxygen vibrational modes. Figure 3.5 shows the fit of calculated reflectivity for SiO_2 compared to the experimentally measured reflectivity as well as the reflectivity calculated from published values of *n* and ***k***[26]. It is clear that the guassian dispersion analysis fits the experimental data well. Figure 3.6 shows a comparison of the imaginary dielectric functions obtained from Guassian dispersion analysis and those calculated from published values of *n* and ***k***.

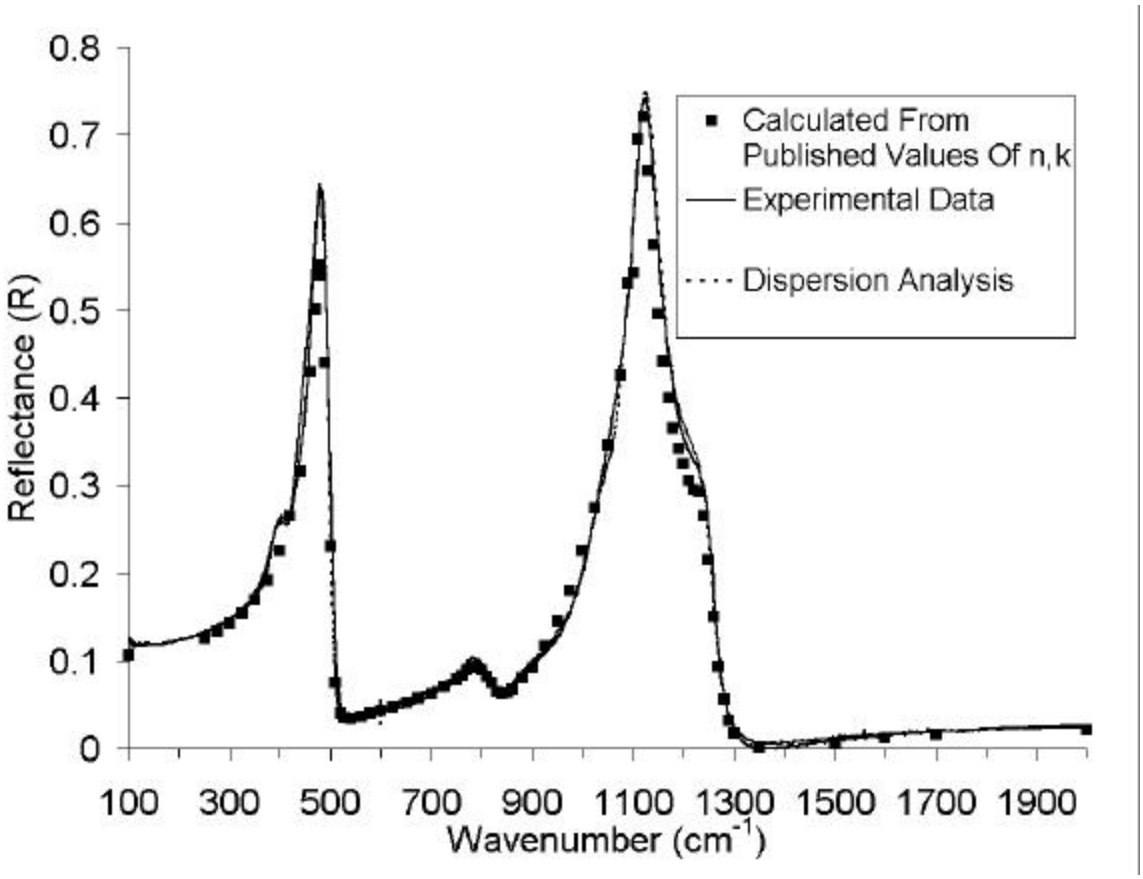

Figure 3.5 Comparison of the reflectance of silica glass from direct measurement, from guassian dispersion analysis and from calculation from published values of n and κ [26].

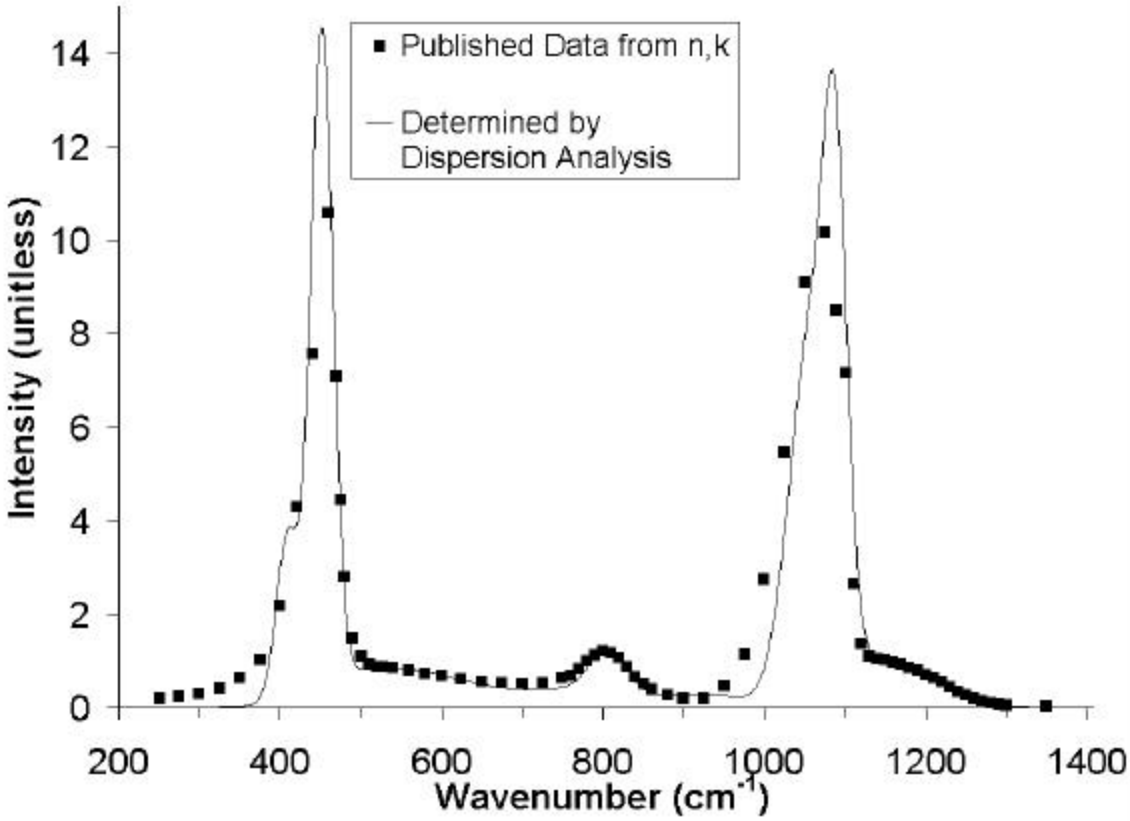

Figure 3.6 Comparison of imaginary dielectric functions of silica glass from guassian dispersion analysis and from calculation from published values of n and κ [26].

There are slight differences between the imaginary dielectric functions. These differences may be attributed to differences in the accuracy of the reflectivity measurements. To determine the instrumental error, a silica sample was independently measured a total of 6 times with a resolution setting of 1 cm^{-1}. The average standard deviation for the 6 reflectivity measurements was 1.37% over the range from 400 cm^{-1} to 1600 cm^{-1}. The fits to the reflectivity were conducted to an r-square fit of at least .960 with an average r-square value of .985. While discussing the error in the measurements and the analysis it is important to note the following. The FTIR spectrometer used for these measurements makes use of KBr components and although data is measurable to

400 cm^{-1}, reflectivity below about 650 cm^{-1} is quite noisy due to low signal throughput of the KBr components. Additional error can be introduced by the roughness of the samples. Specular reflectance is dependent upon a material's reflectivity for an infinitely smooth surface (R_0), wavelength (λ) and the rms roughness (σ) of the surface according to [27]:

$$R(s, l) = R_0 \exp\left(-\left(\frac{4ps}{l}\right)^2\right) \tag{35}$$

If the roughness of the surface is on the same order or greater than the wavelength of the measuring beam, the measured reflectivity will be reduced from the theoretical maximum for the material.

Although many assignments for silica glasses have been made in the literature (see Table 3.1 below), vibrational mode assignments for peaks in silica are not trivial as is evident by the variation in assignments. The assignments listed here are from Raman and IR studies of silica and silicate glasses. The location of a particular vibrational mode should be essentially the same in both the imaginary dielectric function obtained from IR and in Raman spectroscopy, if the mode is IR and Raman active. The different modes arise from bending and stretching of the different bonds between atoms and between extended groups of atoms. The difficulty in assigning specific vibrational modes to dielectric function peaks, results from the large number of modes present and the inaccurate analysis of measurements in the literature. Table 3.1 lists some of the more common modes of silica.

Table 3.1 Peak assignments for Silica glass

Wavenumber (cm^{-1})	Vibrational Mode	Source
440-460	Si-O-Si bending [Q4] SiO_4 tetrahedra Bending	[19, 20, 22, 25, 28]
780	Bending of Bridged $Si0_4$ tetrahedral group	[20]
800	Bending Mode of Bridging oxygen perpendicular to Si-Si axis and within Si-O-Si plane	[20]
800	Network Structure of SiO2 glass	[28]
805	Si-O-Si stretching between tetrahedra	[25]
1000	SiO_4 tetrahedra Stretching	[20]
1060-1065	Si-O-Si Stretching within the tetrahedra	[19, 20, 25]
1060 and 1090	Si-O-Si Stretching (LO and TO)	[28]

A simple silica glass should have only fully bonded SiO_4 tetrahedra making up the network; the exceptions are defect sites and impurities. All the silicon atoms are bonded to four oxygen atoms and all oxygen atoms are bridging oxygen atoms (BO), each oxygen atom bridges between two silicon atoms. Convention refers to a silicon atom with x BO's as a Q_x Si atom (with x= 4,3,2,1,0), and thus silica is made up of all Q_4 Si atoms. The difference between the glass and the crystal form of SiO_4 is that the glass has a variation in bond angles and bond length, leading to a broadening of a particular mode. A comparison of the imaginary dielectric function of both silica[26] and quartz [29] is shown in Figure 3.7. It is clear that the peak positions are similar, and that the glass peaks are broadened.

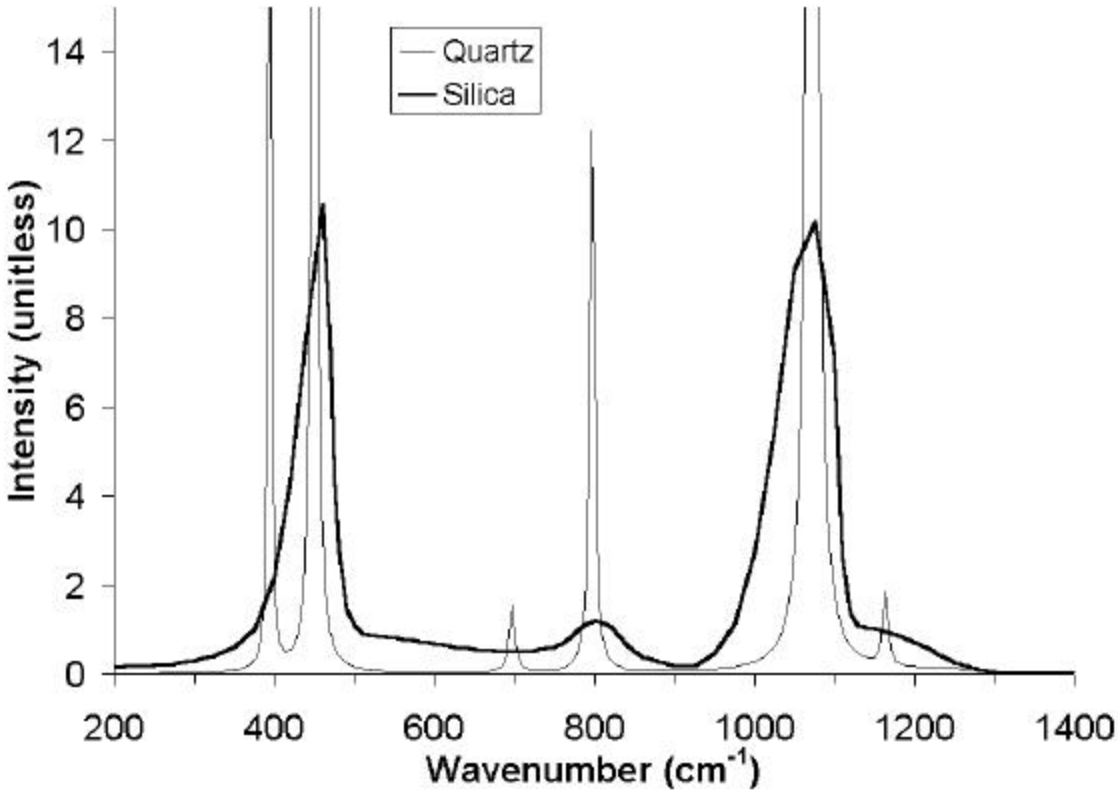

Figure 3.7 Comparison of imaginary dielectric functions of silica glass and quartz.

Although identifying the modes of silica is complex, the effort increases for any addition of another component as in alkali silicate glasses (see Table 2). With the addition of the alkali (a network modifier), the bonding arrangements change as a function of the composition. The higher concentration of alkali metal ions produce more Q_x (with x= 3,2,1,0) Si atoms[14, 30]. Each alkali ion adds one non-bridging oxygen (NBO). Thus, the addition of alkali metal ions adds new vibrational modes, Si-O-[alkali] bending and stretching, and it breaks up the network, altering modes associated with the silica network. The addition of other network modifiers such as other alkali's or hydrogen in the form of water, or hydroxyls adds further complexity and different

vibrational modes. The different network modifiers will each create similar but different bending and stretching modes, as well as affect the network modes differently. The assignments of modes to peaks is therefore very dependent to the concentration of and type of network modifier, and different network modifiers may have peaks in neighboring or overlapping regions of the spectrum.

Table 3.2 Peak assignments for Silicate bond vibrations

Wavenumber (cm^{-1})	Vibrational Mode	Source
850-880	Si-O-[NB], [Q0]	[28]
850	Si-O-[NB], [Q0]	[31]
900-920	Si-O-[NB], [Q1]	[28]
900	Si-O-[NB], [Q1]	[31]
940	Si-OH	[32]
950	Si-O-[NB], [Q2]	[28, 31]
952	Si-OH	[22]
980	Si-OH	[33]
970	Si-O-[NB] stretching	[19, 25]
980	Si-O-[NB] stretching	[20]
1080	Si-O-[NB] stretching	[19]
1100	Si-O-[NB], [Q3]	[28, 31]
1150	Si-O-[NB], [Q3’]	[28]
1200	Si-O- ,[Q4]	[28]

In applying this analysis to the surface of leached glasses, it is useful, for simplicity, to assume a mean field approximation. For example, it is well-known that corroded surface regions exhibit compositional gradients from the surface to the interior. These are often called layers, as in “de-alkalized layers”, however they are mostly diffusion profiles. The IR reflection data represent an average of the reflectivity over the penetration distance of the IR waves. With this approximation, multi-layer analysis is

possible but not practical due to the excessive number of variables introduced and the results are no better than the mean-field analysis presented here.

The sodium and lithium silicate experimental reflectivity curves were fitted using peaks with similar positions and widths as those of the silica glass dielectric function, with the addition of an alkali-silicate peak in the region of a Si-O- [NB] bond between 950 and 1000 cm^{-1} and a silanol peak at approximately 940 cm^{-1}. The peak positions were refined during the fitting process. The positions of the peaks are in general agreement with both the sodium and lithium silicate peak locations obtained from bulk Raman spectra and other IR studies of similar concentrations [34]. A representation of the Gaussian peaks used to fit the imaginary dielectric function of the 20% Na_2O-80% SiO_2 glass before and after leaching is shown in Figs. 3.8a and 3.8b.

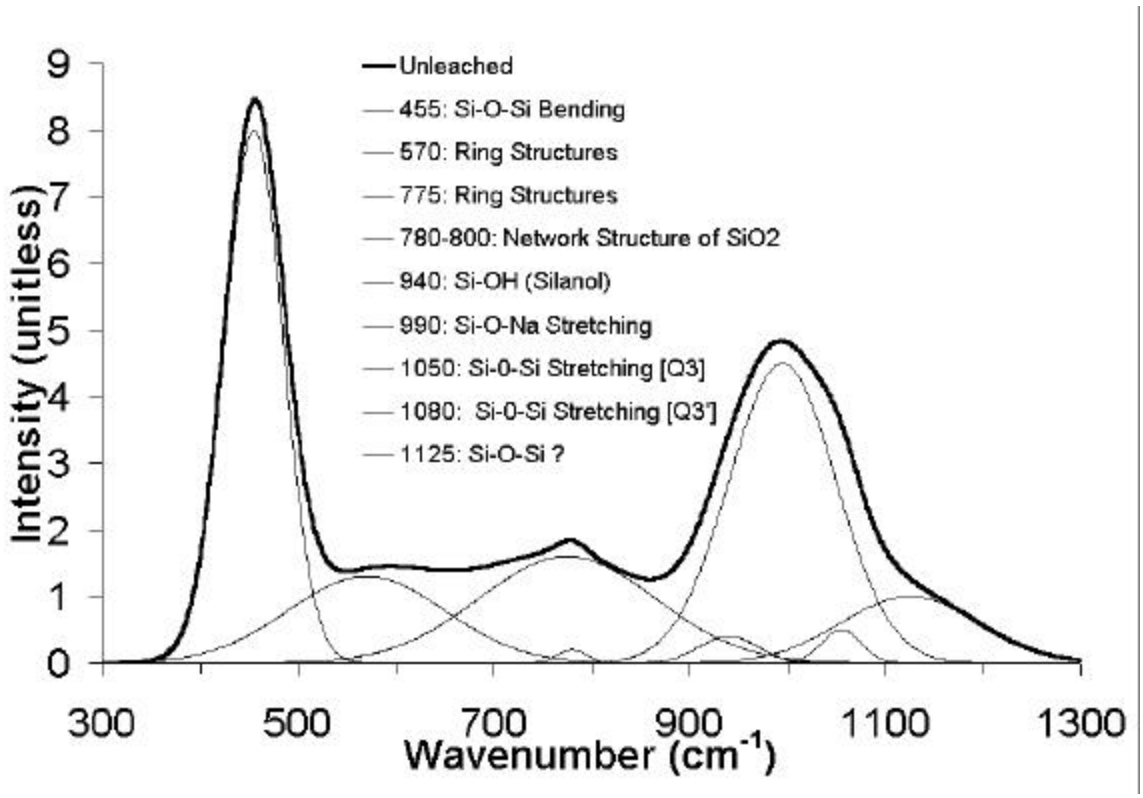

Figure 3.8a Calculated imaginary dielectric function for unleached 20% Na_2O- 80% SiO_2 using guassian dispersion analysis with peak positions listed in the figure.

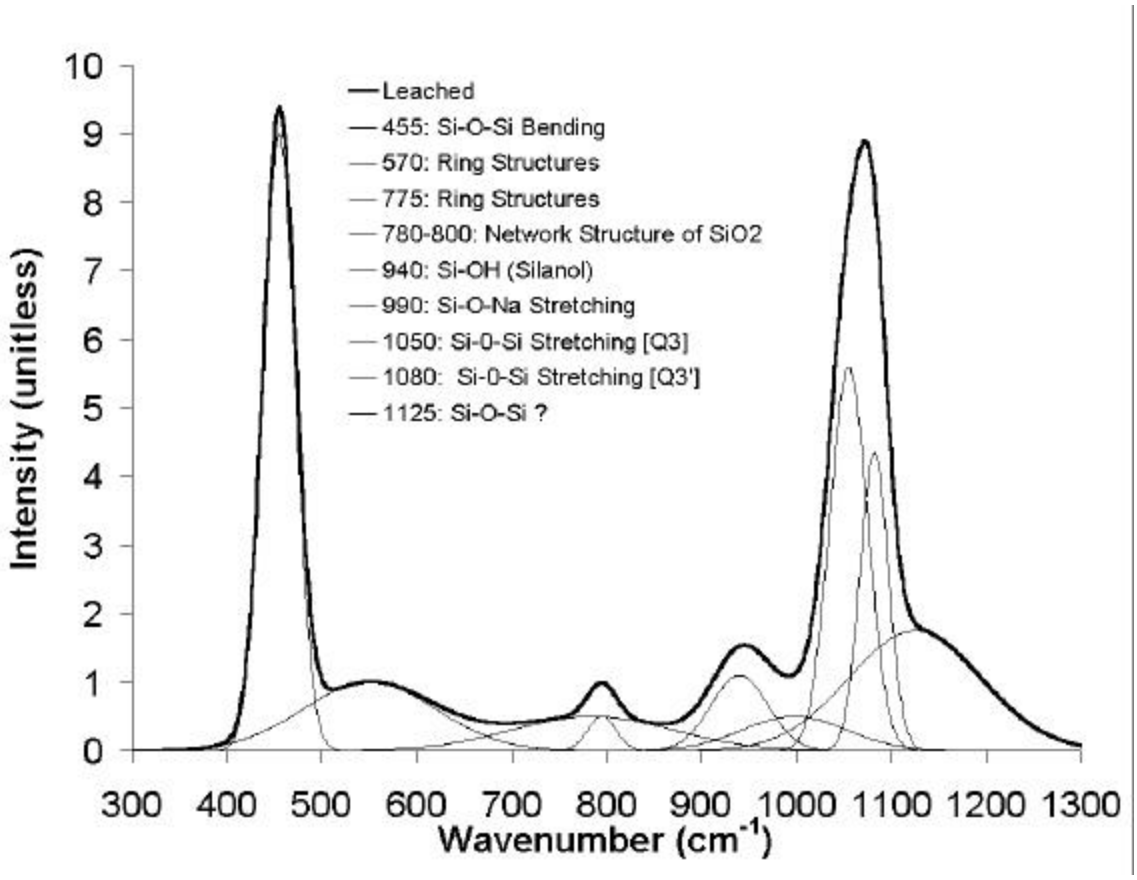

Figure 3.8 Calculated imaginary dielectric function for leached 20% Na_2O- 80% SiO_2 using guassian dispersion analysis with peak positions listed in the figure.

Figure 3.9 compares the measured reflectivity with the calculated reflectivity for the sodium silicate sample before and after corrosion. These fits are typical for all of the data sets. The peak positions in the dielectric function do not change with corrosion time and the peak widths remain relatively constant and are shown in Figures 3.10a and 3.10b. This essentially removes two adjustable parameters from each oscillator peak used in the corrosion analysis, leaving only the peak intensities as variables for fitting the corrosion-induced reflectivity spectra. Figures 3.11 and 3.12 show the integrated area of the Gaussian peaks as a function of corrosion time for the sodium and lithium silicate glasses, respectively. The peak intensities and the integrated

areas do change during corrosion. Assignments of these peaks are given in Table 3.3 and are fairly consistent with Tables 1 and 2. It can be seen that the NBO peaks (995 and 965 cm^{-1}) decrease in area while the silica peaks increase. These time dependent changes in peak area allow a measurement of the dynamics of the dealkalization process in alkali silicate glasses during leaching. Also note that the peak at 940 cm^{-1} assigned to the silanol vibration[33] emerges and grows with corrosion time, as expected.

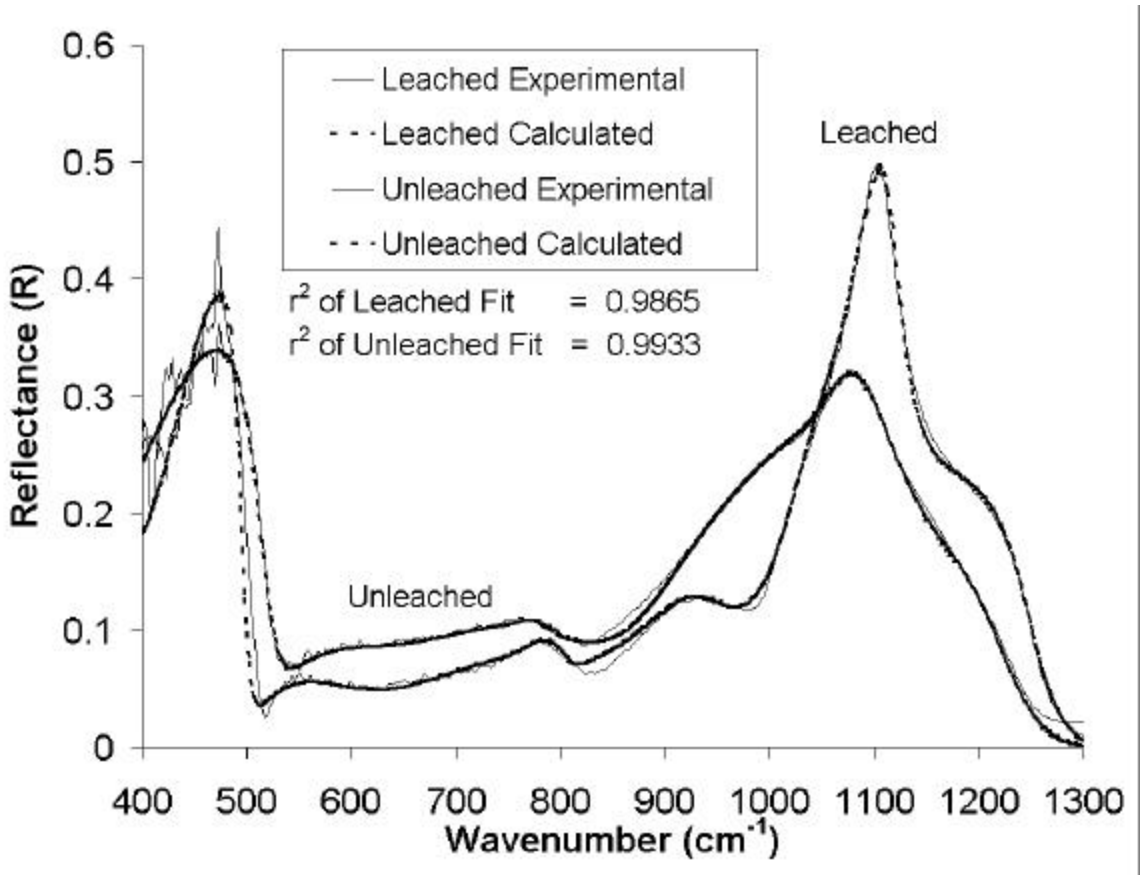

Figure 3.9 Fits of calculated reflectance compared with experimental reflectance for 20% Na_2O- 80% SiO_2 glass unleached and leached for 605 hrs

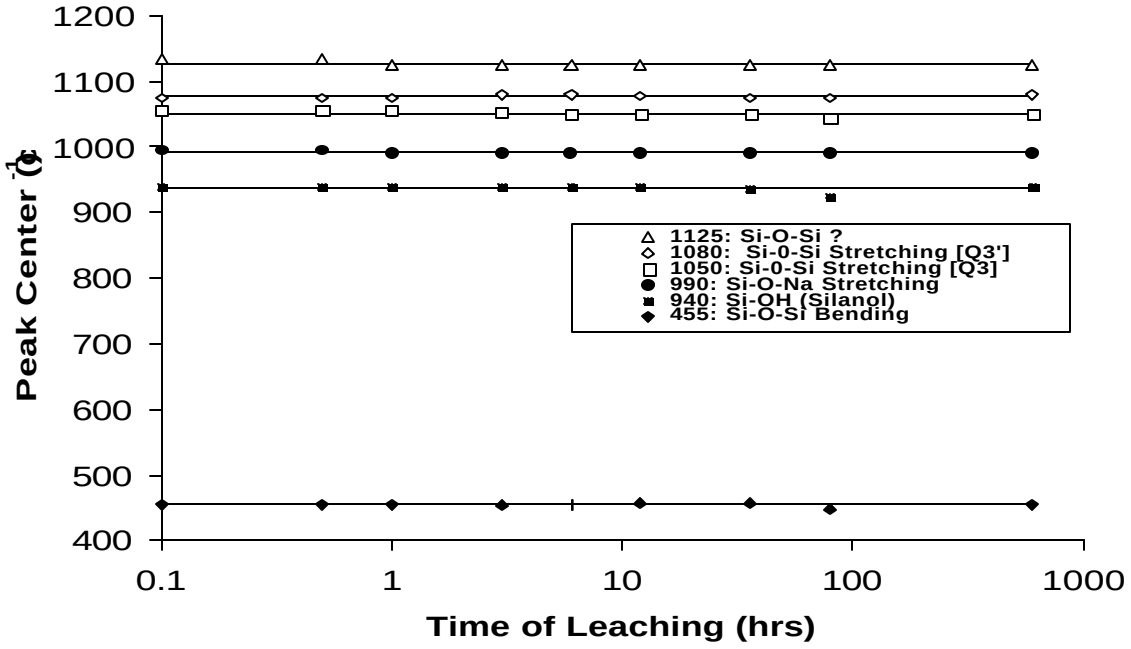

Figure 3.10a Imaginary dielectric peak positions vs. leaching time for 20% Na_2O- 80% SiO_2 glass.

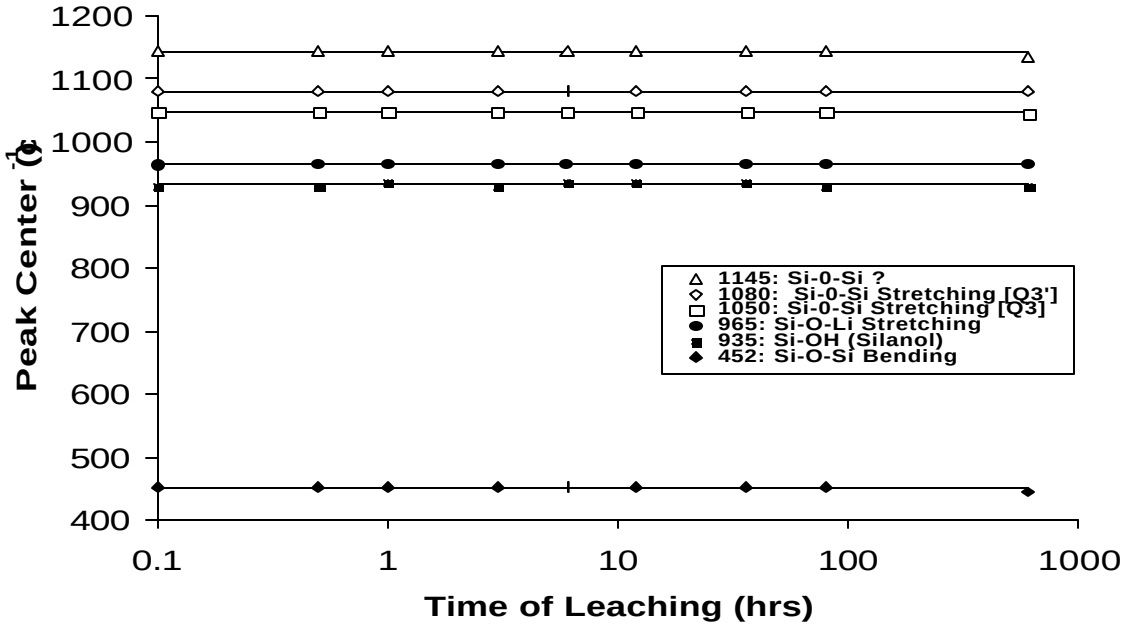

Figure 3.10b Imaginary dielectric peak positions vs. leaching time for 20% Li_2O- 80% SiO_2 glass.

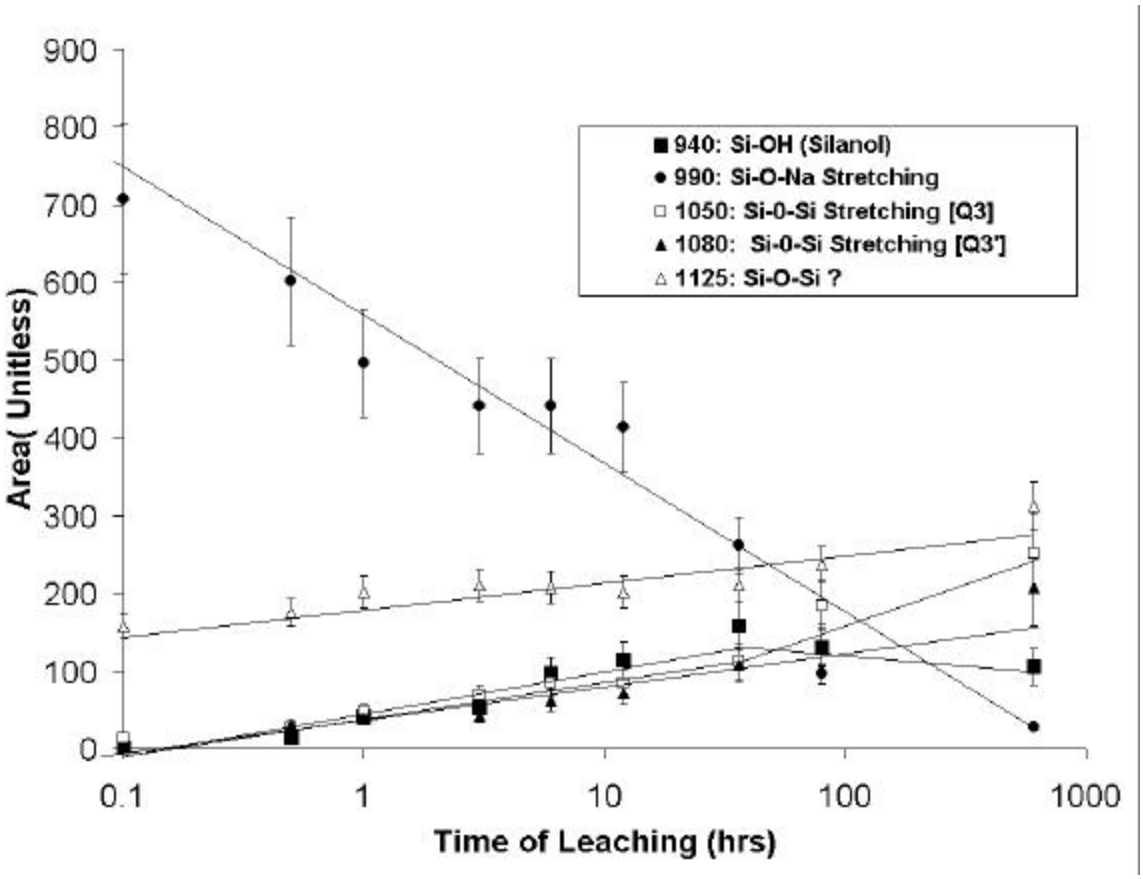

Figure 3.11 Integrated area of Gaussian peaks of the imaginary dielectric function vs. time of leaching of the 20%Na_2O-80%SiO_2 glass. (The lines are drawn to aid the eye.)

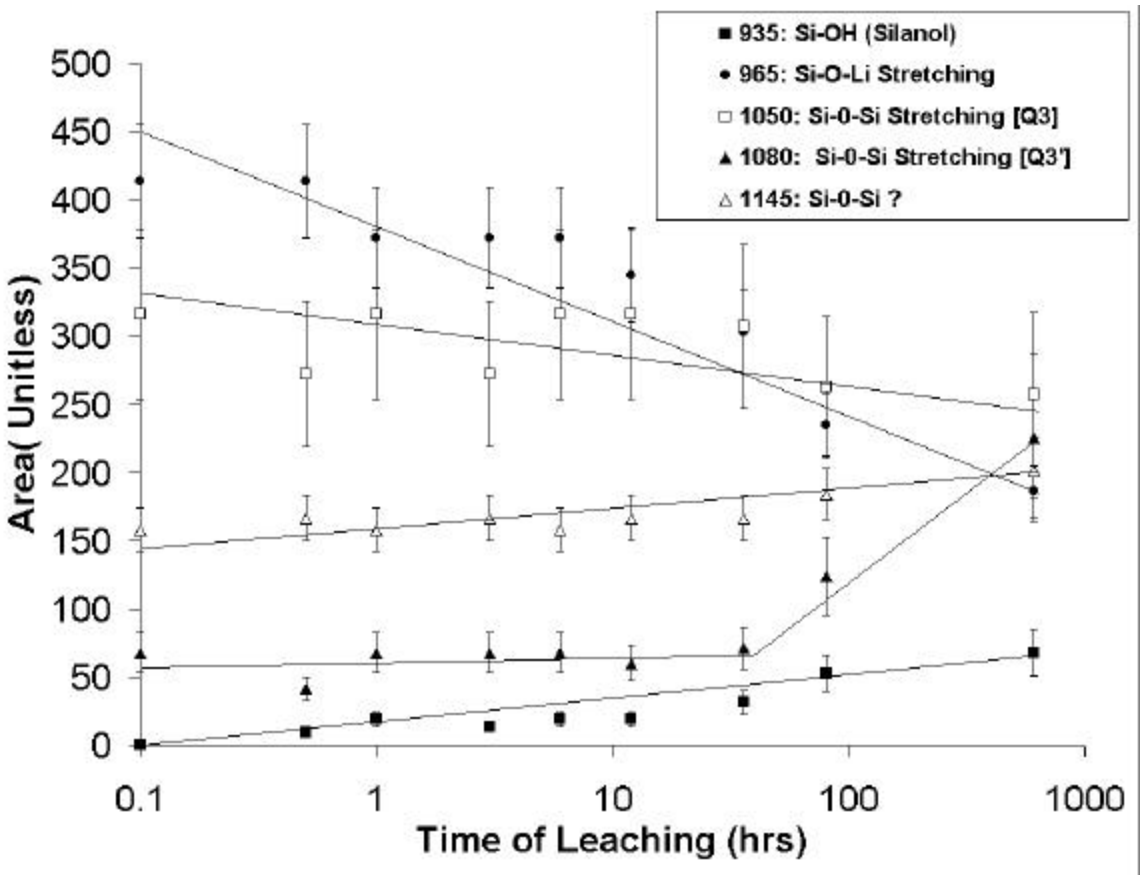

Figure 3.12 Integrated area of Gaussian peaks of the imaginary dielectric function vs. time of leaching of the 20%Li_2O-80%SiO_2 phase separated glass. (The lines are drawn to aid the eye.)

Table 3.3 Peak Wavenumbers used to fit measured data

Wavenumber (cm^{-1})	Vibrational Mode
445-455	Si-O-Si bending [Q4] SiO_4 tetrahedra Bending
570	Ring Structure
775	Ring Structure
800	Network structure of SiO_2
940	Si-OH
965	Si-O-[Li] stretching
990	Si-O-[Na] stretching
1050	Si-O-Si stretching [Q3]
1080	Si-O-Si stretching [Q3']
1125-1145	Si-O-Si stretching [Q4]

Figure 3.13 shows the calculated depth of penetration (δ) for infrared light for the sodium sample both before and after corrosion, as calculated from the equation:

$$d = \frac{1}{k(w)w} \tag{36}$$

The loss coefficient κ(ω) was calculated from the values of the complex dielectric function determined by guassian dispersion analysis and Equation 9. This shows that the penetration depth is less than 0.1 micron in the region of interest both before and after corrosion. The imaginary dielectric function is an exponentially weighed average over the thin layer of glass that is being sampled. As the corrosion progresses and the major composition changes occur beyond the sampling thickness of the IR light, the approach will become progressively less sensitive to the corrosion process.

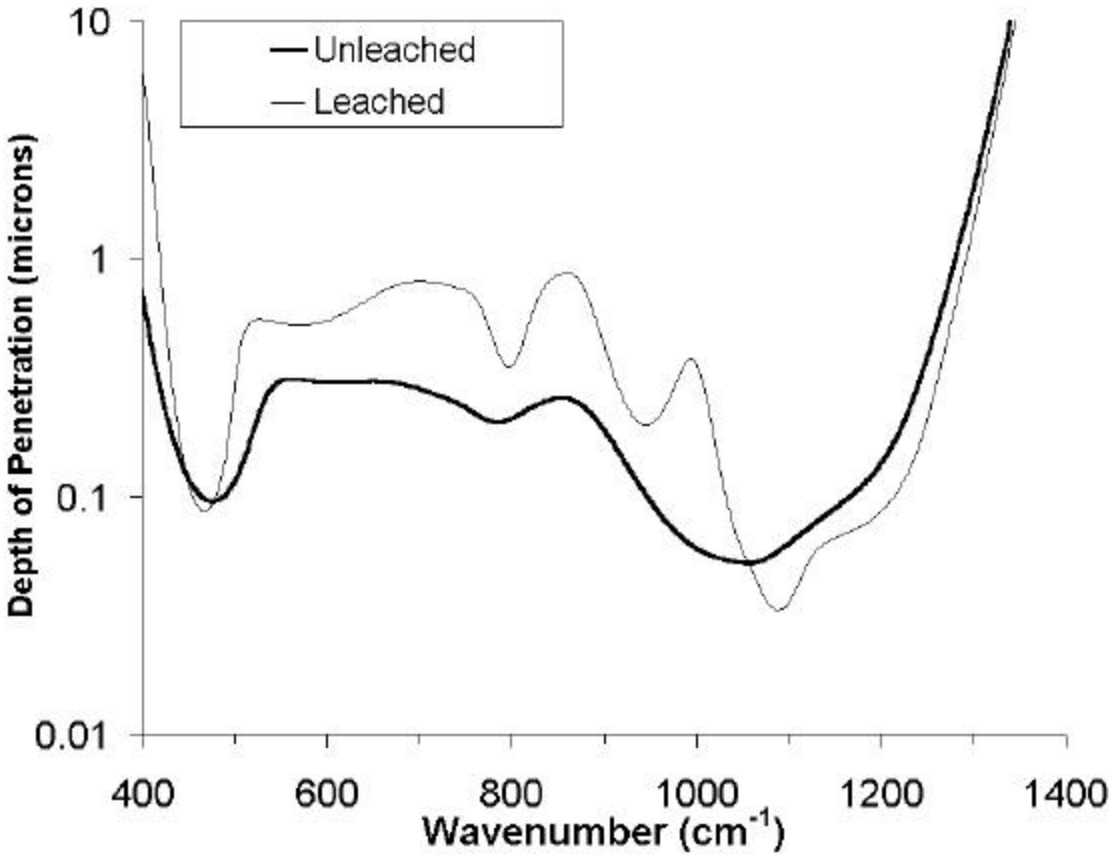

Figure 3.13 Depth of penetration of the measuring beam for the 20% Na_2O -- 80% SiO_2 glass calculated from the loss coefficient obtained from dispersion analysis.

Conclusions and Future Work

In this chapter, a novel analysis technique for infrared reflection spectra of glass surfaces is introduced. The reflection spectra from the leaching process of two alkali-silicate glasses and reflection spectrum from silica were used as examples to determine and follow the dielectric functions of these alkali silicate glasses during the leaching process. Gaussian dispersion analysis was used to extract information about the changes in surface composition during glass corrosion. The results indicate that the frequency of the oscillator peaks is not sensitive to the changes in surface composition during

corrosion. The changes in reflectivity result almost entirely from changes in the area (height and width) of the oscillator peaks. Changes in peak area correlate directly with changes in the number of oscillators in the sample and reveal the dynamics of the dealkalization process in these glasses. Additionally, by properly fitting the reflectivity, the surface optical properties of glasses can be determined.

For truly quantitative corrosion studies, further work is needed to establish oscillator strengths and appropriate peak positions and widths by using bulk glass standards so that guassian dispersion analysis can be used to determine exact surface concentrations of arbitrary glass samples.

Also, the type of analysis presented here is essential in the reduction of all reflection and absorption spectra. Since the functions used are ergotic it is only limited by the investigator's ability to generate oscillator peaks in the imaginary part of the dielectric constant and the accuracy of the measurement. Finally, as this is a mean-field approximation, this approach cannot yield concentration profiles of the surface species and once the corrosion process extends past the penetration distance of the reflected IR light, further changes will not be detected in the spectral analysis.

CHAPTER 4
EFFECTS OF ROUGHNESS ON REFLECTIVITY

Introduction and Background

When making intensity based optical studies it is important to consider the effect of surface roughness and the losses due to scattering. Reflectivity occurs at the interface between two media of different index of refraction and is dependent upon the angle of incidence. Surfaces that are not absolutely smooth can have the effect of locally changing the angle of incidence and reflecting the portion of the incident light at an angle other than that expected.

If the wavelength of the incident light is large compared to the surface irregularities, the effects can be negligible, while in cases of large surface irregularities compared to the wavelength, the light can be reflected in many directions, or scattered. Previous work in this area has been concerned mostly with correlation between polishing and surface changes due to corrosion occurring during the polishing stages or theory relating the specular reflectance for highly reflective materials with different polishing stages.

Darby et al. [35] preformed an infrared reflectivity vs. polishing levels experiment on a sodium silicate glass of 33 % Na_2O concentration by weight. He found that the reflectivity maximum for the Si-O-Na peak increased with finer polishing until the 600 grit level with SiC polishing paper. Finer polishing did not appear to improve the reflectance, and it was reported that apparently the corrosion rate was faster than the

polishing rate. Another study by Gelbov [36], reported that a higher quality polishing with water usually results in more leaching of the surface and a changed reflectance spectrum than of a less smooth surface from faster polish. It was thought this was due to the longer times required for higher quality surfaces and the fact that polishing in water creates a corrosion suitable environment. Both of these studies agree that a higher quality polish of a non-durable glass may improve the surface roughness but at the expense of chemically changing the surface.

In other works[27, 37-39], on the relation of specular reflection vs. roughness, theories have been developed to relate the reflectance with rms roughness. Bennett and Poerteus developed theories to relate the wavelength dependence of specular reflectance relative to the ideal reflectance with rms roughness and diffuse reflectance with rms roughness and an autovarience length, or slope of roughness value. They report both the theories and compare it to some experimental measurements made on aluminum coated steel and aluminum coated plate glass samples. These theories have been found to be in good agreement and have been utilized to determine roughness from reflectivity[40].

Experiment

Sample Preparation

The exact sample material was not considered to be an important factor for this experiment. A borosilicate glass was selected due to its environmental stability and its relative similarity with samples measured in Chapter 3. Pre-cleaned Gold Seal microscope slides produced by Becton Dickinson and Company were cut to 1 cm by 1cm rectangles and ground with 120 grit silicon carbide sandpaper into disks of approximately

1cm in diameter. These disks, samples A through G were polished, or in fact made more rough, with the compounds and sizes listed in Table 4.1.

Table 4.1 Polishing compounds and Particle size for sample preparation

Sample	Polishing Compound	Particle Size
A	CeO_2	1 micron
B	SiC	1200 grit
C	SiC	800 grit
D	SiC	600 grit
E	SiC	400 grit
F	SiC	320 grit
G	SiC	120 grit

The polishing with SiC was made with SiC paper produced by the Buehler Corporation on a polishing wheel with water as a cooling and lubricating agent. The polishing with the CeO_2 was made by placing a few drops of a CeO_2 –water suspension on to a TEXMET polishing cloth, both the CeO_2 compound and TEXMET are manufactured by the Buehler Corporation. For all samples the surfaces were roughened with the next roughest sandpaper before polishing with the smaller particle sizes. Additionally the polishing at each stage was conducted for approximately five minutes. Both the duration and pre roughening were preformed to insure that the final polish was representative of the final polishing stage.

Optical Measurements

To determine if the polishing with a 600 grit silicon carbide paper was sufficient for the experiments conducted in Chapter 2, near normal reflectance of all samples were measured on an FTIR. Two measurements were made on each sample in order to

confirm the measurement. In addition to the FTIR measurements, observations by eye were made.

AFM and Profilometry

In order to correlate the polishing stages with measured roughness values, Atomic Force Microscopy (AFM) and Profilometry measurements were made on the samples. The AFM, in tapping mode, was used only on samples A and B as the roughness of samples C through G were quite large and profilometry was more appropriate. The AFM has a vertical range accuracy of ±1 A° while the profilometer used, an Alpha-Step 500 surface profilometer by Tencor Instruments, has a 10 A° standard deviation repeatability with a 100 A° step profile. The stylus used on the profilometer had a 5 μm radius.

Results

Figure 4.1 show the reflectance of the different samples vs. wavelength. Only one reflectance spectrum per sample is shown, as the difference between reflectance for the same sample was small. Figure 4.2 and Figure 4.3 are AFM images of sample A and sample B.

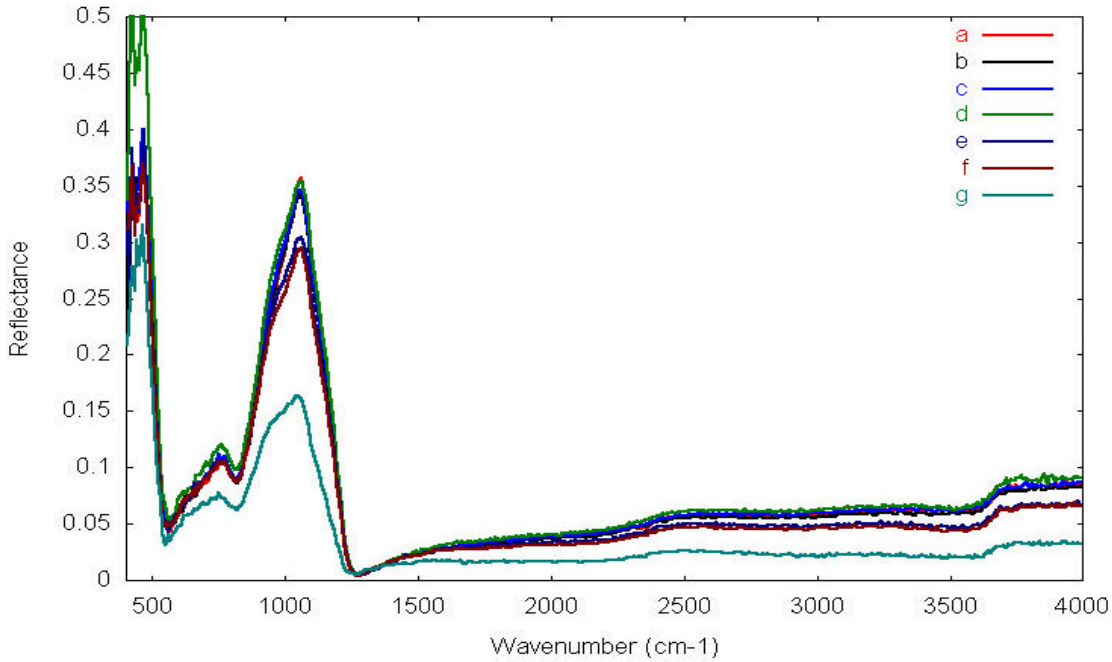

Figure 4. 1 Reflectance vs. Wavenumber for samples A through G

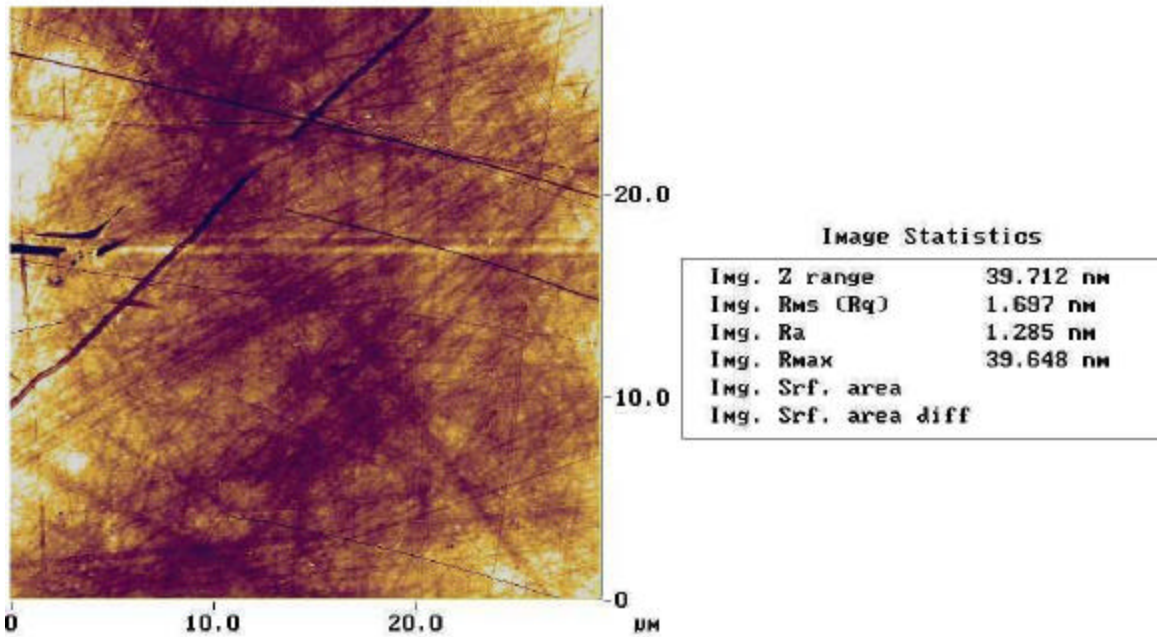

Figure 4.2 AFM image of Boro-silcate glass, sample A, polished with 1µm CeO_2 polishing compound.

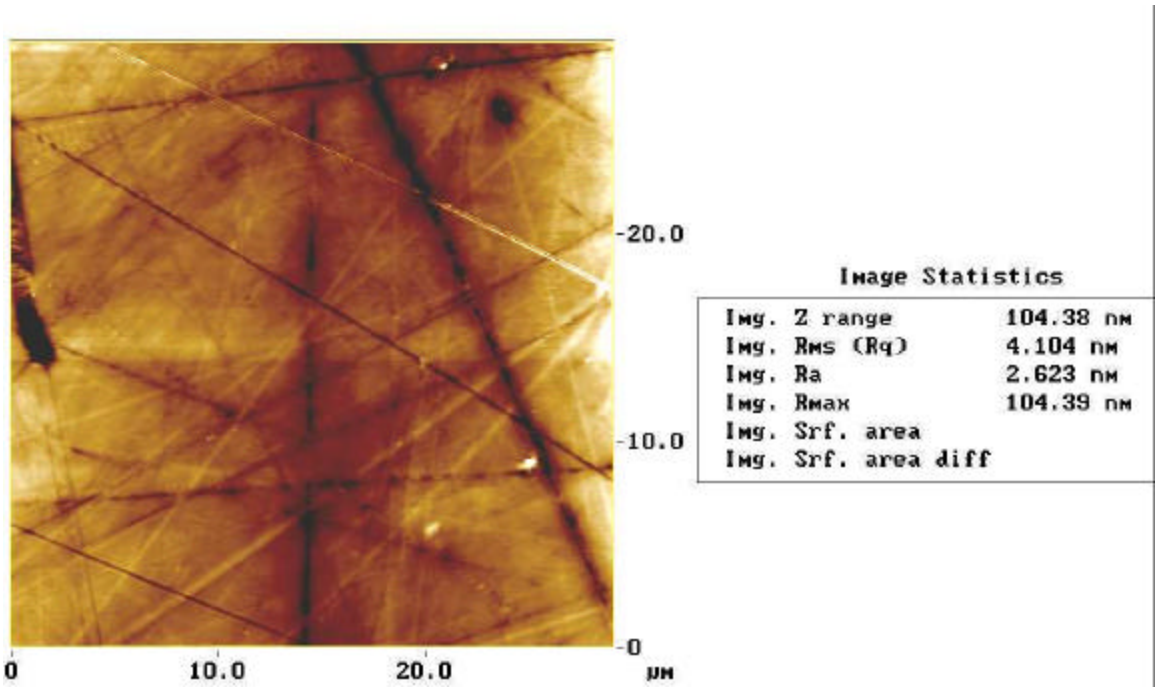

Figure 4. 3 AFM image of borosilcate glass, sample B, polished with 1200 grit SiC polishing paper.

A summary of the data obtained from profilometry measurements is shown in Table 4.2. The profilometer used returns Ra and not rms roughness.

Table 4.2. Summary of Prolimetry results

Profilometry (5µm tip)	Ra (nm)
Sample A	4.4
Sample B	7.79
Sample C	13.15
Sample D	65.43
Sample D	90.89
Sample E	79.2
Sample E	89.67
Sample F	87.35
Sample F	82.6
Sample G	477.69
Sample G	226.4

The observation by eye of the samples yielded the following. Samples A through D were optically clear and the surface was free from scratches. The reflection of a room light was free from scattering. Sample E had visible scratches, but was still very transparent. Sample F had visible scratches and was semi translucent in transmission. The scratches on sample G were difficult to observe, as the surface had more of a frosted appearance and was completely translucent.

Discussion of Results

The reflectivity spectra vs. sample preparation show no significant difference in the overall reflectivity for samples A through D, or polishing above the 600 grit stage does not improve the overall spectra with in the variability of the measurments. It is observed that samples A and D have a slightly higher peak intensity at 1060 cm^{-1} than both samples B and C. It is not thought that these differences are significant.

It can be seen that for samples E and F the reflectance spectra appear very similar to each other, but significantly reduced from the reflectance spectra from samples A through D. Though the polishing regimes were different, the Ra values obtained from profilometry measurements are similar. The closeness of both the roughness measurements and the spectra are expected, but not that the two different polishing stages would yield such similar results, particularly when the observations by eye of the sample surface were different. The similarity is believed to come from some irregularity from the polishing procedure, from sampling region of the profilometer, errors in the profilometer or a combination of all of these. The AFM and Profilometry are typically used for surfaces much smoother than the samples used in this study particularly the

rougher polished samples. It is believed that due to this, and the variability of the duplicate measurements, that the error in the roughness measurements is quite large and that the measurements may be used as a general gage of the increasing roughness and not necessarily a quantitative measure of the actual roughness.

Theory

Definitions of Roughness

Few surfaces are perfectly smooth and exhibit both roughness and waviness. The surface roughness is considered the finer irregularities superimposed on larger scale periodic (or non-periodic) variations in surface smoothness. The definitions typically used to quantify the results of a profilometers trace are R_t, R_a, and rms, from ANSI B-46-1-1978. R_t is defined as the distance from highest peak to lowest valley. R_a is also known as the centerline average or arithmetical average. A mean surface line is drawn such that the material above the line is equal to the unfilled area below the line. The Ra is defined as follows:

$$Ra = \frac{1}{l}\int_0^l |y| \partial l \,, \tag{37}$$

where l is the length of trace and y is the distance from the mean surface line to the measured height. The rms, also know as R_q, is closely related to R_a and is defined as follows:

$$Rq = \left[\frac{1}{l}\int_0^l y^2 \partial l\right]^{\frac{1}{2}}, \tag{38}$$

Ra is related to Rq by a factor of 1.11 for a sine wave and is approximately 1.4 for lapped surfaces**[41]**.

Reflectance vs. Surface Roughness

Bennett and Porteus's theories are based upon a statistical treatment of electromagnetic reflection from rough surfaces for radar waves reflecting from rough water surfaces. These statistical theories are thought to be valid at optical frequencies as well. The equation developed by Bennett and Porteus for normal incidence specular reflectance is:

$$R_s = R_0 \exp\left(-\frac{(4ps)^2}{l^2}\right), \tag{39}$$

where R_s is the measured reflectance, R_0 is the theoretical reflectance for a smooth surface, σ is the rms roughness, and λ is the wavelength. They also developed equations for non-normal specular reflectance and diffuse reflectance vs. roughness. In the case of FTIR measurements the acceptance angles of the detectors are small enough with regard to the signal origin that the measurements can be considered primarily specular. Equation 39 is plotted for various rms roughness values over the 400 to 4000 cm^{-1} spectral range in Figure 4.4.

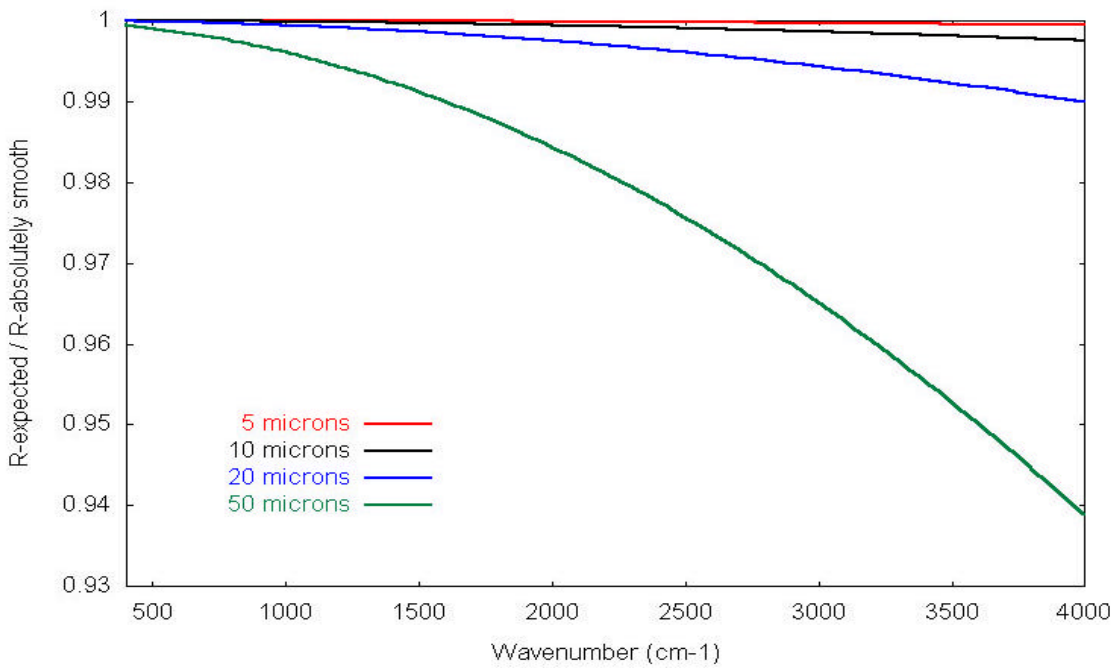

Figure 4.4 Expected reflectivity ratio to maximum for rms roughness values of 5,10,20 and 50 microns

The measured spectra were fit using Equation 39 and sample A's reflectance as that of R_0, with particular attention paid to the peak at approximately 1060 cm^{-1}. Figure 4.5 plots the expected response of the peak at 1060 cm^{-1} with rms roughness. Samples A through D are have nearly identical spectra and is it expected from Figure 4.5 that their rms roughness values would be less than 100 microns. The data from the profilometry measurements supports this, assuming that rms roughness is 1.4 R_a, but with sample D having values on the edge of this range. The fits are not shown for samples A through D. Samples E, F and G are shown, with fits, in Figures 4.6, 4.7 and 4.8 using values of rms roughness of 280, 300 and 660 microns respectively.

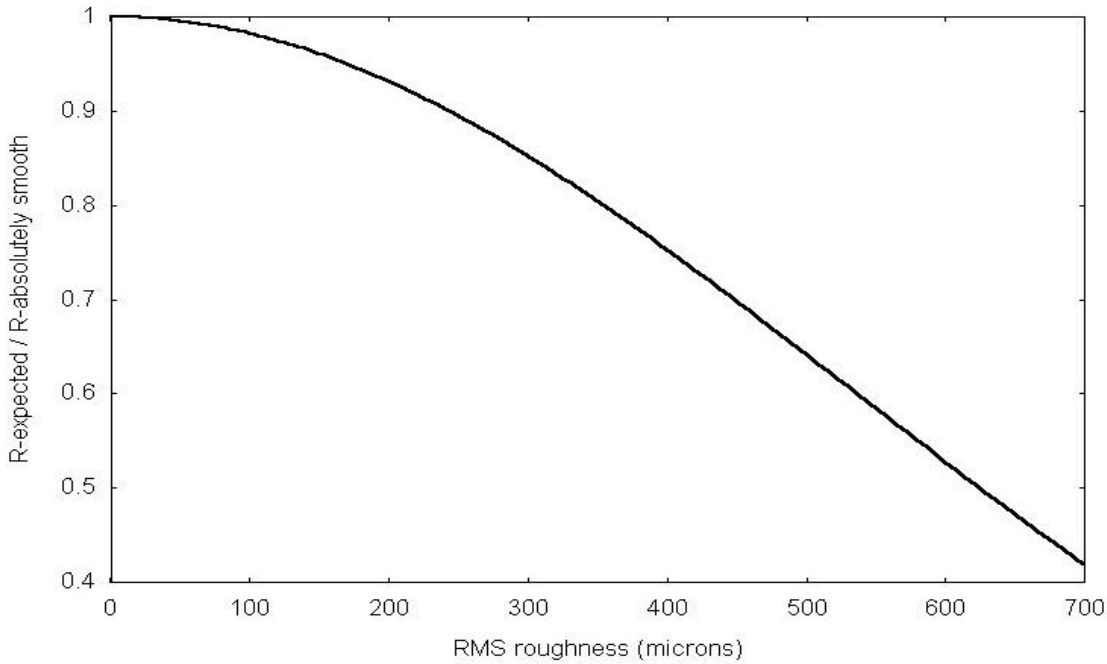

Figure 4.5 Expected response of reflectivity vs. rms roughness at 1060 cm^{-1} from Equation 39.

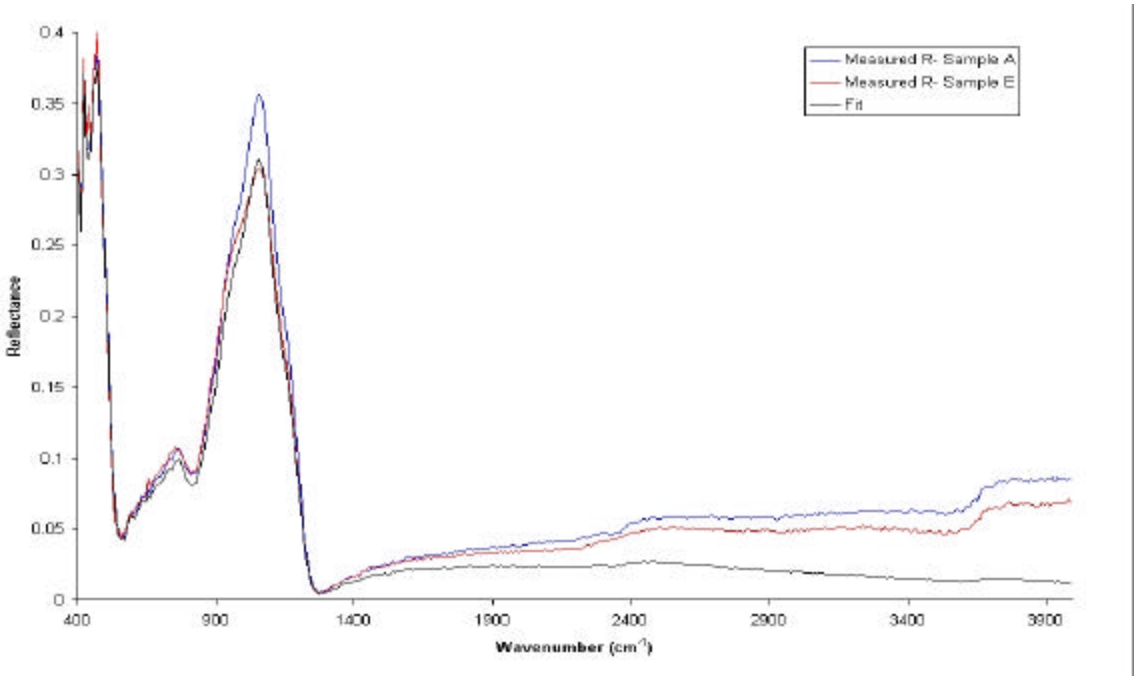

Figure 4.6 Fit of 1060 cm^{-1} peak for sample E.

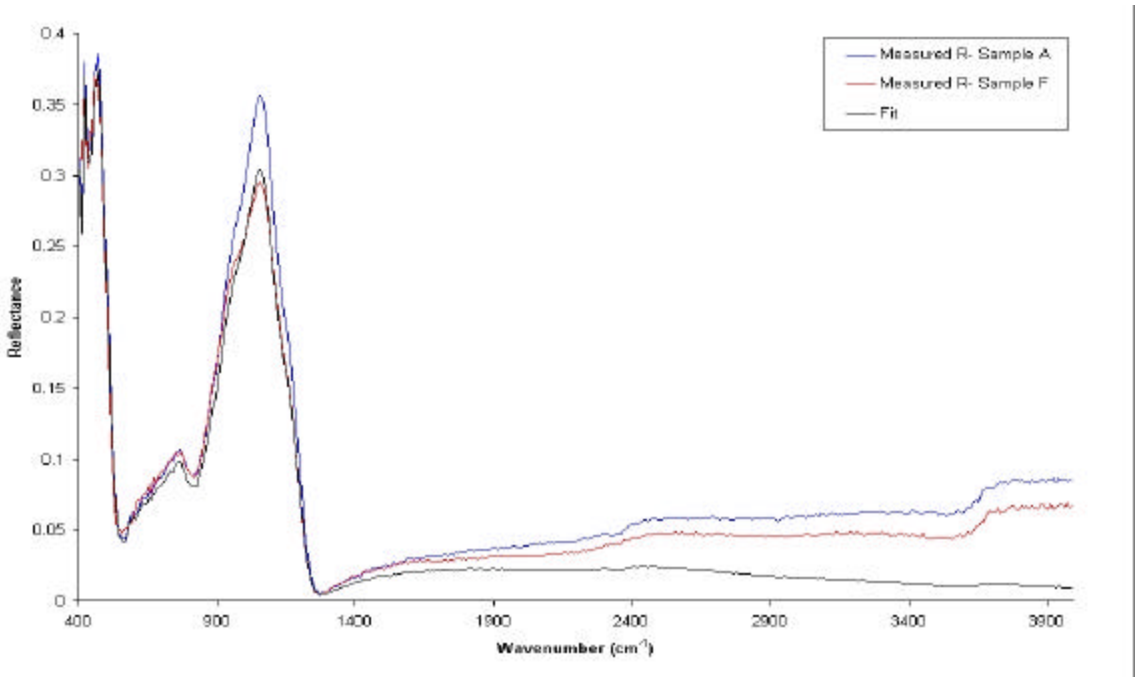

Figure 4.7 Fit of 1060 cm^{-1} peak for sample F.

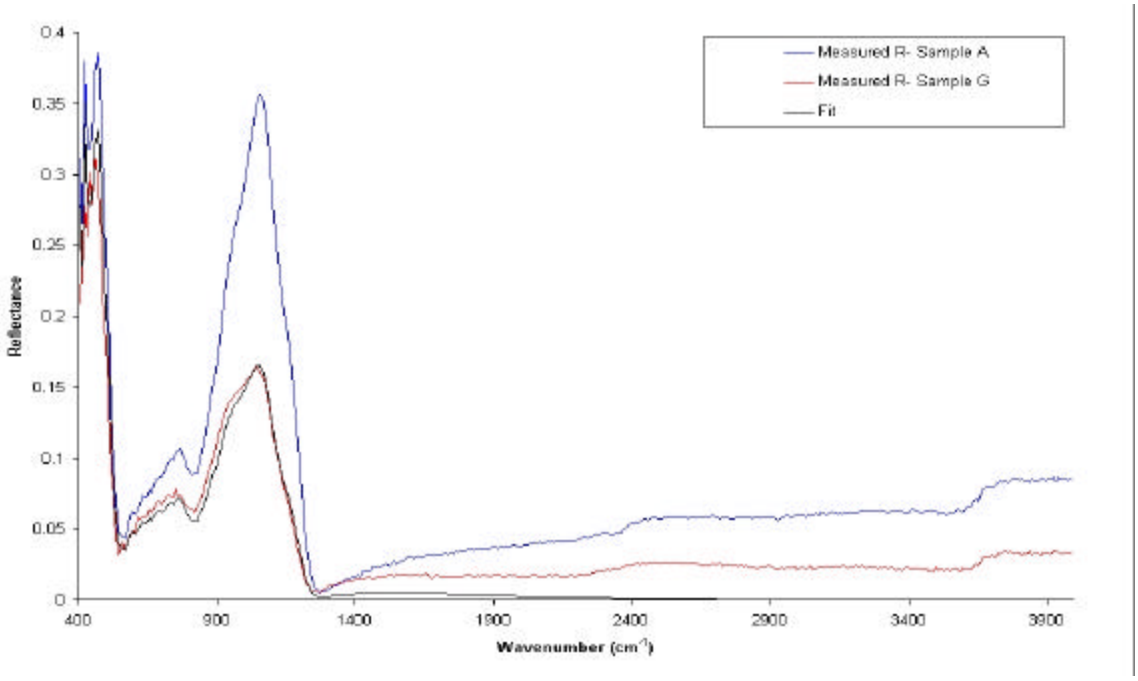

Figure 4.8 Fit of 1060 cm^{-1} peak for sample G.

The values of rms roughness obtained for samples of E, F, and G by fitting the measured spectra, do not match well with the estimated values of rms roughness (1.4 * R_a) based on the profilometry measurements, but do follow the same trends.

One difficulty in applying Equation 39 to the present study is the limitation of the useful range of the equation. Equation 39 is only valid when the σ/λ <<1. For the samples A-D the σ/λ is much less than 1 for the spectral range, but do not differ significantly in their measured spectral response. For the samples E, F, G the σ/λ ratio is much larger, see Figure 4.9, particularly at for the larger wave numbers and thus are not expected to fit the experimental spectra in these regions. It is apparent from the fits and the reported useful σ/λ range that Samples E, F and G are out of the useful range of Equation 39.

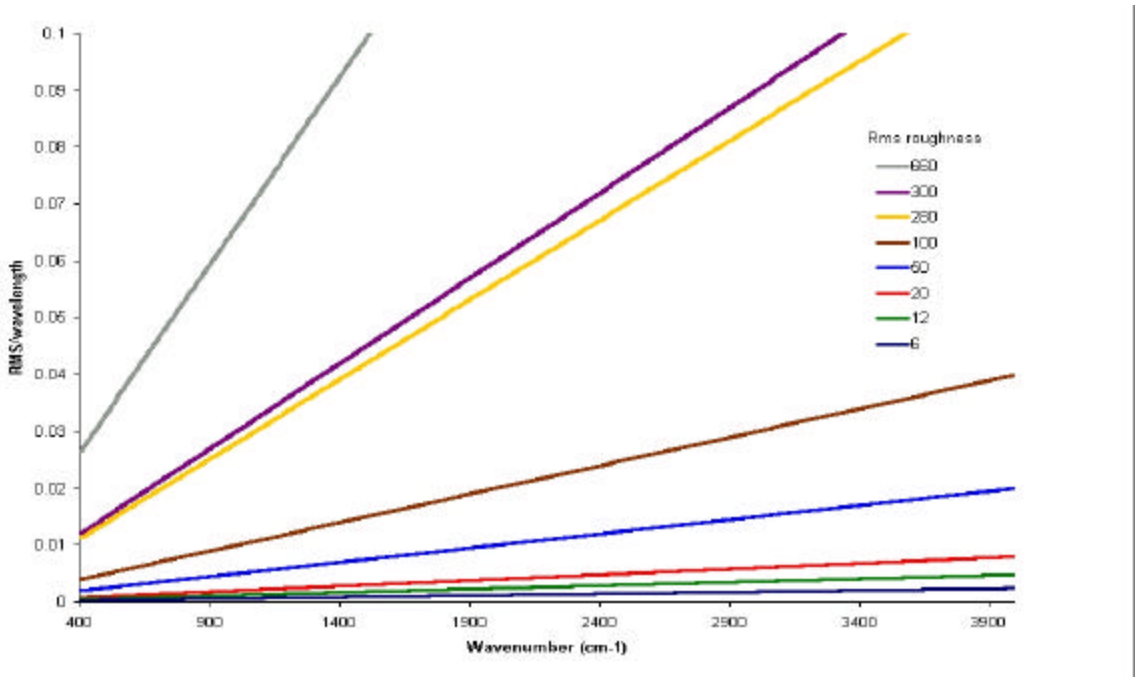

Figure 4.9 RMS/wavelength for range of RMS values vs. spectral range of FTIR.

Conclusions

The motive of this experiment was to confirm the polishing procedure used in Chapter 3 for the reflectance study of corrosion was sufficient. From both of the works by Darby and Glebov, it appears that the polishing of environmentally sensitive glass samples is best at a less than perfect polish. This is due to the time it takes to perform finer polishing and the corrosive environment that the samples experience during that time. Also the increase in signal from the finer polish isn't significant considering the variability of the FTIR measurements.

The studies of Bennett and Porteus dealt with highly polished surfaces of high reflecting materials. The correlation of this theory with these non corrosive, variably polished and partially reflecting samples is not established. The variability of the FTIR measurements for the more highly polished samples of A, B, C, and D, is greater than the deviation expected for the low values of rms roughness. For the rough samples, E, F, and G, the theory is not expected to hold through out the spectral range, and does not, but the trends expected by Equation 39 are followed.

CHAPTER 5
LIQUID ATTENUATED TOTAL REFLECTANCE

Introduction

The work conducted in this chapter deals with the calculation of the dielectric properties of de-ionized water and ethyl alcohol from liquid cell ATR measurements by guassian dispersion analysis. Also liquid cell ATR measurements of mixtures of de-ionized water and ethyl alcohol are compared with the expected response of the liquid ATR cell as calculated from a model for optical properties of chemicals based on the additive nature of dielectric functions.

Background

Identification or qualitative analysis of materials is often achieved by optical measurements. Due to the abundance of absorbing bonds of many materials in the infrared and the wide availability of FTIR spectrometers, the FTIR infrared absorption spectra is often the tool of choice when characterizing polymers, glasses, liquids and many other materials. Some of the difficulties involved with the absorption spectra have been the shifting of absorption bands with concentration of chemicals and overlap of these bands in multi chemical solutions.

Due to these problems, the nature of these measurements has always been qualitative. There have been attempts to derive quantitative information, or concentrations, from the absorption spectra, but these have usually been based on Beer's Law or other empirical analysis, that have the same difficulties as mentioned above.

These types of empirical analyses can not be universally applied and are only useful for fully characterized systems.

ATR liquid cell

Optical analysis of liquid samples can be performed, like any other sample, by measuring the transmitance or reflectance. Transmission measurements are often performed with the use of a cuvette, and approximations for absorbance are made. Generally these approximations neglect surface reflections, but due to the low index of many chemicals, and thus low reflectivity, the approximations are fairly accurate. Reflection measurements are usually more difficult with liquids and single or multiple reflection cells are often used. These cells have a crystal, of known index of refraction, and use it as an interface with the liquid.

Multiple reflection cells are recommended for use with liquids with low absorbance, as they increase the systems sensitivity [42]. An example is the Spectra-Tec model HATR 0001-703 shown in Figure 5.1. Figure 5.2 shows a comparison of the absorbance of water, as taken from the ATR cell, and absorbance as calculated from published values of optical properties for water [43] using Equation 11 from Chapter 2. The amplitude of the calculated peak was scaled, to account for path length, to approximately that of the ATR peak at 1600 cm^{-1}. The measured peak at 3400 cm-1 is clipped, as the transmission was zero for the much of the peak. This is due to the high absorption of water for light at those frequencies. The shapes of the peaks (1600 cm^{-1} and 3400 cm^{-1}) are approximately the same but the locations of the ATR peaks are shifted to lower wavenumbers than those of the published values.

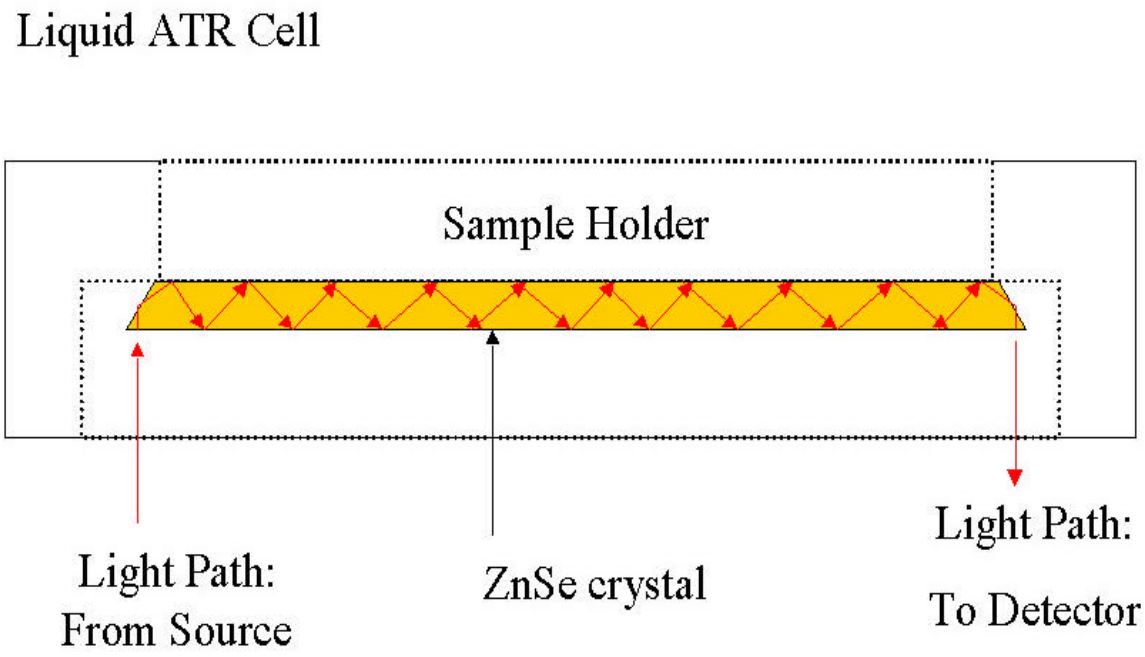

Figure 5.1 Spectra-Tec model HATR 0001-703.

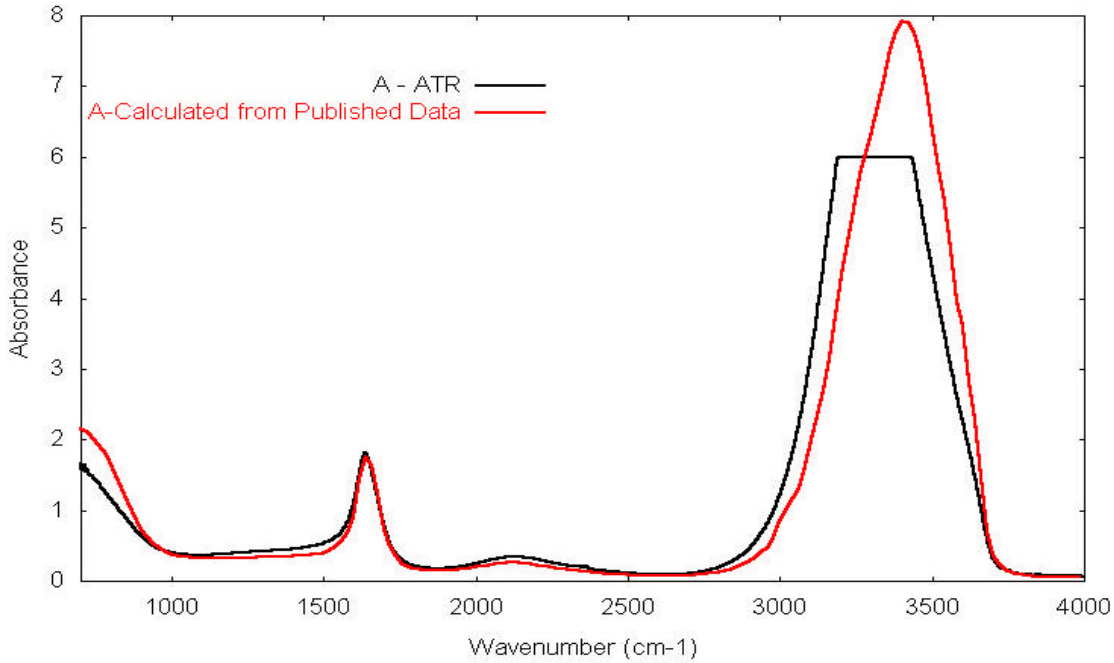

Figure 5.2 Measured Absorbance and Calculated Absorbance from published data for de-ionized water

Analysis of ATR spectra

The manufacturer of the spectrometer defines that

$$T(w) = \frac{I(w)_{out}}{I(w)_{in}} \tag{40}$$

and uses Equation 9 to estimate absorbance. As can be seen from Figure 5.2 the approximation is close, but shifts the peak locations. This shift can be problematic when trying to subtract out the effects of a single chemical.

From Figure 5.1, it can been seen that the light interacts with the sample in a much more complicated geometry than either transmission or a single surface reflection, but since the geometry is known, the light path and optical interaction can be calculated. The formula for this cell is the following:

$$\begin{aligned} I(w)_{out} &= I(w)_{in} * (1 - R(0, n(w)_{Air}, n(w)_{ZnSe})) \\ &* R(68.5, n(w)_{ZnSe}, n(w)_{Air})^2 * R(45, n(w)_{ZnSe}, n(w)_{Sample})^{10} \\ &* R(45, n(w)_{ZnSe}, n(w)_{Air})^9 * (1 - R(0, n(w)_{ZnSe}, n(w)_{Air})) \end{aligned} \tag{41}$$

Where $R(\theta, n_t, n_i)$ is the coefficient of Reflectivity between two media with complex index of refraction of n_t and n_i at an angle θ. $I(\omega)_{in}$ is the incident intensity of the beam before the Liquid ATR cell. Since the beam impinges the interface between two media at other than normal incidence, the coefficient of reflection depends on the polarization of the beam relative to the surface. The two orientations, electric field parallel to the interface or TE, and magnetic field parallel or TM , have reflection coefficients defined as follows:

$$R_{\mathrm{TE}}(\Theta, n_t, n_i) = \left[\frac{n_t^2 \cos(\Theta) - n_i \sqrt{n_t^2 - n_i^2 + n_t^2 \cos(\Theta)^2}}{n_t^2 \cos(\Theta) + n_i \sqrt{n_t^2 - n_i^2 + n_t^2 \cos(\Theta)^2}} \right]^2 \tag{42}$$

$$R_{TM}(\Theta, n_t, n_i) = \left[\frac{n_i \cos(\Theta) - \sqrt{n_t^{\,2} - n_i^{\,2} + n_t^{\,2} \cos(\Theta)^2}}{n_i \cos(\Theta) + \sqrt{n_t^{\,2} - n_i^{\,2} + n_t^{\,2} \cos(\Theta)^2}} \right]^2 \tag{43}$$

Where again, n_t is the complex index of refraction of the medium the beam is transmitting through and n_i is the complex index of refraction of the medium that the beam is incident upon. Theta (θ) is the angle of incidence from normal. The optical properties of the ATR crystal-ZnSe- are well known [44] and the real part of the index of refraction is shown in Figure 5.3. The polarization can be estimated by an equal mixture of TE and TM. Air's optical index of refraction is generally approximated as that of a vacuum, n(ω)=1+ 0i. Thus by solving

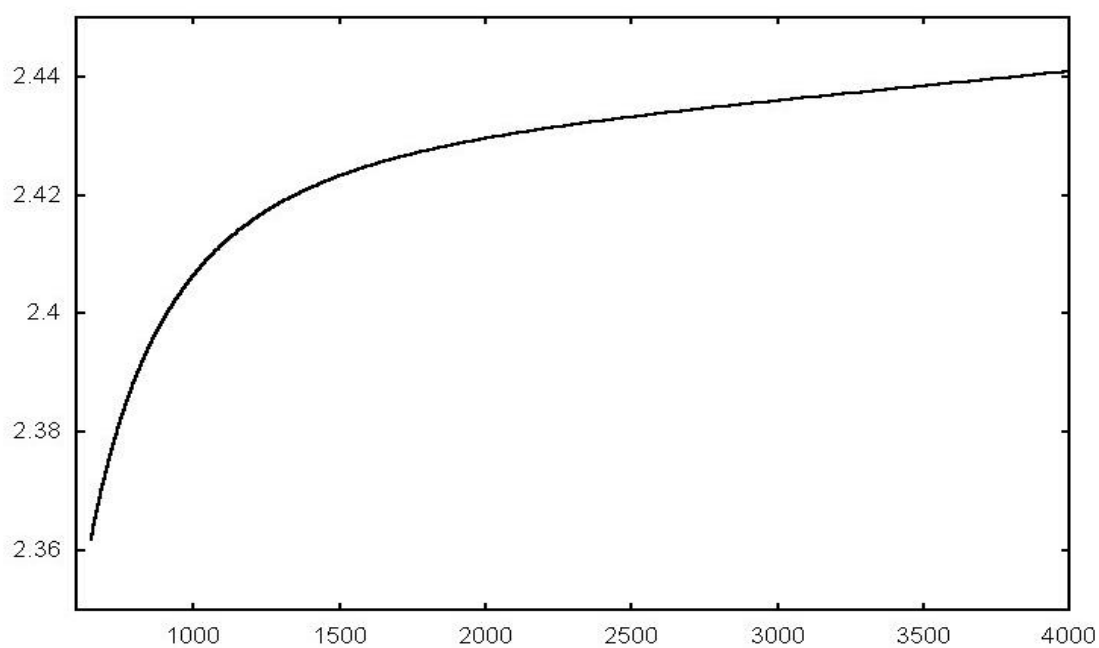

Figure 5.3 Index of refraction (n) for ZnSe.

the equation for a known sample- air, or measuring directly, the profile of the incident beam, $I(\omega)_{in}$,can be determined. Furthermore with the assumption of a vacuum for air,

the 45 degree reflectance between air and ZnSe is 1 at all wavenumbers in the useful spectral range for this cell, this simplifies Equation 41 to:

$$\frac{Signal(w)}{Background(w)} = *R(45, n(w)_{ZnSe}, n(w)_{Sample})^{10} \tag{44}$$

The shift in Figure 5.2 is due to the fact that the signal in the ATR undergoes a multiple reflection process and does not simply transmit through the sample as one would expect from using the approximations given by the manufacturer. Due to the differences between transmission and reflection, there is a shift in location of the loss[45]. In samples with very large absorption losses the shifts can be significant. Figure 5.4 depicts the change of normal reflectivity in air, with large changes in the amplitude of a guassian shaped peak in the imaginary dielectric function. The peak is centered at 1000 cm-^{1} with a width of 100 cm^{-1}. Figure 5.5 depicts the change in the calculated alpha for the same amplitude changes in the imaginary dielectric function. The base index for the calculations was 1.5.

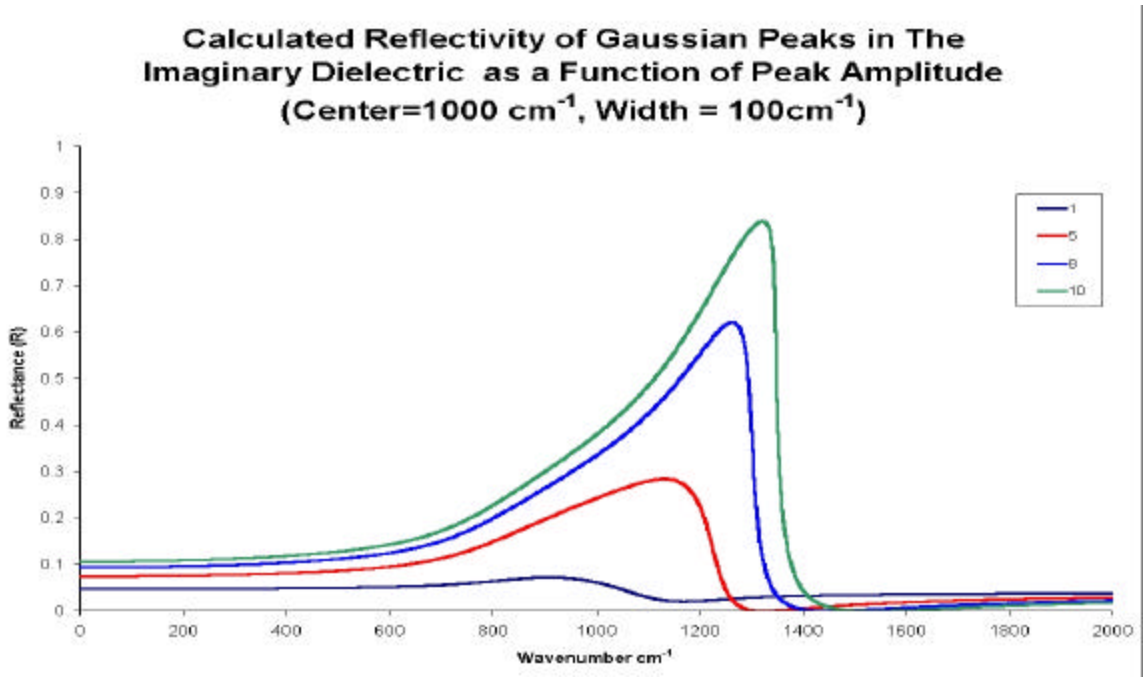

Figure 5.4 Change in normal reflectivity as a function of imaginary dielectric peak height

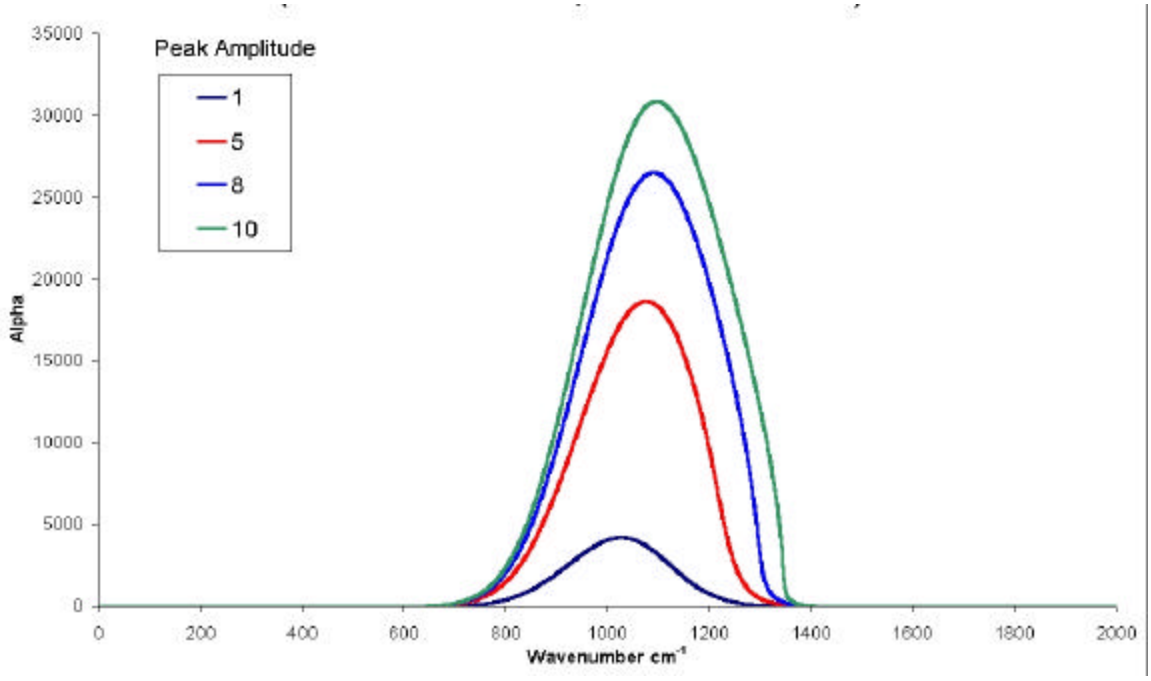

Figure 5.5 Change in Alpha as a function of imaginary dielectric peak height

As is shown in Figures 5.4 and 5.5 the location of the reflectivity maximum and minimum and alpha change with changes in the amplitude of the imaginary dielectric peak. Though the ATR cell does not involve normal reflections in air, the principle is the same. Furthermore, the location and amplitude of reflection peaks will be affected by not only amplitude changes, but also changes in absorption peaks in the nearby spectral region.

Figure 5.6 shows the effect of increasing the amplitude of an absorbing peak in the dielectric function on the ATR absorbance as calculated by the manufacturer. The calculation is based upon Equation 44 and Gaussian shaped peak centering at 1500 cm^{-1} in the imaginary dielectric function. Figure 5.6 shows that the ATR cell response to a fixed location absorption peak is to shift the location to lower wave numbers with an increase in peak amplitude. This is analogous to an increase in concentration, but is a simplified case as it is an individual peak, uninfluenced by other peaks in the spectral region.

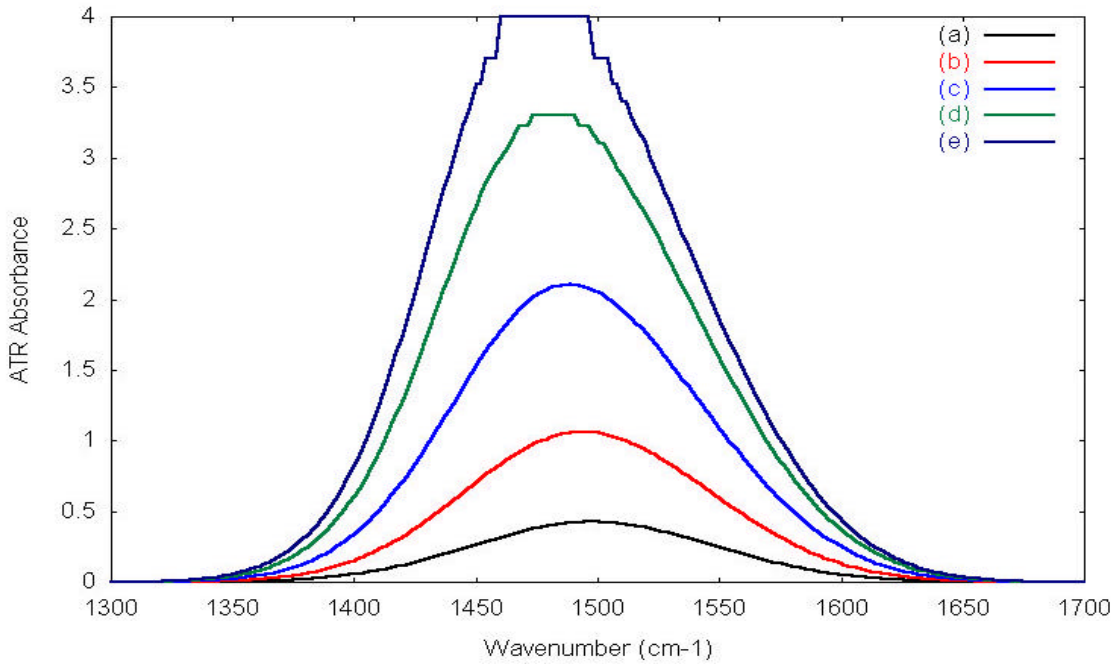

Figure 5.6 Changes in ATR absorbance with increasing peak amplitude of imaginary dielectric function. Values of Amplitude: (a)=.1,(b)=.25,(c)=.5,(d)=.8,(e)=1.

Though the scales are different for emphasis, it is interesting to note that the shift in alpha for an increase in amplitude is to higher wavenumbers, while the ATR absorbance shifts to lower wavenumbers.

The use of the ATR liquid cell as a quantitative analysis tool is problematic with the current analysis. The approximations recommended by the manufacture of such equipment yield spectra that look close to that of absorbance, but are not. Even though the approximations are close, absorbance does not lend itself to direct quantitative analysis.

Quantitative Optical Analysis

Historically optical measurements have been qualitative in nature, though many attempts have been made to derive quantitative information from them. Beer's Law is well known in chemistry as an empirical method to approximate the concentration

of solutions from absorbance. Another method has recently been developed that makes use of the more fundamental theories of dispersion analysis.

Beer's Law

One type of data analysis techniques used to derive chemical composition from optical measurements makes use of Beer's Law. Beer's Law, also known as the Beer-Lambert, or the Bouguer-Beer Law is

$$A(w) = KxC \tag{45}$$

where A(ω), taken as the maximum absorbance value, is directly related to the concentration, C, by the product of the path length, x, and a constant K. Also, the ratio of two peaks from different chemicals is used in some cases to determine relative concentrations. The use of Beer's law is pervasive in the analysis of chemical concentrations, and may be a good approximation over small concentration changes, with the use of standards, under controlled conditions.

The reason that Beer's law is so limited in its scope is that as the concentration of a solution changes, the location and shape of the absorbance peaks change. Additionally if the peak being used as the reference peak is close to other peaks from the solvent or other solutes, the absorbance peak of the solute of interest will be effected. Both the shifting effects and effects of neighboring peaks are due to the change in dispersion as the concentration changes, and due to dispersion effects from distant peaks. Furthermore, changes in the peak shapes are ignored with Beer's Law. Only the maximum amplitude of a peak is considered, while the width and integrated intensity is ignored. Beer's Law does not take these effects into consideration, and thus as concentrations change, systems deviate from the linear approximation made by Equation 45 [46].

Quantitative Dispersion Analysis

Dispersion Analysis is well suited for quantitative analysis. If the local electric field equal to the applied electric field approximation holds, then the area of the peaks in the imaginary dielectric function will be linearly proportional to the concentration of molecules exhibiting absorption. As such, for chemical systems, each chemical will contribute to the total mixture dielectric function linearly with concentration as:

$$\boldsymbol{e}_{total}(\boldsymbol{w}) = \sum_{j} C_j \boldsymbol{e}_j(\boldsymbol{w}) \tag{46}$$

Dispersion analysis, Kramers-Kronig analysis, or measurement of two extrinsic properties is necessary to obtain the dielectric functions, as discussed in Chapter 2.

Although measurement of two extrinsic properties and subsequent calculation of intrinsic optical properties can be more accurate, dispersion analysis has some advantages over the other methods. Dispersion analysis does not require more than one extrinsic property to be experimentally measured. As a process of performing dispersion analysis the dielectric function is de-convoluted into peaks, of which the areas are easily calculated and in some instances the individual vibrational modes can be examined, as in Chapter 3. Dispersion analysis doesn't have errors introduced into it by limitations of the measured data, such as Kramers-Kronig type analysis. Furthermore, since dispersion analysis starts at the fundamental optical properties, and calculates and compares to the measured extrinsic property, as long as a function can be generated to solve the measured property in terms of its dielectric function, dispersion analysis can be performed.

Considerable effort would be necessary to calculate the optical properties with the other techniques, in cases of complicated geometry, such as ATR.

Experiments

Chemical Preparation

Ethyl alcohol, de-ionized water and mixtures of 25%, 50%, and 75 % ethyl alcohol, with the balance being de-ionized water, were prepared. A graduated cylinder with graduate markings of 1ml was used to measure the chemicals and to pour into a clean 50ml beaker. The chemicals were prepared one at a time to a total volume of 20ml. The beaker was cleaned and rinsed with ethyl alcohol and dried before the next chemical was mixed.

The Attenuated Total Reflectance Liquid Cell

A FTIR with a spectral range from 400 cm-1 to 4000 cm-1 was used for the measurements. A Spectra-Tec model HATR 0001-703 liquid ATR attachment was used for the measurements. The cell is shown above in Figure 5.1. The cell equipped with a ZnSe crystal reduces the spectral range to 650 cm^{-1} to 4000 cm^{-1}.

Experimental Procedure

The FTIR spectrometer chamber was purged with dry N_2, evaporating from a liquid nitrogen dewar. The Liquid ATR cell was rinsed with ethyl alcohol and dried. Prior to making any measurements, a background spectra of the liquid ATR cell was recorded. The background spectrum recorded was the signal through the ATR liquid cell without any liquid sample in the chamber and only the purged air inside the FTIR sample chamber. The background is essentially the infrared source spectra as transmitted

through the empty liquid cell. The background was repeatedly measured until it was stable and the purge reached a steady state.

The ATR liquid cell was removed from the FTIR spectrometer. The ATR cell was first rinsed with de-ionized water and then with ethyl alcohol. The ATR cell was dried with a laboratory dry air hose. This was done to accelerate the evaporation of the ethyl alcohol. A pipette was used to transfer liquid from the 50 ml beaker containing the chemical mixture to the trough. The cell was then returned to the FTIR sample chamber. This procedure was repeated for each sample, typically with the next sample being prepared while current sample was being measured.

Additionally, the above procedure was repeated on different days for the pure samples of de-ionized water and ethyl alcohol. This was done due to establish criteria for assigning error to the measurements and subsequent calculations and due to the difference of the measured spectra from the expected spectra.

Results

Figure 5.7 a-e shows the measured spectra, in a signal to background format, from the ATR liquid cell for the different mixtures of the water-ethyl alcohol system. Figures 5.7 a and b, show the pure liquids measured on different days. Figure 5.8 shows all of the measured spectra on a single plot. The signal to background format is not the typical format to present liquid ATR spectra, but for later calculations the measurements are presented in signal to background format. Approximated absorbance is the usual format and is shown in Figure 5.9.a,b and c.

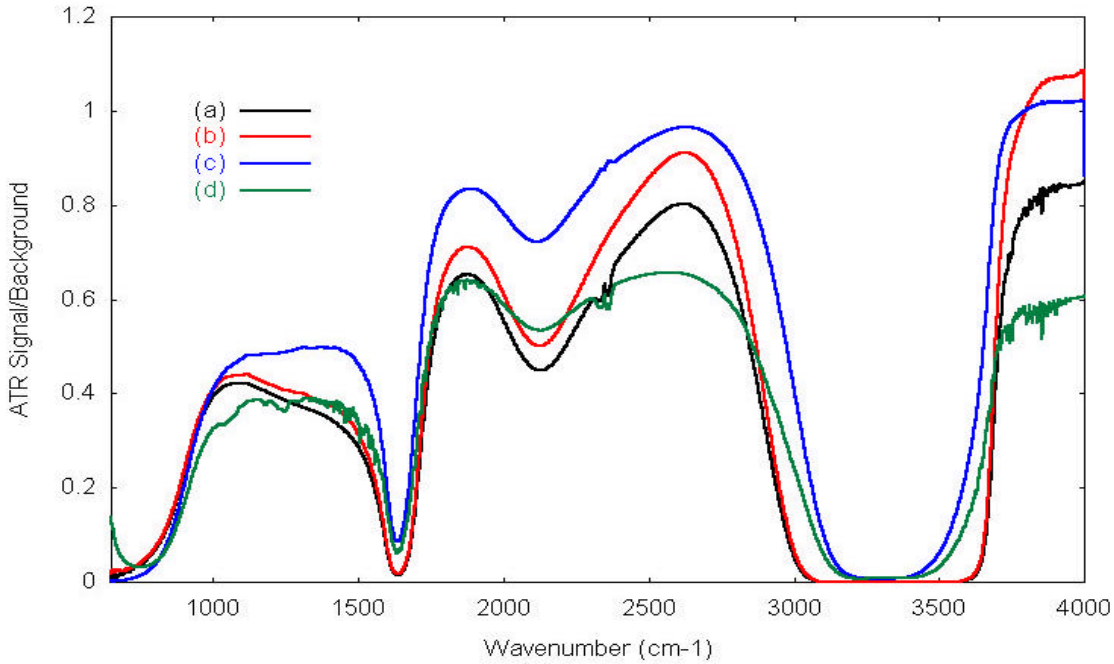

Figure5.7a Measured Liquid ATR spectrum for de-ionized water; (a) measured on the day the mixtures were measured, (b),(c) and (d) measured on different days.

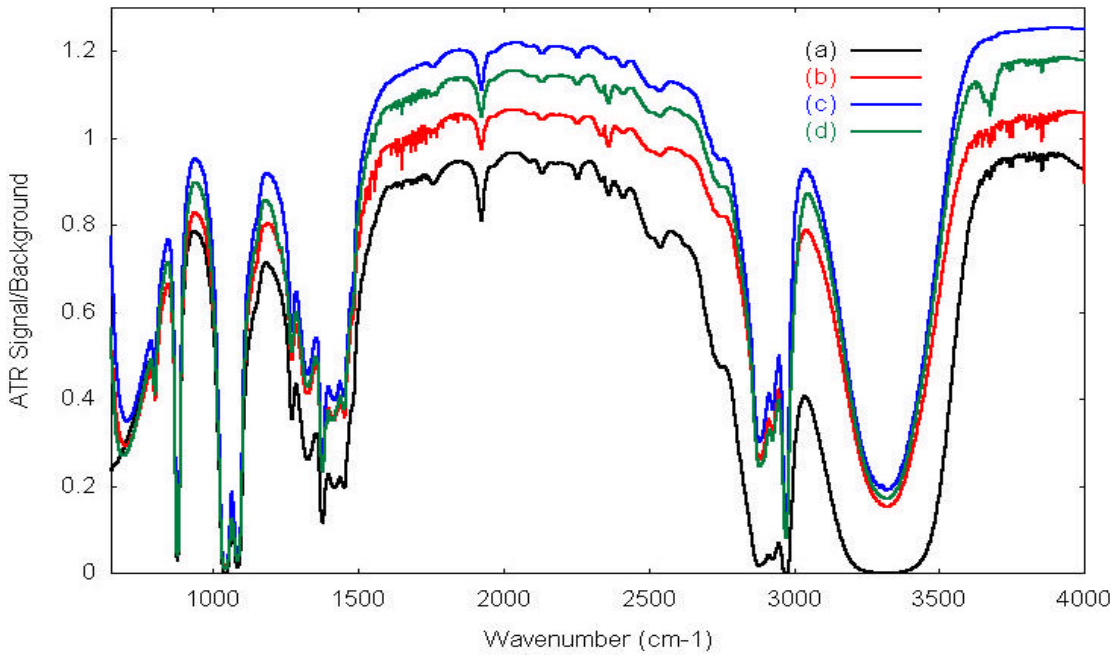

Figure5.7b Measured Liquid ATR spectrum for ethyl alcohol; (a) measured on the day the mixtures were measured, (b),(c) and (d) measured on different days.

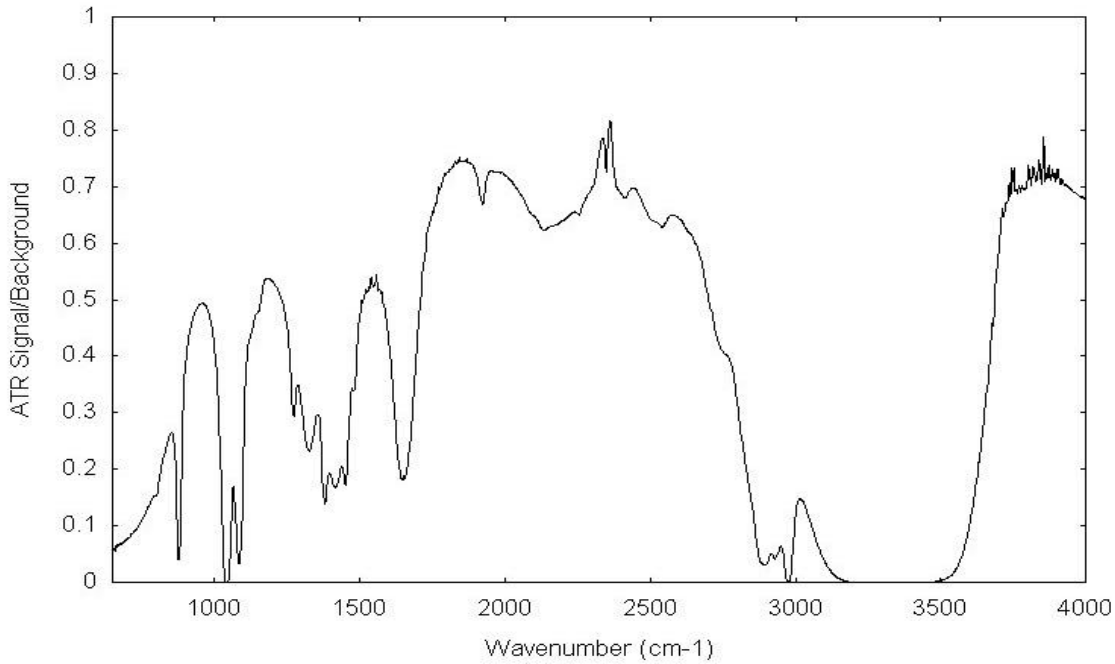

Figure5.7c Measured Liquid ATR spectrum for 75% ethyl alcohol-25% DI water

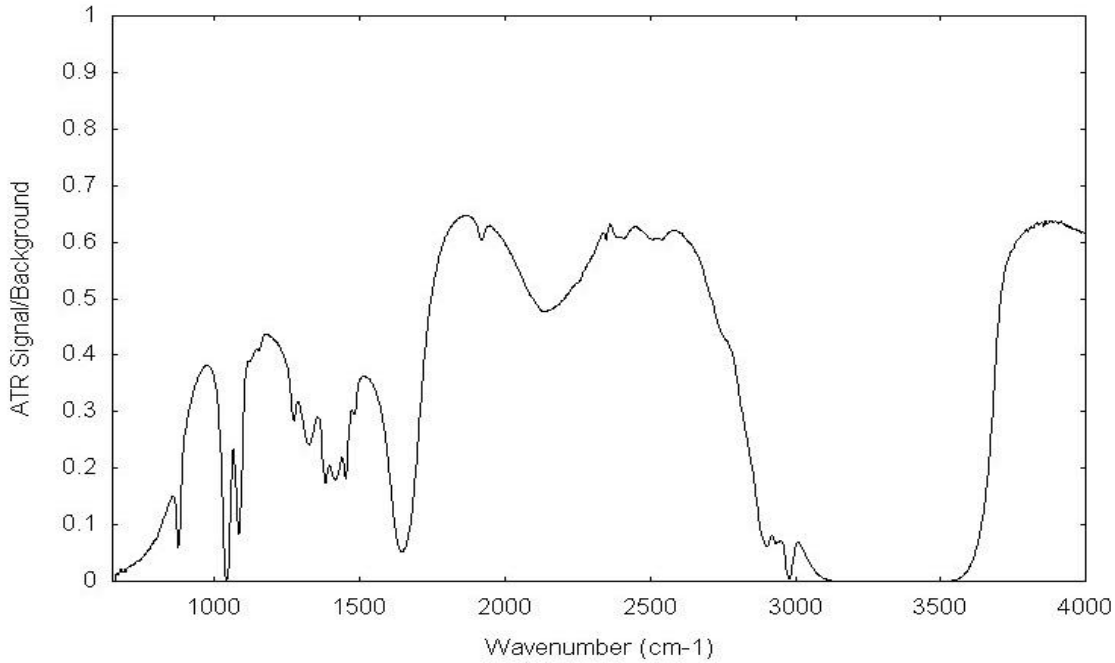

Figure5.7d Measured Liquid ATR spectrum for 50% ethyl alcohol-50% DI water

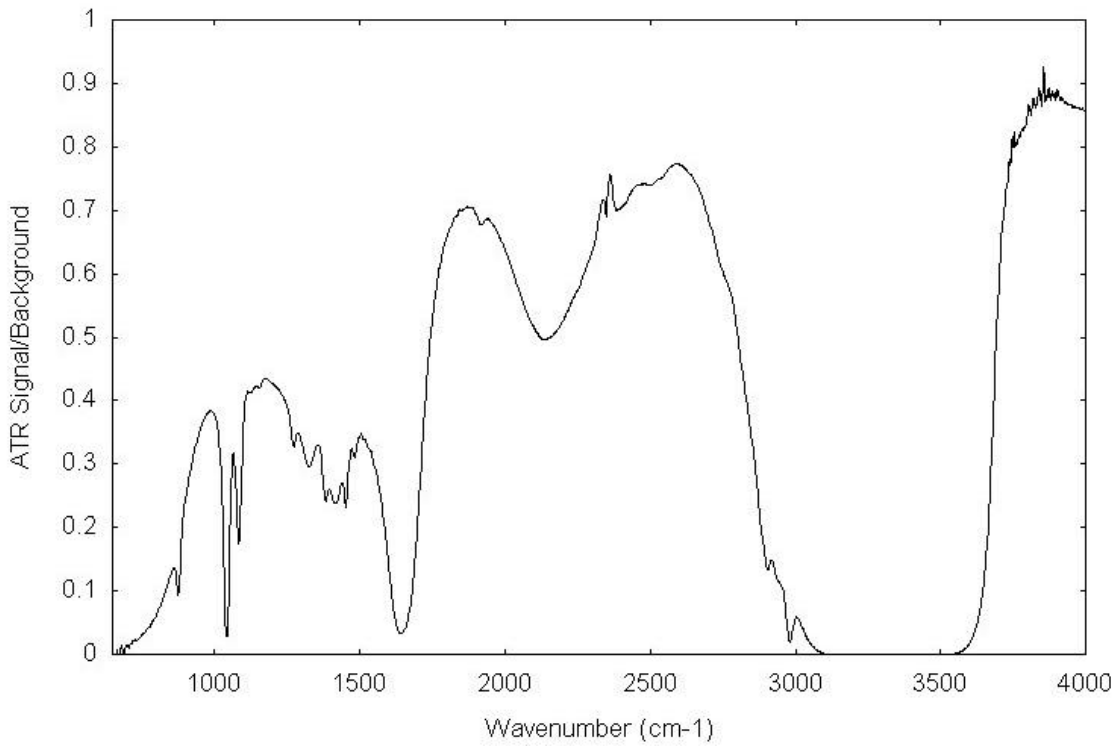

Figure5.7e Measured Liquid ATR spectrum for 25% ethyl alcohol-75% DI water

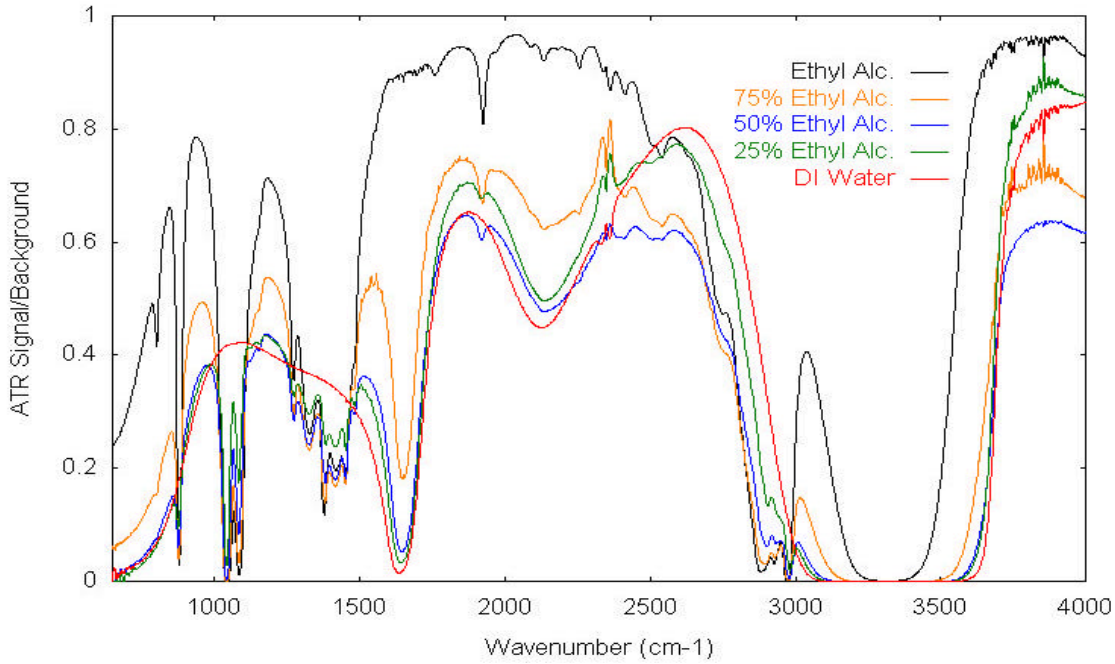

Figure5.8 Measured Liquid ATR spectrum for ethyl alcohol- DI water system

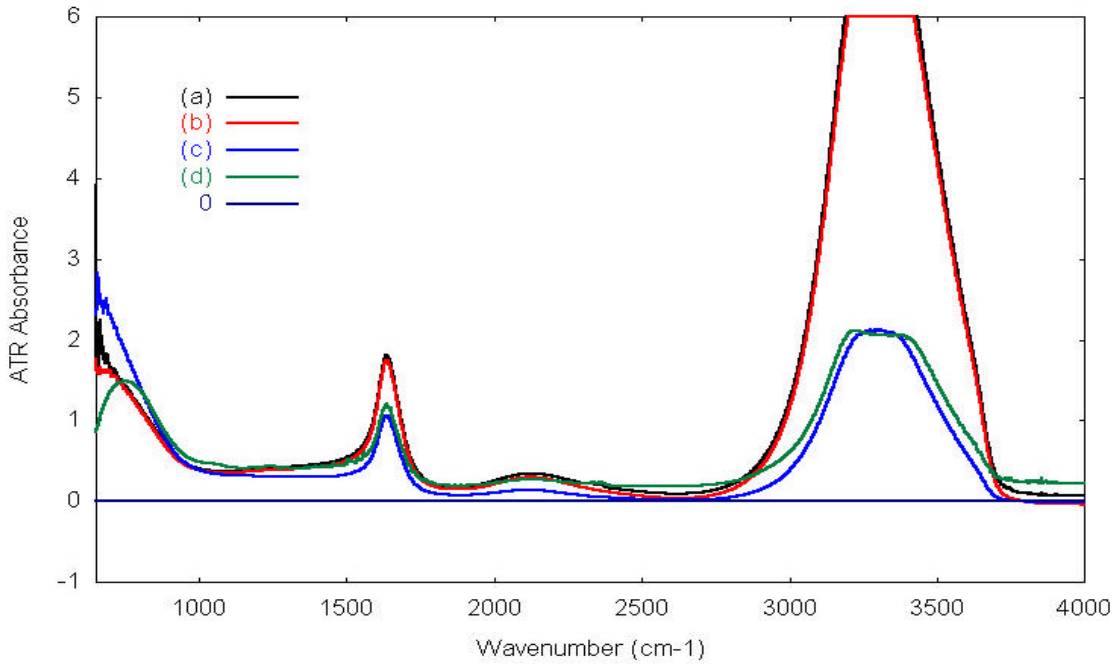

Figure 5.9a ATR spectra of water for various days plotted as Absorbance
(a) measured on the day the mixtures were measured; (b),(c) and (d) measured on different days.

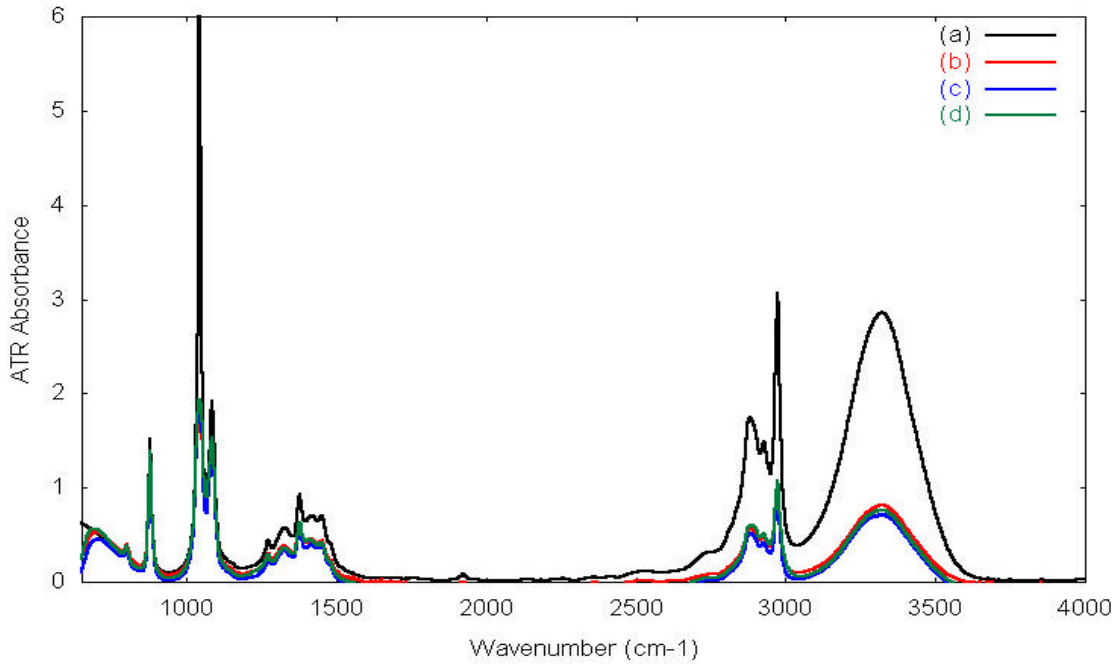

Figure 5.9b ATR spectra of ethyl alcohol for various days plotted as Absorbance. (a) measured on the day the mixtures were measured; (b),(c) and (d) measured on different days.

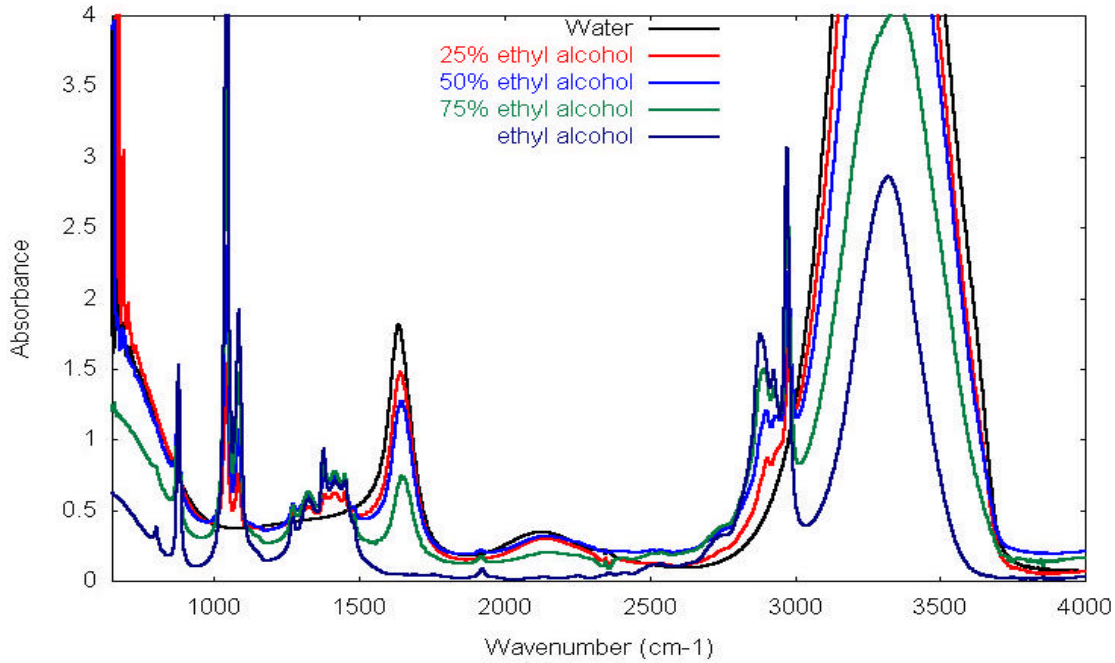

Figure 5.9c ATR spectra of Water -ethyl alcohol mixtures plotted as Absorbance.

Discussion of Results

Although a background spectrum was taken prior to measurements, it is believed that there were fluctuations in the measurements due to the FTIR system, external to chemical compositional changes. Additionally some of the signals had portions that were greater than the background signal, which is not theoretically possible. These suspicions were confirmed by the measurements of the pure chemicals over a range of days as shown in Figure 5.7a and b. Although a procedure was used to eliminate any background effects, it is thought that since the ATR liquid cell was removed from the FTIR spectrometer during the experiments that possible differences in the placement of the stage may have caused a change in the signal. The changes in the signals for both chemicals appeared to be just a multiplication of the other signals, though not in a strictly linear fashion. No resolution was found for this variation. The standard deviation of the measurements for both water and ethyl alcohol are shown in Figure 5.10.

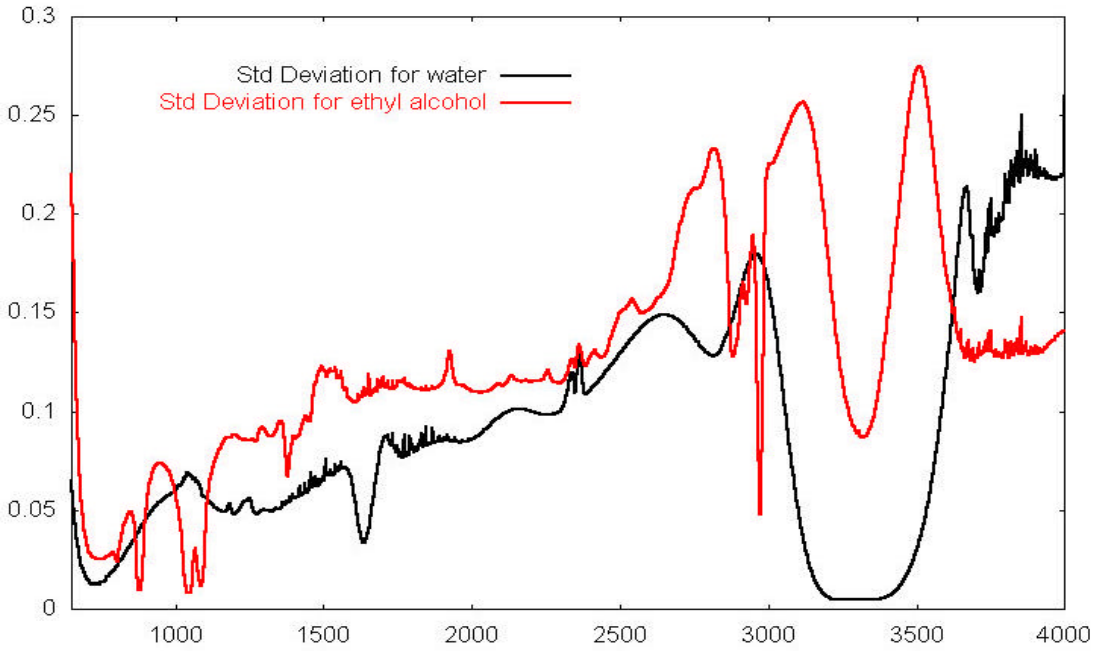

Figure 5.10 Standard deviation of measurements of water and ethyl alcohol.

The data set taken on a single day with carefully measured chemicals was used for the analysis, as they were found to be the most consistent and they had values that where close to unity in the spectral range near 4000 cm^{-1}. The region near 4000 cm^{-1} has no absorption bands and theoretically should be unity.

The plots in absorption vs. wavenumber show that although there are very visible differences in the amplitude of the signals, that the differences are just in the amplitude, and the overall shape and contours stay the same. Typically this is not a problem since these measurements have been historically used to identify the presence of a chemical and not quantify the amount present. The identification is made by matching the contours of the spectra to that of previously measured spectra. It is clearly visible that all of the spectra in Figures 5.9a and 5.9b are of the same chemicals, respectively. There may not be a driving force to deal with this problem because in the typical analysis there

isn't a need for absolute consistency of amplitudes of measurements, but only consistency of the relative amplitudes. This may partially explain the variation in the measurements.

Before the data was analyzed the spectra was baseline corrected. This was done by uniformly multiplying each spectrum until the signal in the 4000 cm^{-1} region was approximately unity. The resulting corrected spectra are shown in Figure 5.11a and b. A linear correction was made, even though the multiple measurements made of a single chemical did not scale linearly. Also shown in Figures 5.12 a through d, is absorbance vs. wavenumber for smaller spectral regions. The peaks in this region are typically analyzed by using Beer's Law.

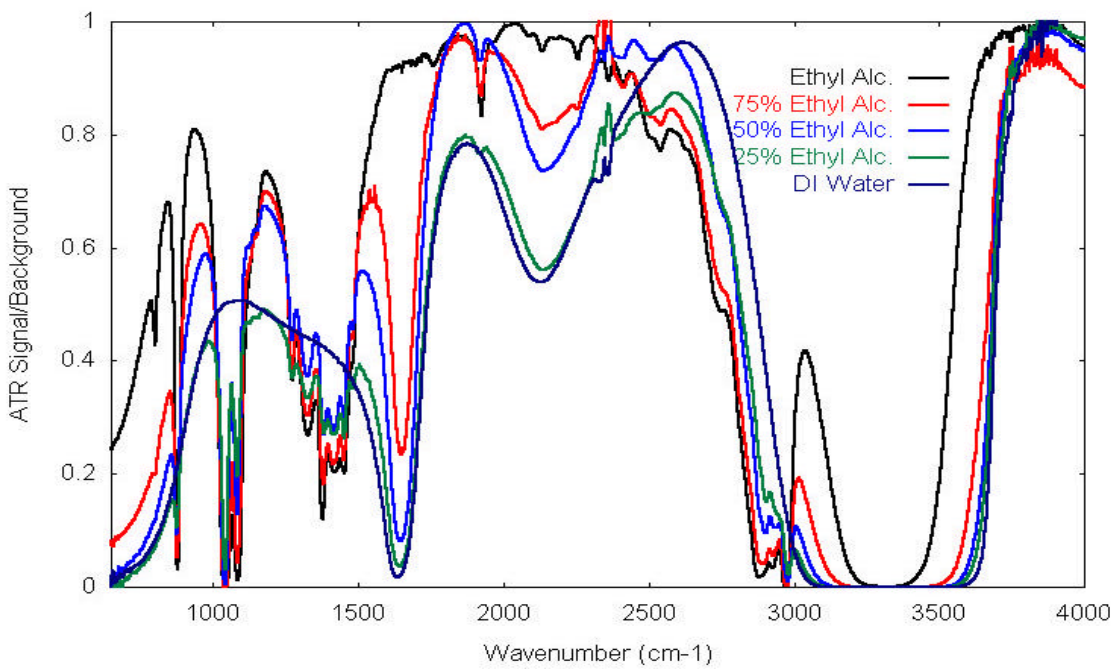

Figure 5.11a Baseline corrected spectra for ethyl alcohol –water system, plotted as Signal to background.

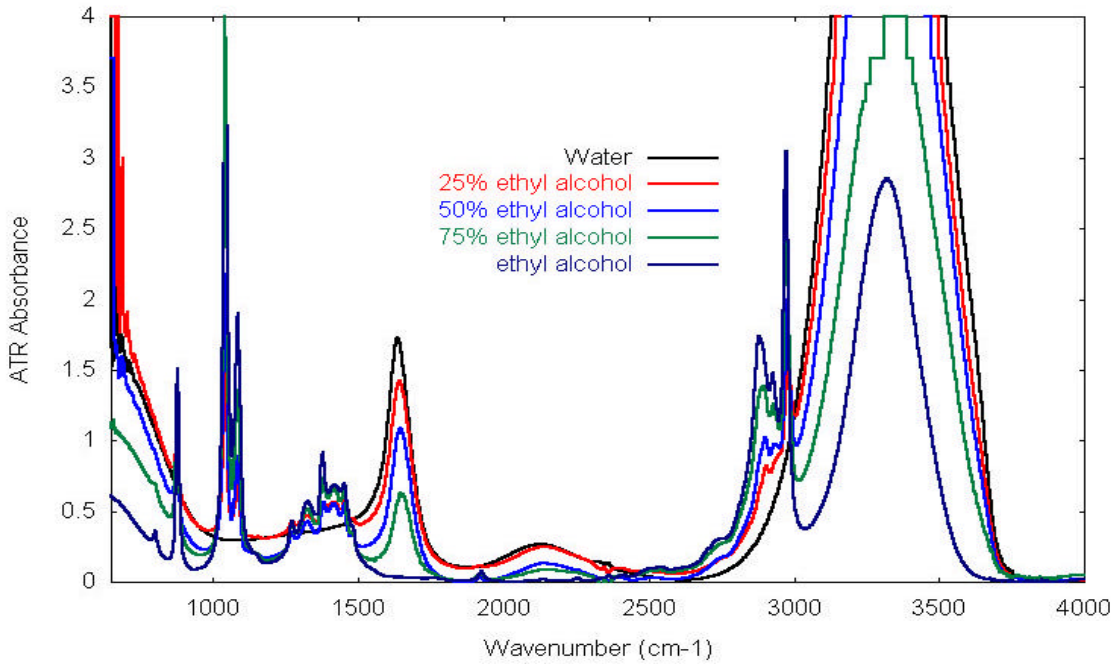

Figure 5.11b Baseline corrected spectra for ethyl alcohol –water system, plotted as ATR Absorbance.

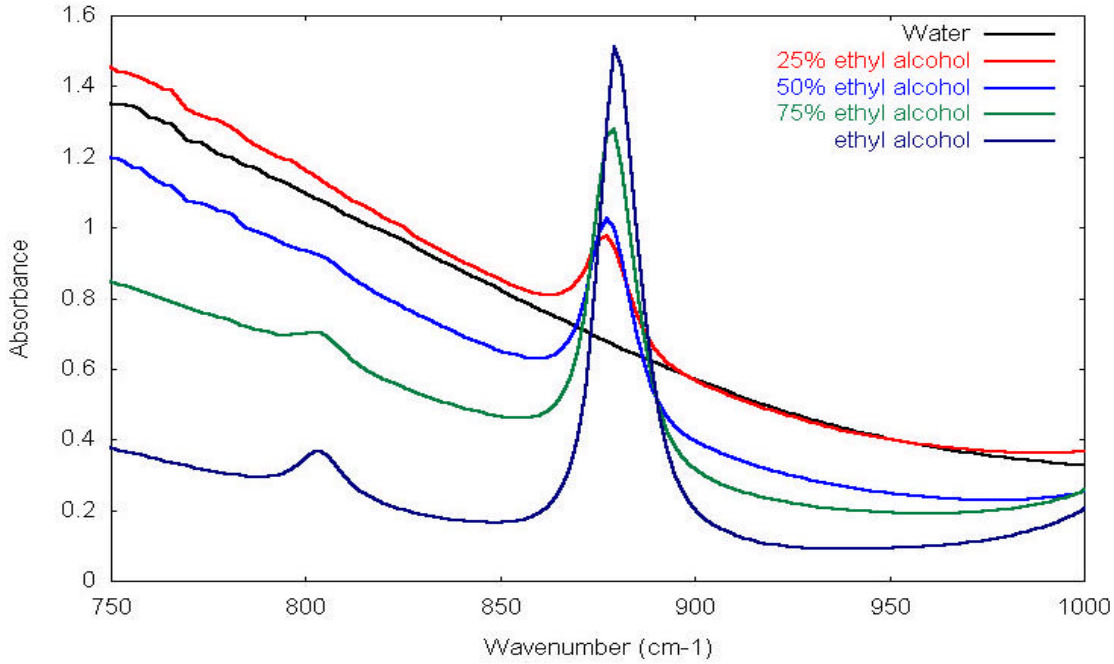

Figure 5.12a Baseline corrected spectra for ethyl alcohol –water system, plotted as ATR Absorbance for spectral region 750 to 1000 cm^{-1}.

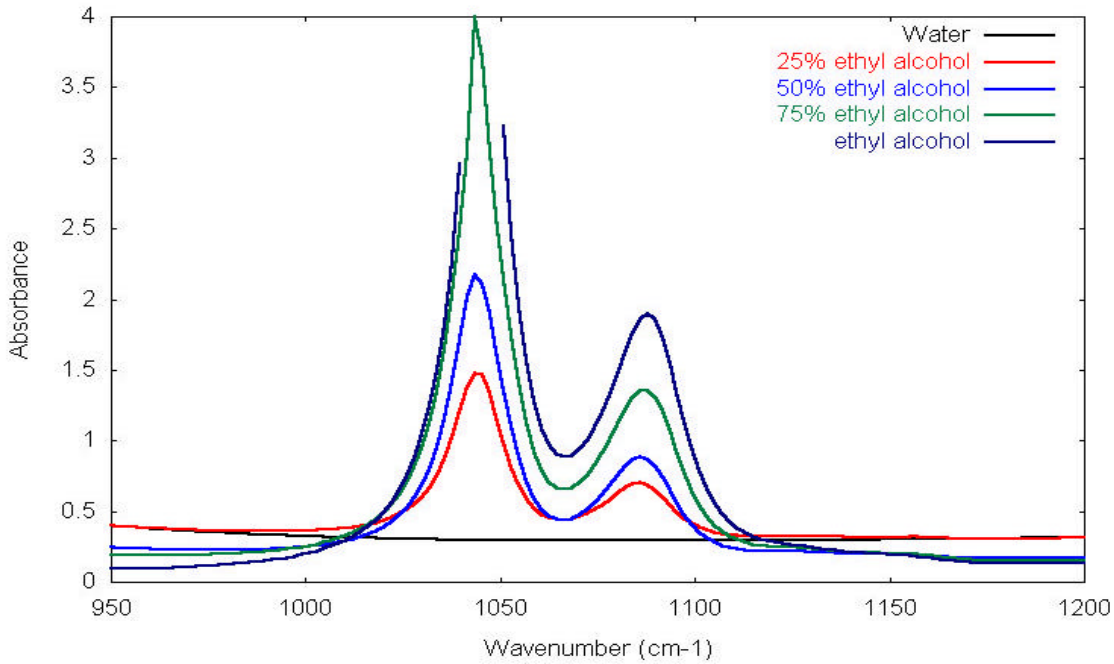

Figure 5.12b Baseline corrected spectra for ethyl alcohol –water system, plotted as ATR Absorbance for spectral region 950 to 1200 cm^{-1}.

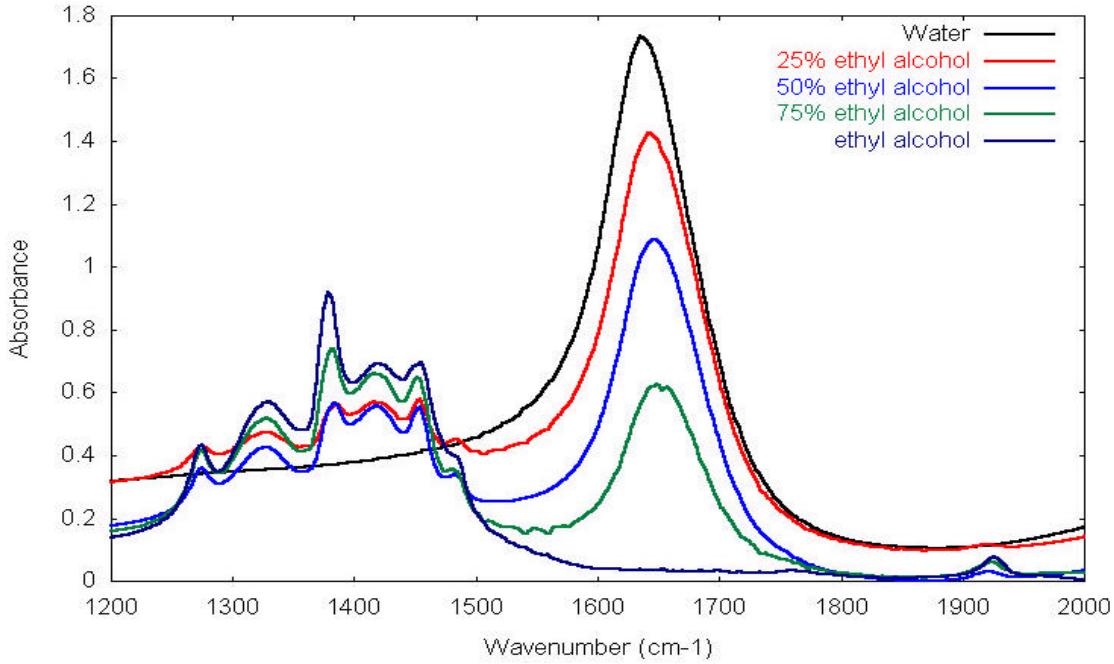

Figure 5.12c Baseline corrected spectra for ethyl alcohol –water system, plotted as ATR Absorbance for spectral region 1200 to 2000 cm^{-1}.

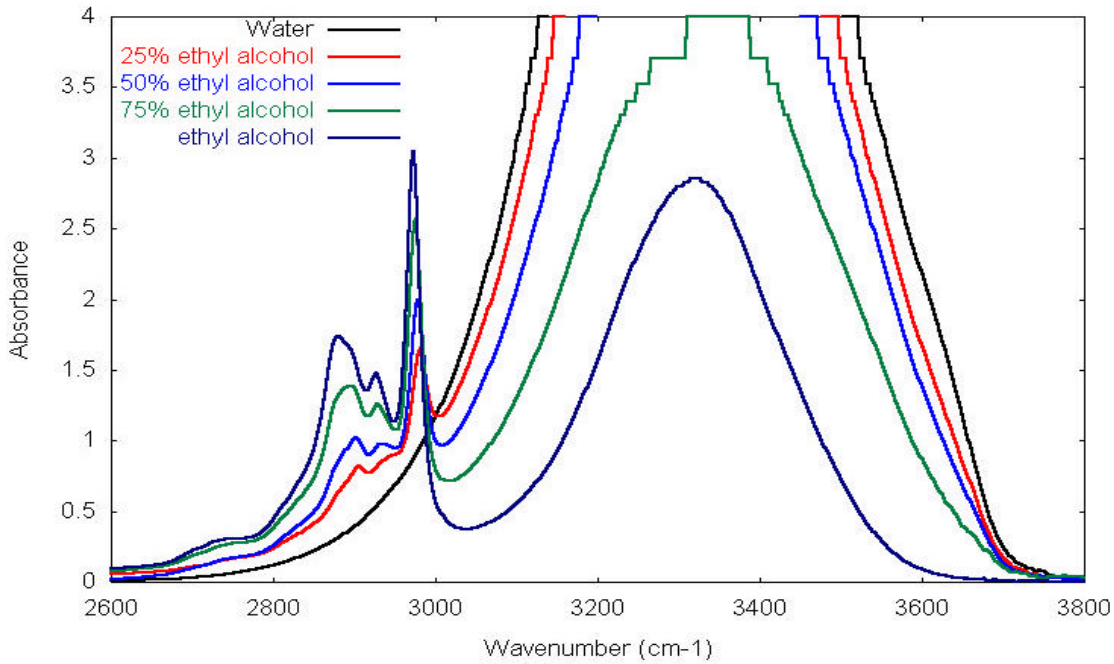

Figure 5.12d Baseline corrected spectra for ethyl alcohol –water system, plotted as ATR Absorbance for spectral region 2600 to 3800 cm^{-1}.

It is clearly visible from Figures 5.12 a through d, that the absorption peaks both change location with time and the ethyl alcohol and water peaks overlap. Even in cases where the spectral region of one chemical is relatively flat such as in Figure 5.12b or 5.12c, the overall effect on the absorbance is still influenced by the chemical with the flat absorbance. The absorbance of water in Figure 5.12 b is approximately .4 across this region, where the ethyl alcohol has a base of approximately .1 with two peaks. As the concentration of ethyl alcohol increases the peaks increase and shift, but the baseline decreases due to the loss of water's contribution. Similar effects are shown in Figure 5.12c and d, where the peaks merge into each other. With more than two chemicals the complexities will increase.

Analysis by GDA

The baseline corrected water and ethyl alcohol spectra were fit with Gaussian Dispersion Analysis using Equations 32 through 34 for the modeling the dielectric function, and Equation 44, for the liquid ATR cell. The resultant fits for water and ethyl alcohol are shown in Figures 5.13 a and b.

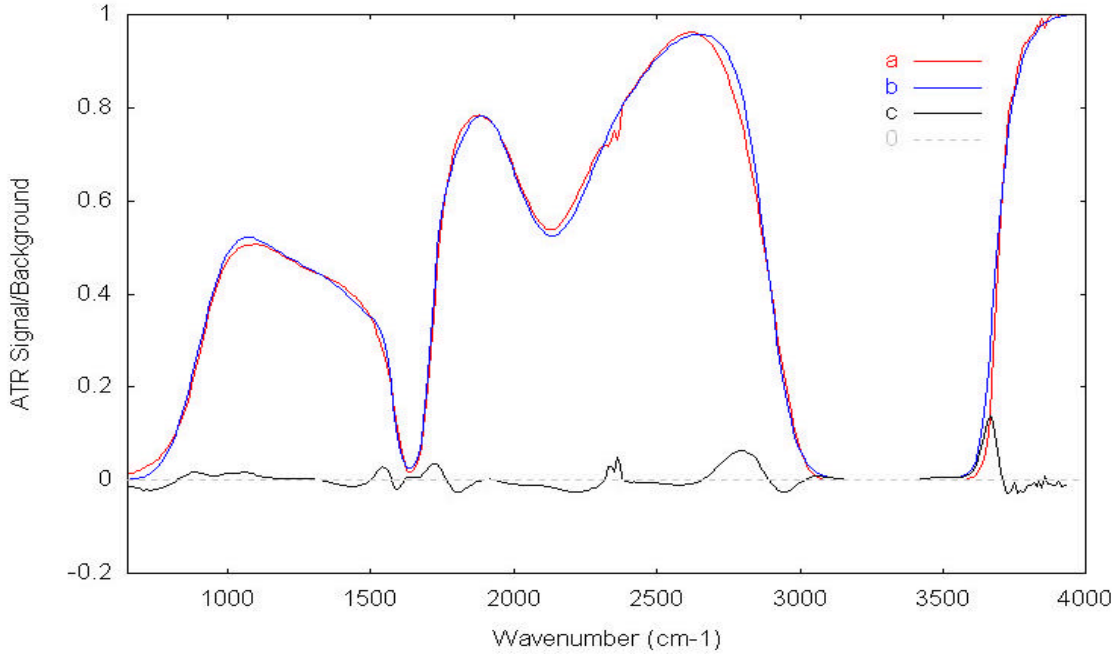

Figure 5.13a ATR water spectra fit with Gaussian dispersion analysis.
(a) Baseline corrected water spectrum; (b) Calculated spectrum; (c) Difference between (a) and (b); (0) Zero line for reference.

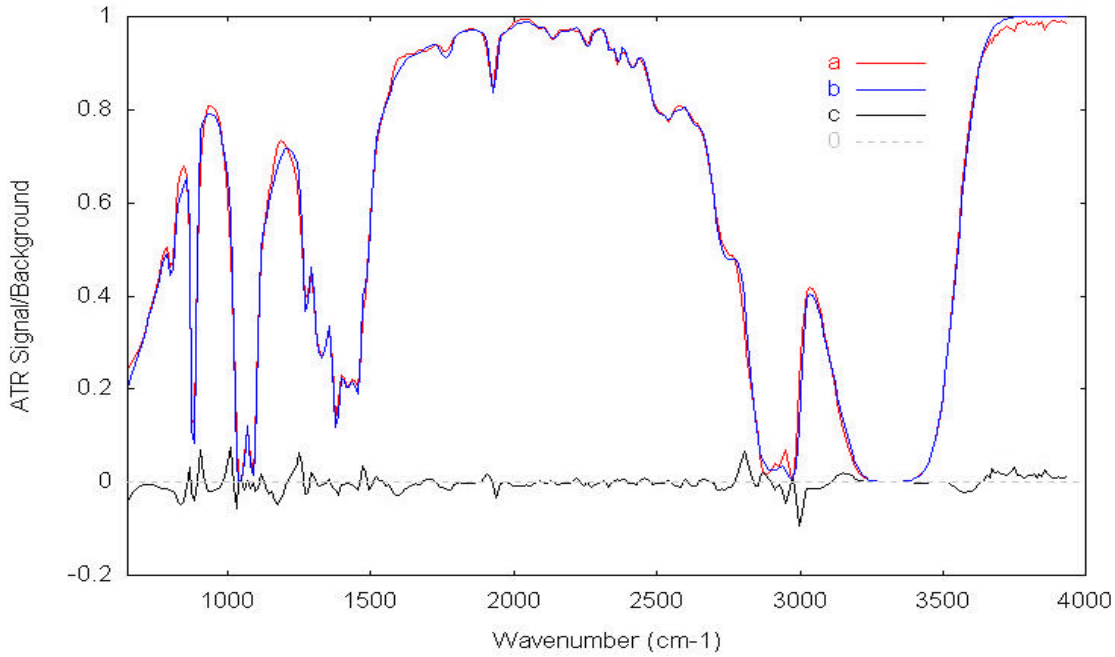

Figure 5.13b ATR ethyl alcohol spectra fit with Gaussian dispersion analysis. (a) Baseline corrected ethyl alcohol spectrum; (b) Calculated spectrum; (c) Difference between (a) and (b); (0) Zero line for reference.

The fit to the signal to background of both water and ethyl alcohol are very close. The dielectric function of water used to calculate the spectrum in Figure 5.13a is shown in Figure 5.14a compared to a published spectrum from Querry[43].

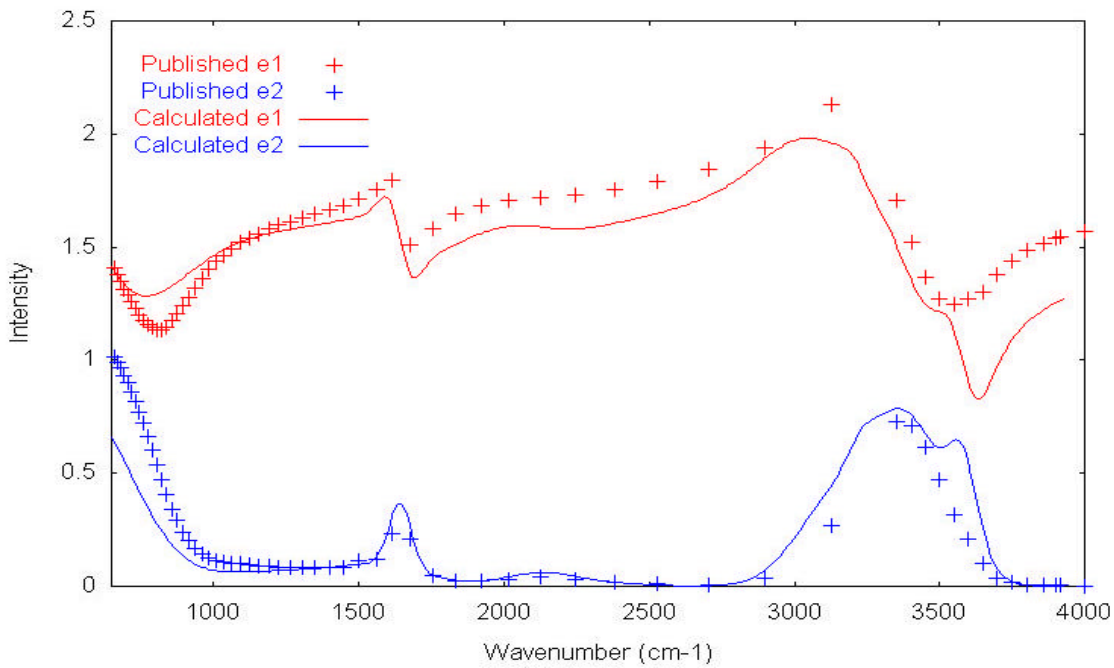

Figure 5.14a Comparison of published and calculated real (e1) and imaginary (e2) dielectric functions of Water.

The dielectric function calculated to fit ethyl alcohol is shown in Figure 5.14b. The calculated dielectric function for water in Figure 5.14a, matches fairly well with the published data. The exceptions being an additional peak in the fitting dielectric function in the 3600 cm^{-1} region and the low wavenumber region near the 650 cm^{-1} edge. The additional peak in the 3600 cm^{-1} region may be due to some impurity in the measured water, while the differences in the low wavenumber region may be due to the low through put of the FTIR system at those frequencies. Additionally, there is some doubt as to the accuracy of the measured spectra and published values. The expected response from the published values of dielectric is shown in Figure 5.15. The predicted spectrum, based upon the published values of the optical properties, of water falls in between many of the measured spectra.

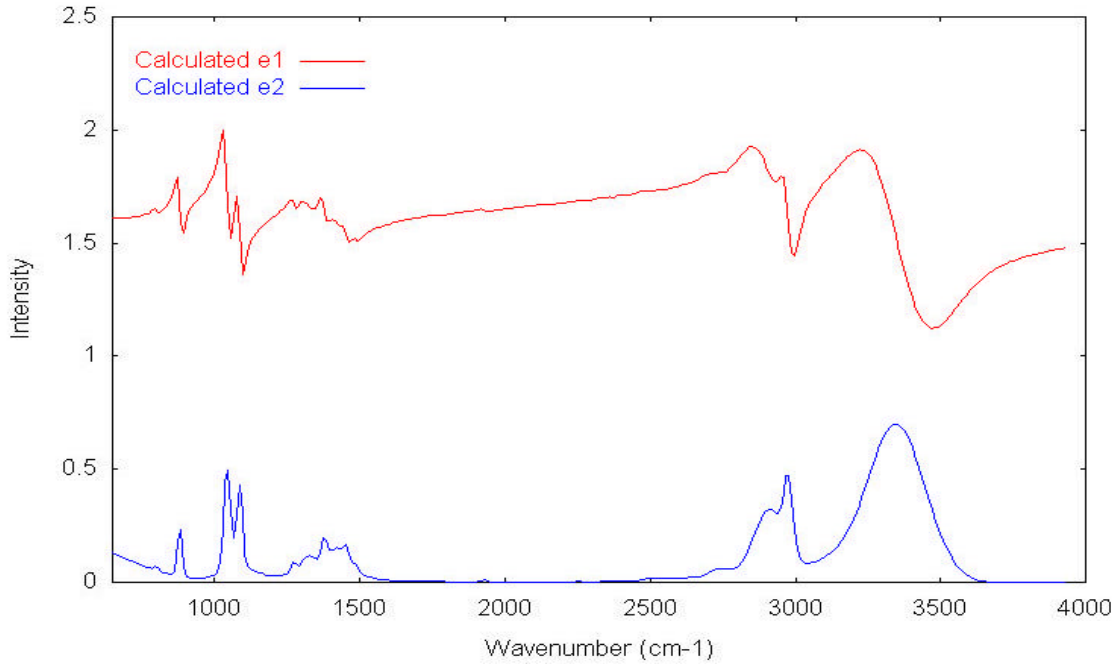

Figure 5.14b Calculated real (e1) and imaginary (e2) dielectric functions for ethyl alcohol.

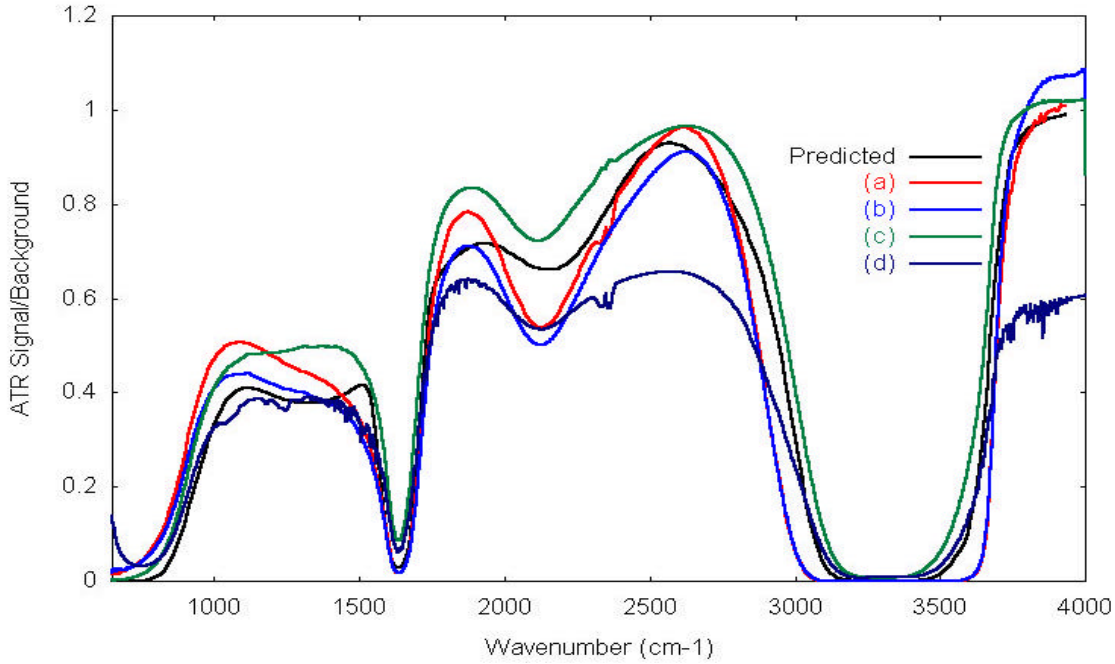

Figure 5.15 Predicted optical response for water in ATR cell with measured spectra a, b, c, d.

The calculated dielectric functions for water and ethyl alcohol were combined in proportion to the chemical compositions measured; 25%, 50% and 75% ethyl alcohol. The resulting calculated dielectric functions were used to calculate the expected liquid ATR signal for each chemical mixture. Figure 5.16-a,b and c compare the calculated ATR response with the measured. Additionally, due to the uncertainty of the measured spectra, and consequently the accuracy of the calculated dielectric functions, a second set of dielectric functions were calculated for the mixed chemicals using the published data for the optical properties of water. No published values are available for ethyl alcohol. A direct fit of the published values was used in order to develop a function that could interpolate data in between the published points. The results are shown in Figures 5.17 a, b. c.

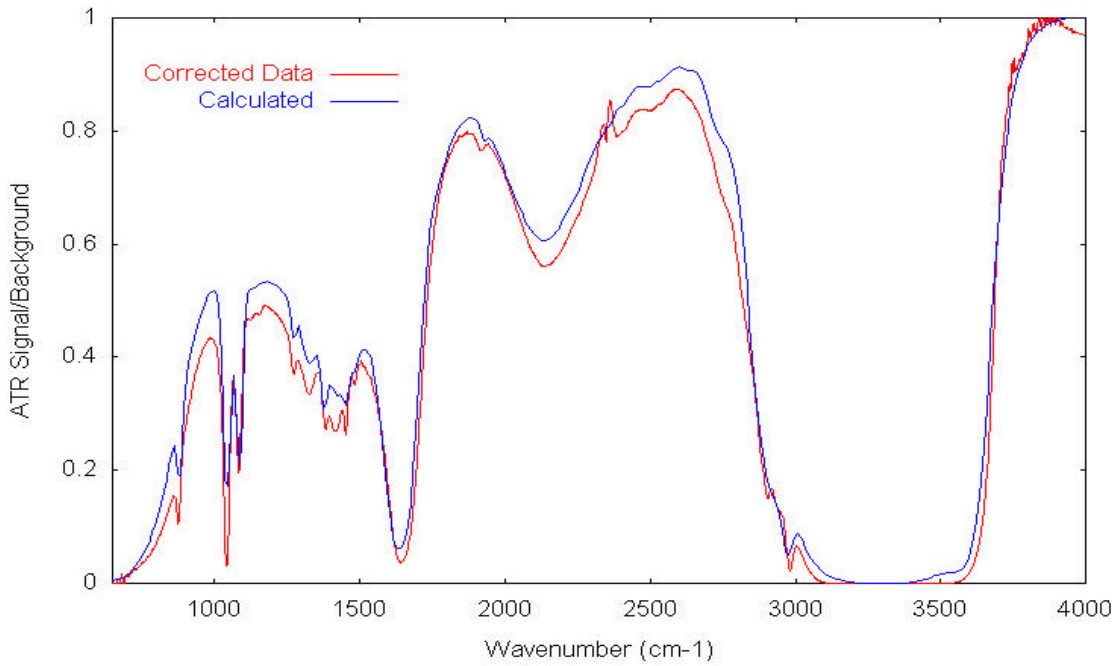

Figure 5.16a Calculated and corrected measured ATR spectra for 25% ethyl alcohol using dielectric function obtained through dispersion analysis.

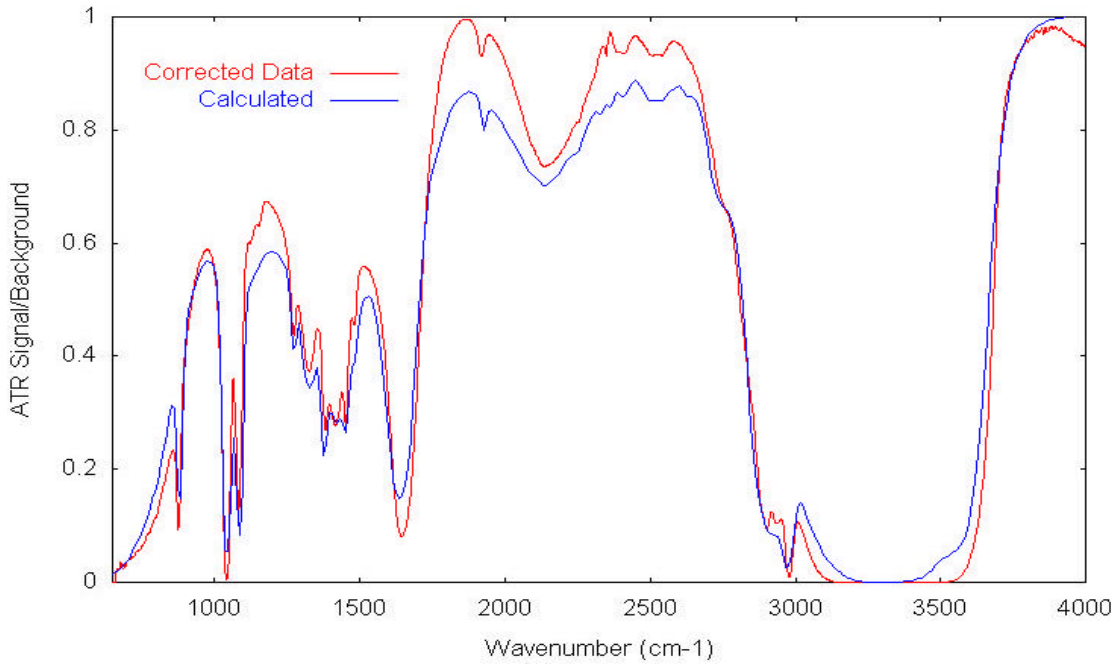

Figure 5.16b Calculated and corrected measured ATR spectra for 50% ethyl alcohol using dielectric function obtained through dispersion analysis.

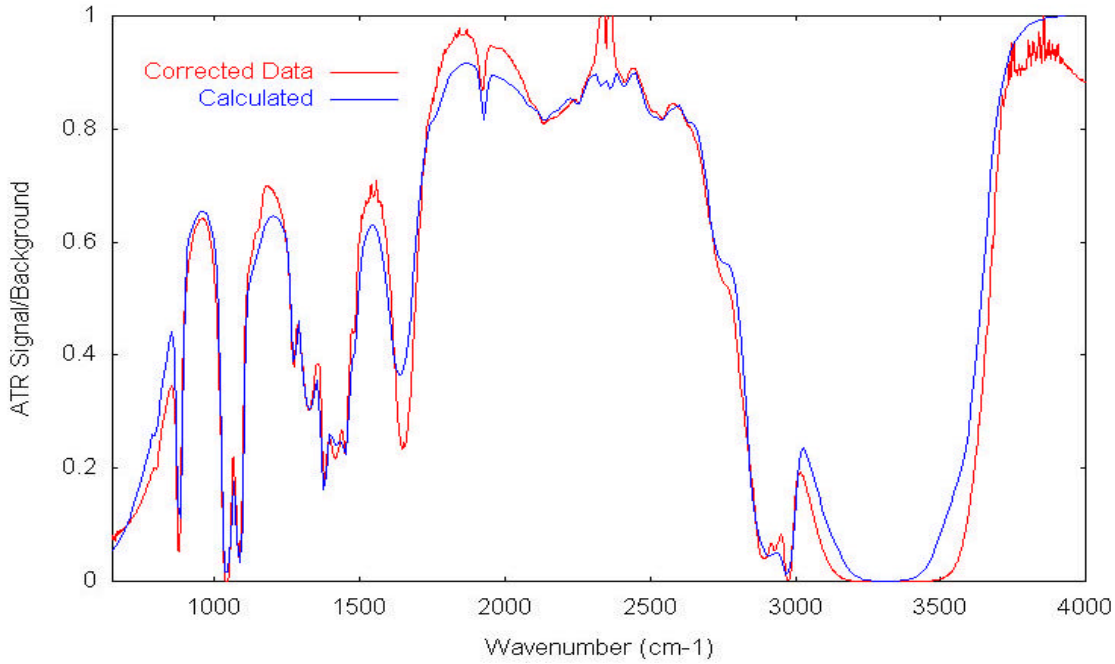

Figure 5.16c Calculated and corrected measured ATR spectra for 75% ethyl alcohol using dielectric function obtained through dispersion analysis.

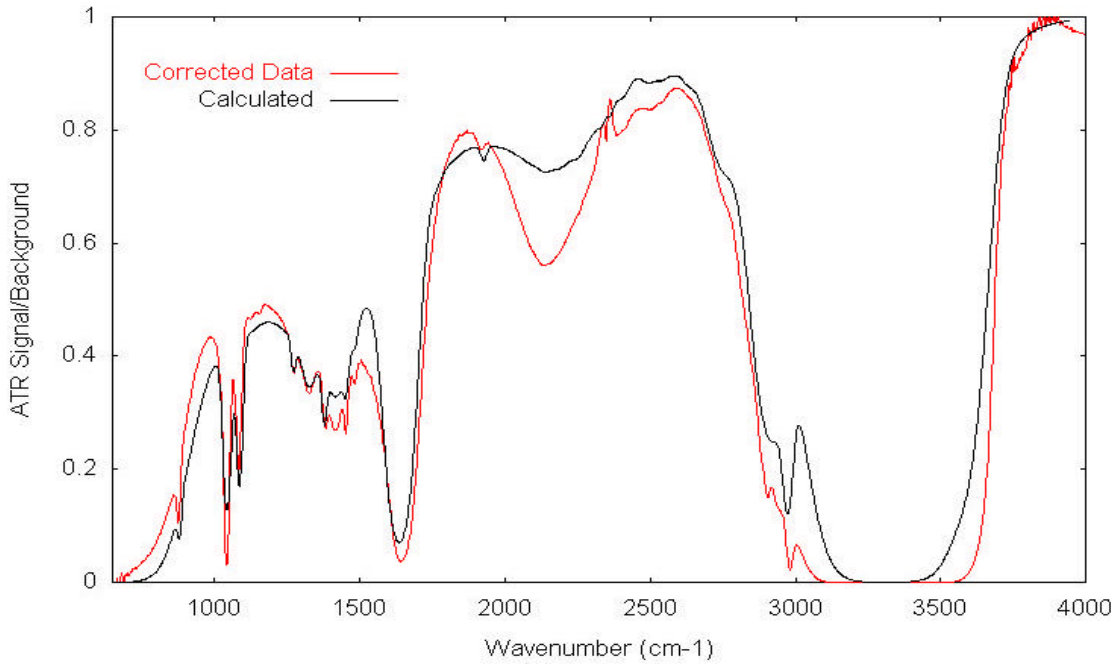

Figure 5.17a Calculated and corrected measured ATR spectra for 25% ethyl alcohol using a dielectric function obtained through dispersion analysis for ethyl alcohol and from published data for water

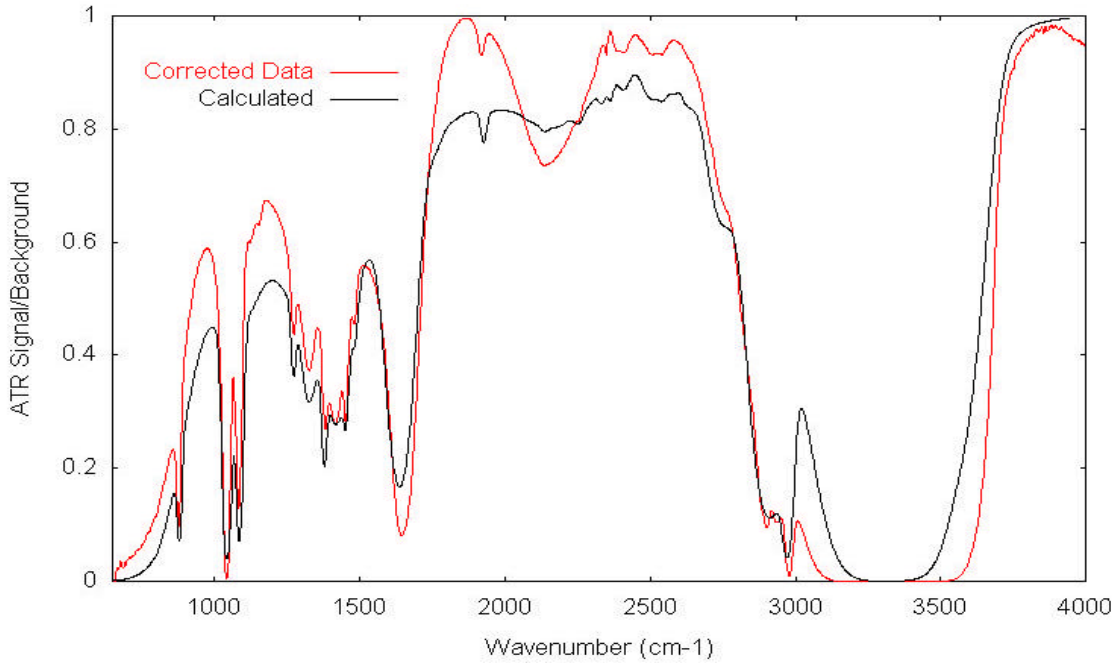

Figure 5.17 b Calculated and corrected measured ATR spectra for 50% ethyl alcohol using a dielectric function obtained through dispersion analysis for ethyl alcohol and from published data for water.

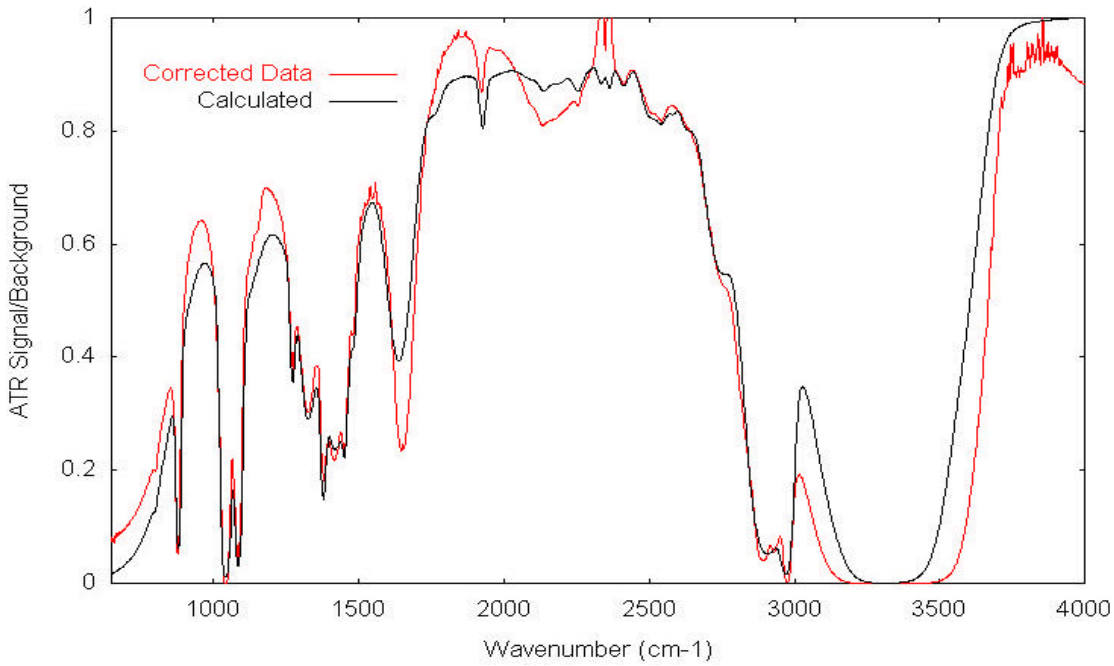

Figure 5.17c Calculated and corrected measured ATR spectra for 75% ethyl alcohol using a dielectric function obtained through dispersion analysis for ethyl alcohol and from published data for water.

A visual inspection determined that the calculated dielectric function yielded a better correlation with the measured data than did the published dielectric properties. Figure 5.18 shows the ATR absorbance in the spectral range from 2600 to 3800 cm^{-1}, for all of the calculated spectra using dielectric functions obtained by Gaussian dispersion

analysis. This region is shown due to its larger sensitivity. The calculated spectra peaks clearly shift, and in the same direction as that of the measured spectra.

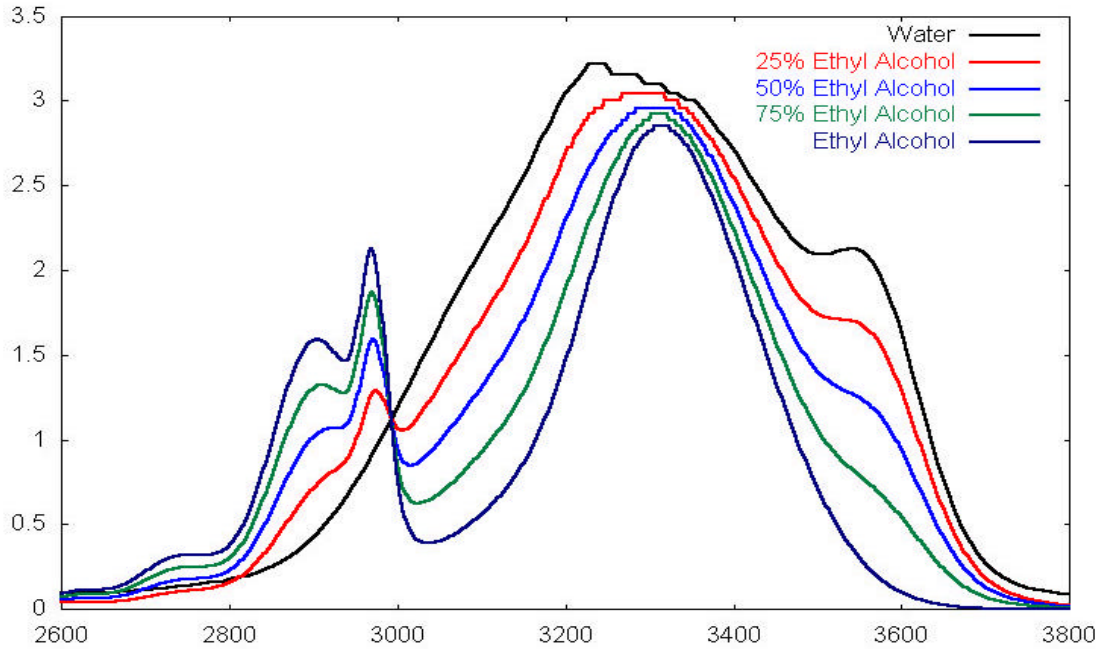

Figure 5.18 Calculated ATR spectra, spectral range 2600 to 3800 cm^{-1}, for ethyl alcohol – water system using a dielectric function obtained through dispersion analysis

Estimation of error

For both sets of calculated spectra, the calculated spectra follow the contours of the measured spectra very well, but the errors involved in these calculations are large. Due to problems with the ATR liquid cell's repeatability, the spectra for both water and ethyl alcohol are uncertain and the standard deviations large. The uncertainty of the initial data is coupled with errors due to fitting of spectra, potential errors in the Equation 44. No numerical value is put onto the error.

The error associated with the dielectric function of ethyl alcohol is unknown, as there is no published data to compare the calculated value with. Furthermore, historically, the published dielectric function of water has had many changes and updates.

The published spectrum presented here was based upon a Kramers-Kronig analysis of $\alpha(\omega)$ measured from 500 cm^{-1} to 8000 cm^{-1}[43]. The values near the edge of the spectra may have errors introduced to the Kramers-Kronig analysis. Though the predicted spectrum is calculated and compared with the measured spectrum, it is impossible to determine which is accurate and where the error is introduced. With out accurately known optical properties for a pure chemical, the error of Equation 44 cannot be determined.

Conclusions and Future Work

The spectra calculated from the dielectric functions determined by dispersion analysis of the spectra of ethyl alcohol and de-ionized water fit reasonable well with the measured spectra in a qualitative sense. Due to the large uncertainty of the measured spectra, this method of analysis would be no better in quantifying an unknown chemical solution than other analysis. With improvements in the measurements, this technique has the potential for accurately determining the concentrations of simple solutions, by simply varying the mixing value of the dielectric functions of the components. For systems with unknown chemicals, dispersion analysis could be employed to fill in regions of the spectra unaccounted for by the known components.

The widespread use of quasi-absorbance, as calculated from ATR type measurement, and absorbance from transmission as the final parameters to describe a material is a hindrance to quantitative optical analysis. The literature is pervasive with inaccurate data and analysis, which compounds the effort. Determining the dielectric function is critical in the quantitative evaluation of chemical systems by optical means and the reduction of consistent optical spectra to their dielectric functions is needed.

CHAPTER 6
OPTICAL PROPERTIES OF $Te_2As_3Se_5$

Introduction

Chapter 7 involves the use of an infrared transmitting fiber optic probe and calculations of predicted optical signals for different chemical mixtures. The material of the probe is glass with $Te_2As_3Se_5$ as its composition. This glass's optical properties have been previously measured, and it was thought that its refractive index was close to 2.6 [47]. In order to perform modeling calculations of the fiber's response it is necessary to know the optical properties as a function of wavelength. In this chapter, experiments and calculations were performed to determine the optical properties of the $Te_2As_3Se_5$ glass over the range used for the experiments in Chapter 7.

Experiment

The $Te_2As_3Se_5$ glass samples were prepared by members of the Lucas research group in the Laboratoire des Verres et Céramiques, University of Rennes, Rennes France. The glass fabrication method is described in detail in reference [48]. The samples tested were 1cm diameter disks of about 2.5 mm thick with parallel faces. The samples had been polished to an apparent optical finish by the French researchers.

An infrared transmission spectrum was previously recorded on two glass sample by members of the Lucas group with a standard FTIR spectrometer in the range from 400 cm^{-1} to 5000 cm^{-1}. In addition, FTIR near normal reflectance and transmission spectra were recorded, at the University of Florida in Gainesville, for the spectral range from 400

cm^{-1} to 4000 cm^{-1}. Measurements were also made with an Atomic Force Microscope (AFM) in tapping mode on one sample in order to determine the surface roughness.

Results

Figure 6.1 shows the transmission of all the samples, recorded both in Rennes and Gainesville. Figure 6.2 shows the reflectance of the samples measured in Gainesville. The results from the AFM measurement and its automated analysis are shown in Figure 6.3.

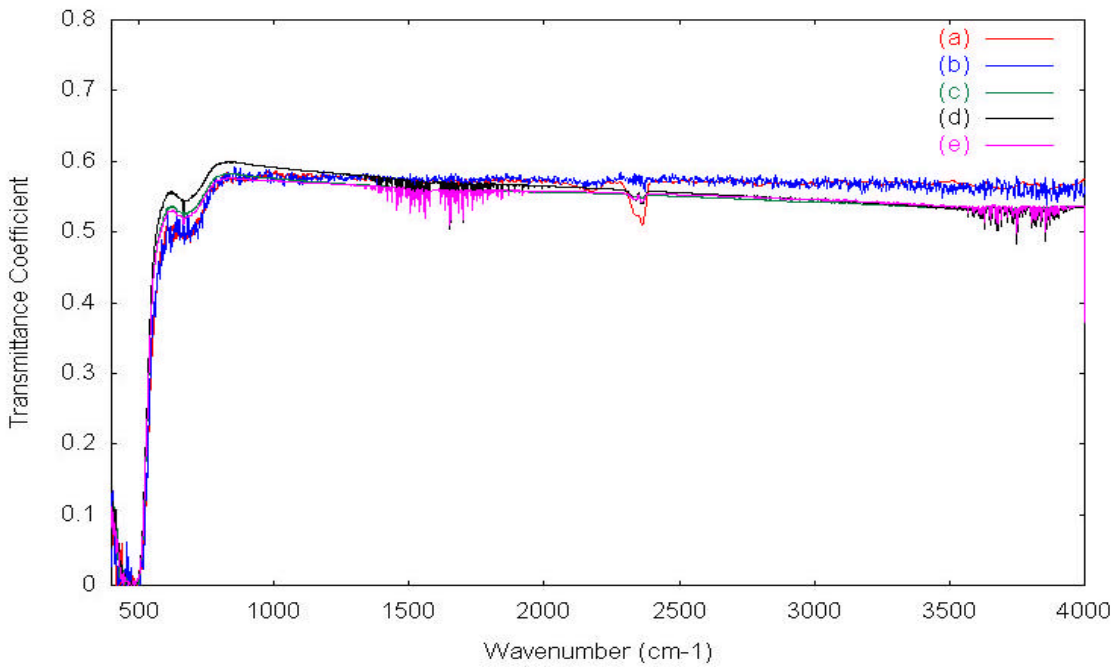

Figure 6.1 Infrared Transmission spectra of $Te_2AS_3Se_5$. (a) and (b) measured by researchers in Rennes France, (c), (d), and (e) measured in Gainesville Florida.

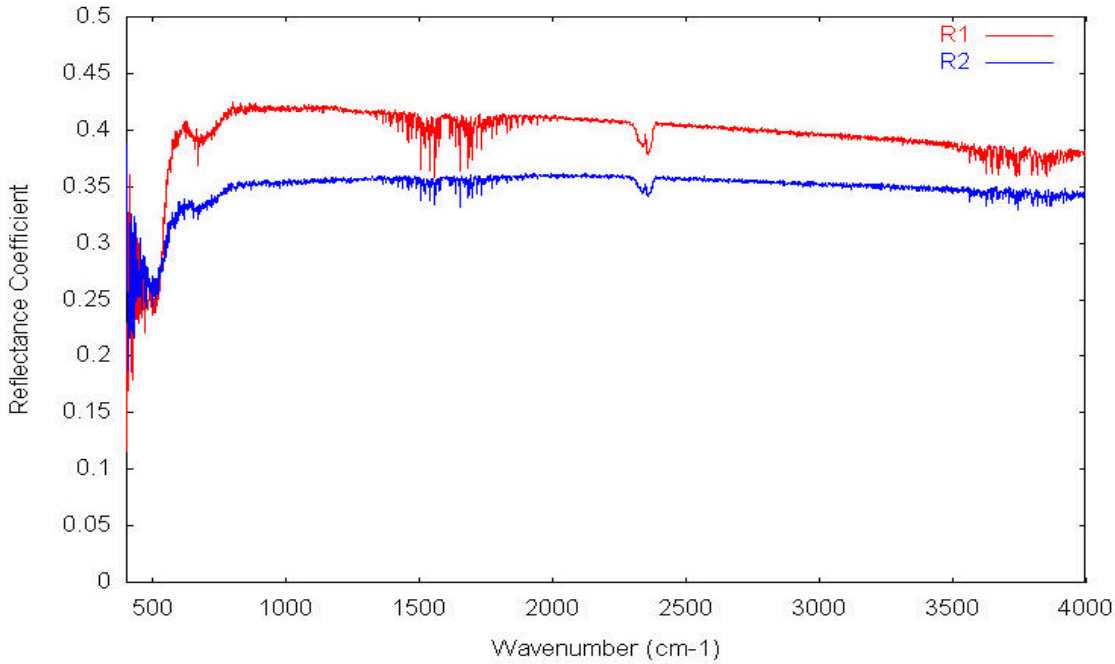

Figure 6.2 Infrared Reflection spectra of $Te_2AS_3Se_5$.

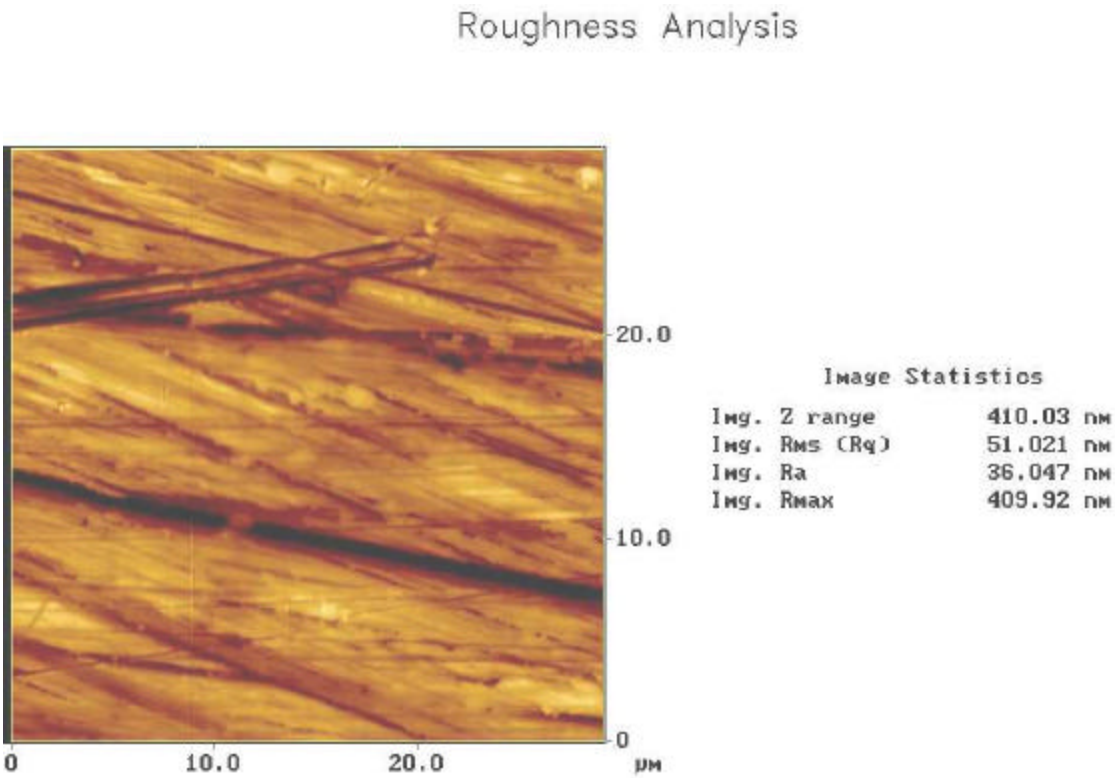

Figure 6.3 AFM image and Roughness Analysis of $Te_2As_3Se_5$

Discussion of Results and Analysis

As shown in Figures 6.1 and 6.2, the transmission and reflectance spectra are nearly flat for the spectral region from 700 to 4000 cm^{-1}. The exception is the double peak loss near 2300 cm^{-1}. These peaks are from the absorbance of CO_2 in the atmosphere. Background spectra are used to eliminate effects such as these, but in many infrared measurements CO_2 effects are pervasive, and ignored. The flat region is indicative of a non-absorbing region, and it is expected that the index of refraction would only have a real component. Referencing back to Equations 4-7 from Chapter 2 for transmission taking into account multiple reflections and assuming that α is zero, Equations 4 and 5 reduces to

$$T_{total}(w,x) = \frac{(1-R(w))^2}{1-R(w)^2} \tag{47}$$

with

$$R(w) = \left(\frac{(n-1)}{(n+1)}\right)^2 . \tag{48}$$

This results in only one dependent variable. The measured transmission is approximately 57.5 % of the background beam. Using Equations 47 and 48 and the value of .575 for T, the calculated index of refraction is 3.16. This is much higher than the previously reported value of 2.6. The expected transmission coefficient for a material with an index of 2.6 would be 67%.

Gaussian dispersion analysis was used to fit the transmission curves over the entire region from 400 to 4000 cm^{-1}. The measurements made in France were used, as

the measurements made in Gainesville have a slight slope in the flat region. It was thought that perhaps the surface roughness of the samples measured in Florida and the resulting scattering reduced the transmission. The AFM measurements show that the surface roughness is approximately 51 nm. The theoretical result of a 51 nm rms roughness for single surface reflection would be as follows:

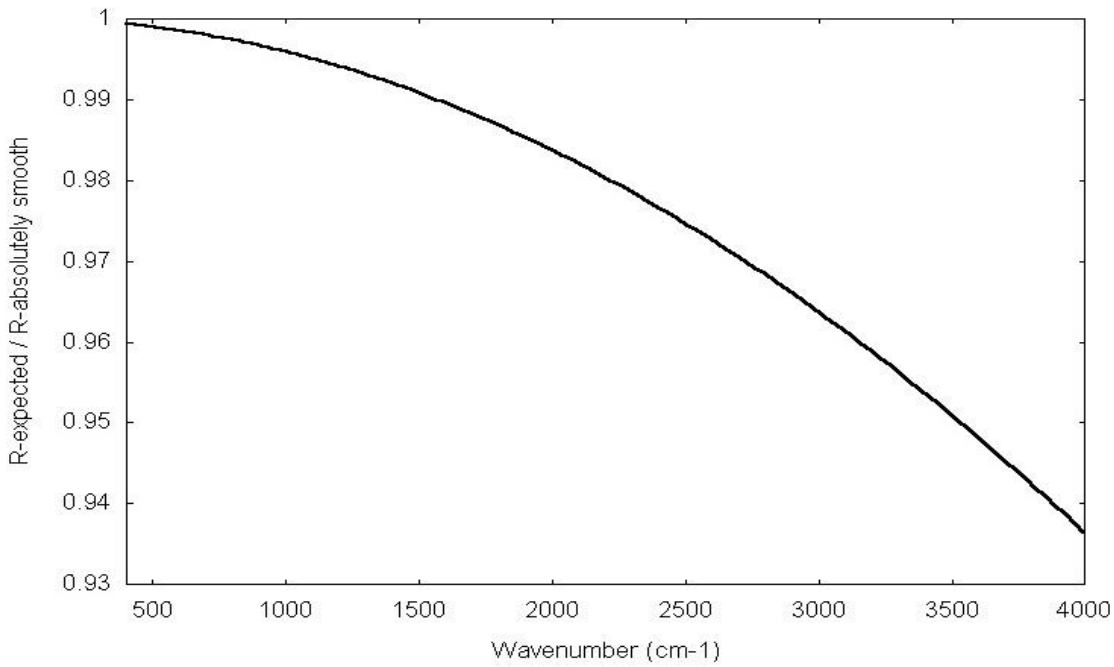

Figure 6.4 Expected response of single surface reflectivity for a rms roughness value of 51nm in the spectral range from 400 cm^{-1} to 4000 cm^{-1}.

The expected loss due to scattering is about a maximum of 6.5% for a single surface reflection at 4000 cm^{-1}. The difference in the measured transmission spectra is from about 57.5% transmission for the glasses previously measured in France to 53% transmission for the glasses measured in Florida, or about an 8% difference. The 6.5% difference is for a single surface reflection and the transmission measured has multiple reflections. There is no equation for surface effects for transmission, but the reduction in signal for the samples in Florida could very well be due to surface scattering. In order to

account for the scattering due to multiple reflections the equations for multiple reflections were re-derived and expanded to take into consideration the losses upon reflection and transmission.

$$T_{total}(w,x) = \frac{(1-r(w))^2 t(w)^2 \exp(-a(w)x)}{1-(r(w)\exp(-a(w)x)l(w))^2} \tag{49}$$

and

$$R(w) = r(w)l(w)(1+T_{total}(w,x)\exp(-a(w)x)) \tag{50}$$

with r(w) the single surface reflection, l(w) the percentage of light coherently reflected from the surface, and t(w) the percentage of light transmitted coherently.

Table 6.1 shows the parameters used to fit the transmission of the glasses measured in France. Figure 6.5 shows the measured transmission with calculated transmission and the calculated index of refraction. No losses due to scattering were considered as the surface roughness of those samples was unknown, but believed to be low.

Table 6.1 Parameters used to fit transmission and reflectivity of $Te_2As_3Se_5$

Peak Position (Wavenumber)	Peak Amplitude	Peak Width
450	1.5	50
670	0.035	70
930	0.00057	90
1900	0.00055	80
2060	0.0003	50
2180	0.0017	40

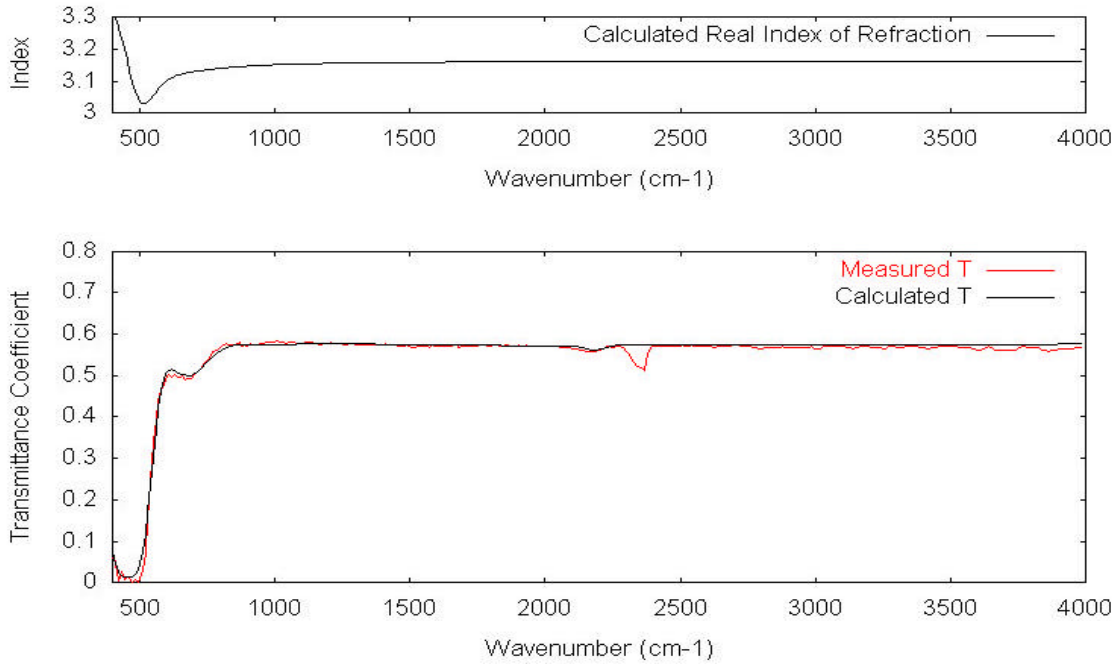

Figure 6.5 Measured FTIR transmission and calculated transmission for $Te_2As_3Se_5$ glass.

The fit of the transmission spectra by the calculated spectra is excellent. The CO_2 peak is ignored. The peaks located in the 2000 cm-1 region are due to Se-H bonds. Hydrogen contamination of these glasses is typical.

The parameters in Table 6.1 were also used to calculate the expected reflectivity shown in Figure 6.6a. Again scattering due to surface roughness was thought to be present. The highest measured reflectivity is plotted with the calculated reflectivity. A value of 51 nm of rms surface roughness was used in the calculation. Both scattering loss values in Equations 50 were assumed to be the same and Equation 40 from Chapter 4 was used to calculate this loss factor. The transmission loss coefficient is estimated to be equal to the reflectivity loss coefficient here, but the reflection is more sensitive than

transmission to surface scattering losses[37]. Again the fit is excellent. The highest reflectivity was used for this, as it is believed that loss due to deviation from the surfaces being parallel may have occurred in the other measurement. The expected transmission was also calculated using Equation 49. The fit was close in most of the spectra, but over compensated for the scattering loss in the higher wavenumber region. Figure 6.6b plots the measured reflectivity with variances in the index of refraction to show the sensitivity of the analysis technique.

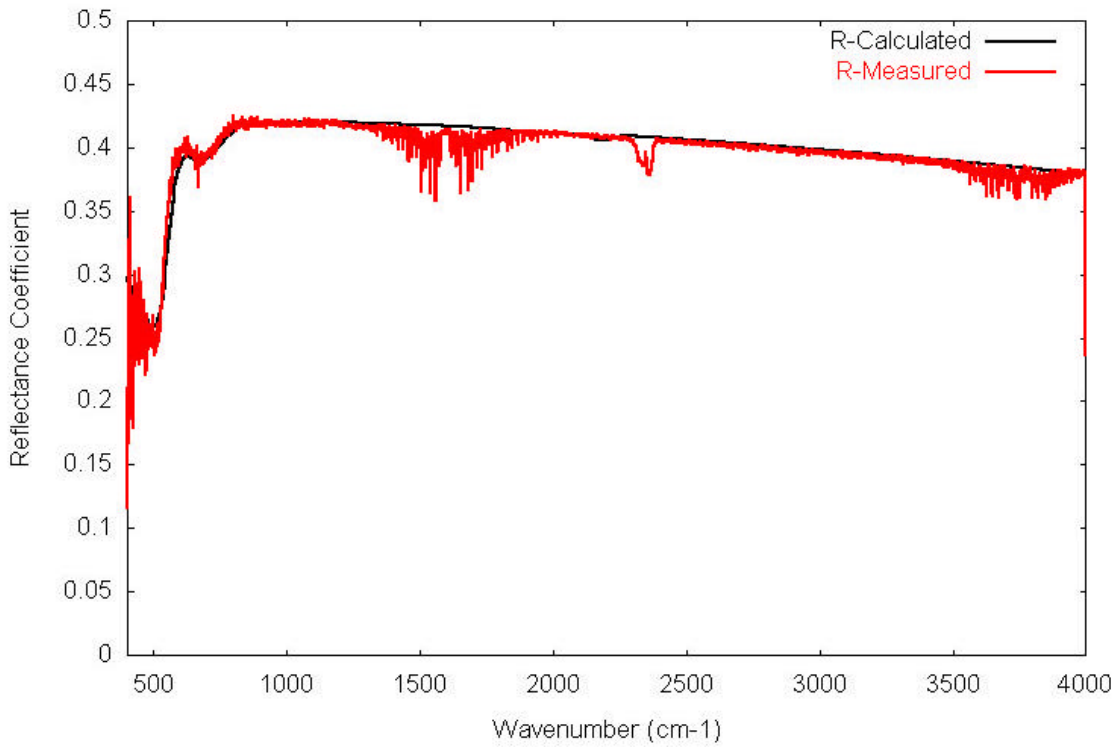

Figure 6.6a Measured FTIR reflectance and calculated reflectance for $Te_2As_3Se_5$ glass.

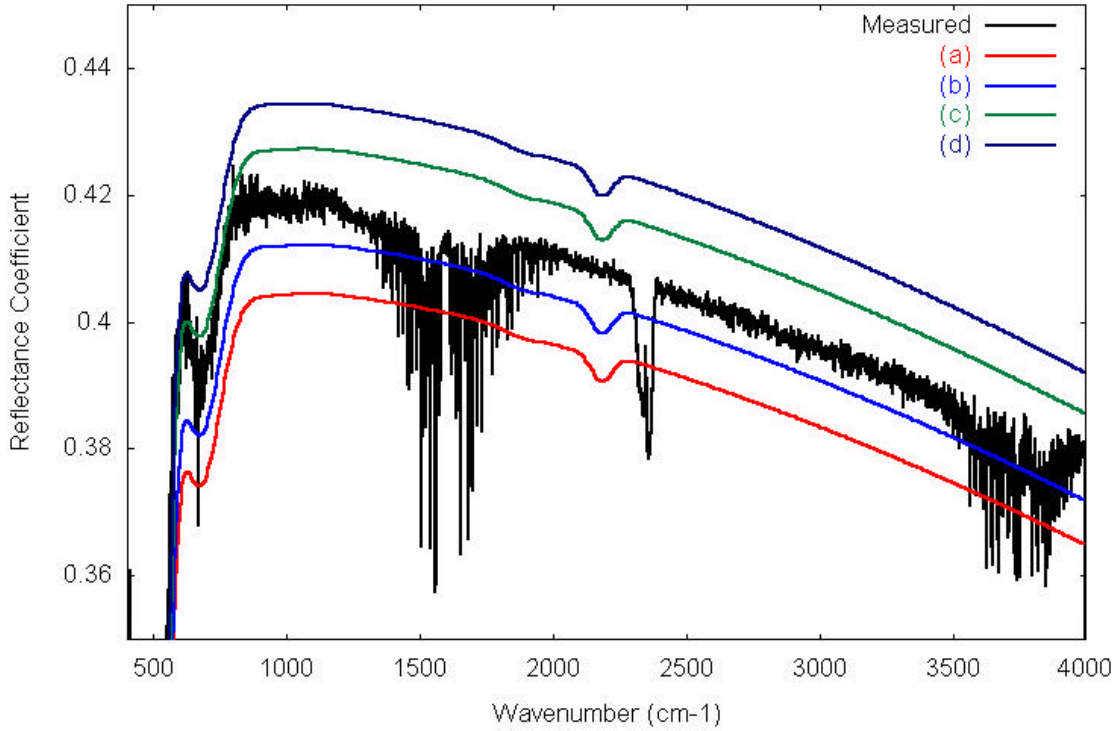

Figure 6.6b Measured FTIR reflectance and calculated reflectance for $Te_2As_3Se_5$ glass with variations of the base index of refraction of 3.16. (a) n=3.06, (b) n= 3.11, (c) n=3.21, and (d) n=3.26.

The calculated dielectric properties of for $Te_2As_3Se_5$ glass are shown in Figure 6.7. These dielectric functions will be used in subsequent calculations in Chapter 7 for the estimated response of a fiber optic probe made of $Te_2As_3Se_5$ glass.

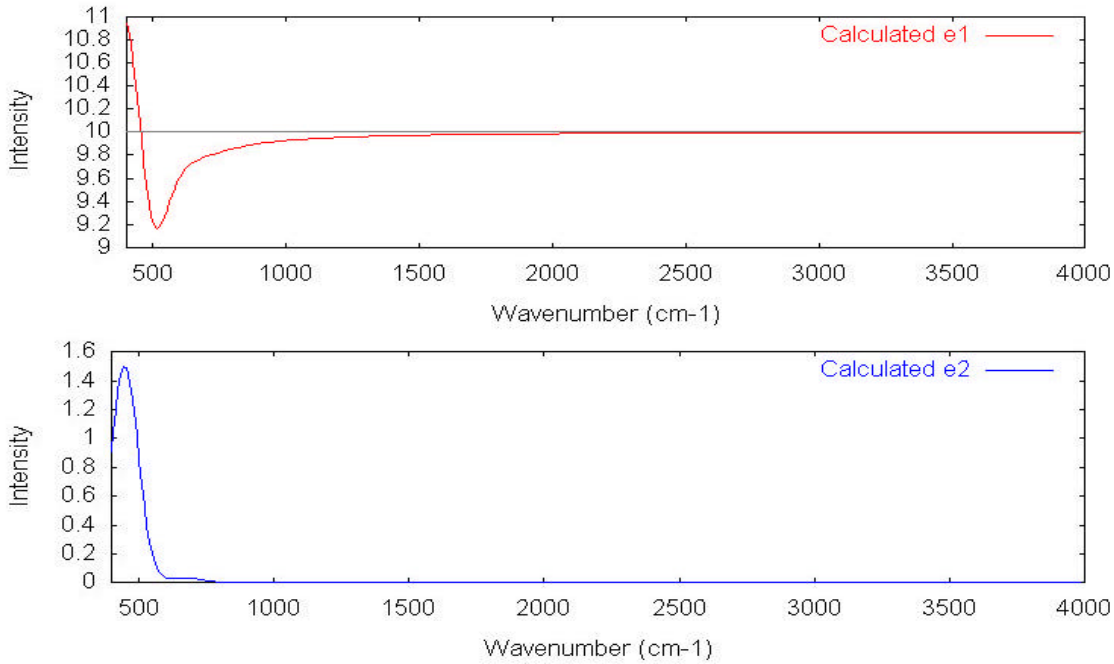

Figure 6.7 Calculated real (e1) and imaginary Dielectric functions for $Te_2As_3Se_5$ glass.

Conclusions

The transmission and reflection measurements were made on a glass of unknown optical properties. By using optical theory and Gaussian Dispersion Analysis an approximation of the optical properties was made that is consistent with the measurements. The effect of the surface roughness was estimated to have a larger effect when multiple reflections are present and the equations for multiple reflections were expanded to Equations 49 and 50, and incorporate the effects of scattering. More work needs to be done to understand the role of scattering upon transmission. This type of analysis may have use in the future for determining the optical properties of other glasses. Additionally, the optical properties of this glass should be confirmed by other means.

CHAPTER 7
FIBER OPTIC CHEMICAL SENSING PROBE

Introduction

Though there are many options for chemical analysis in the laboratory, the options for performing remote analysis are few. Of the current remote analysis techniques available, most are optical in nature. One of the most promising remote analysis tools is the use of broadband optical fiber probes often called fiber evanescent wave spectroscopy or FEWS. Currently, the analysis of the measurements taken with these broadband optical probes is problematic, as absorption bands from different chemicals can overlap. The work presented here gives measurements taken with such a probe along with conventional analysis of the data and discussion of its inadequacies. A model of the propagation of light in the fiber probe is developed and compared to the measured data.

Background

Current Methods of Remote Chemical Analysis

Most all of the current remote sensors described in the literature are based on optical detection means. Most are just sensors, and do not perform chemical analysis. Optical type detection systems typically rely on delivery of light by optical fiber and delivery of the signal to the detector by optical fiber. Some non-optical type remote sensors have been used to monitor processes or chemical stability but are not able to analyze chemical makeup. Some of the optical sensors use a single wavelength of light

and make use of changes in signal intensity to detect compositional changes, similarly to the use of the non optical type sensors, where changes can be monitored but the exact cause of the change cannot be determined[49]. These types of systems are useful only as a measure of a known system's stability over time, and can only be used to measure quantitative changes if a calibration curve is used and the system is known completely. [50, 51]

Current remote optical sensors that are capable of more than stability monitoring include Raman methods, photoluminescence, evanescent wave spectroscopy and broad band transmission methods [50-60]. The design of these types of sensors usually takes the form of one of the three shown in Figure 7.1. Figure 7.1a shows a typical sensor for transmission measurements although Raman or photoluminescence measurements can be made as well. Figure 7.1b shows the typical evanescent wave and/or fiber Attenuated Total Reflectance (ATR) cell, and Figure 7.1c is an fiber optical probe that delivers and collects evanescently excited florescence or Raman signals with the same fiber.

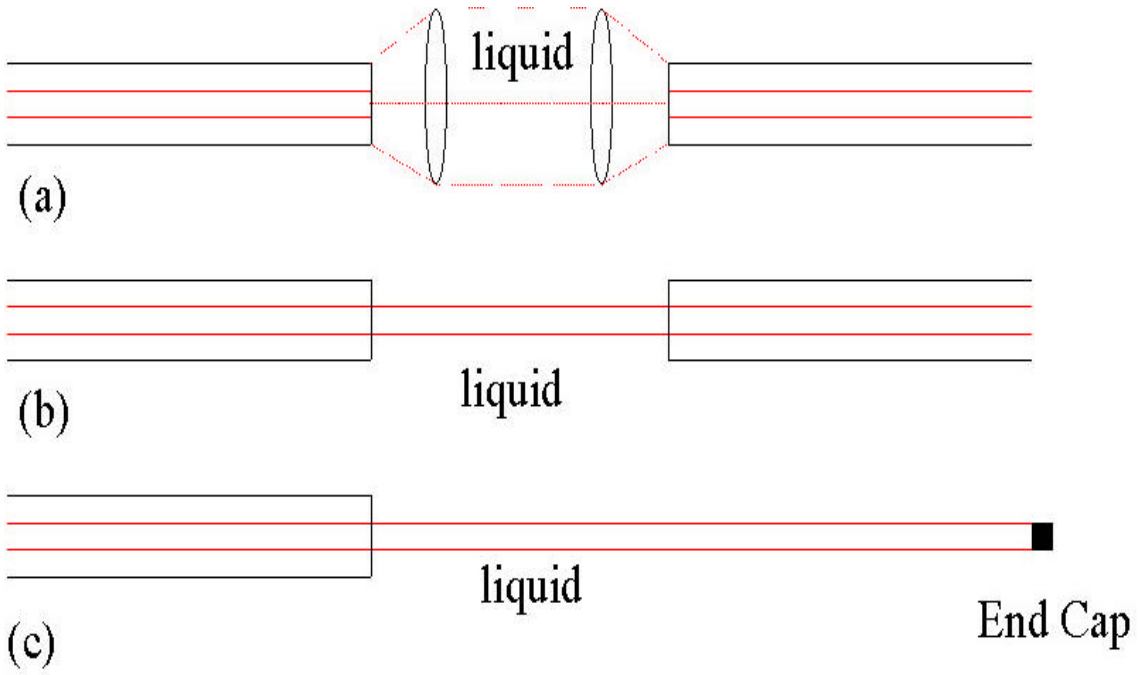

Figure 7.1 Existing types of Remote optical sensors.

The disadvantage to these systems varies with each type of probe and how it is used. The transmission probe is relatively simple, but require lenses at the sampling point. The evanescent wave/ATR probe is the most promising, but there are difficulties in interpreting the results. The single fiber capped probe is limited to systems that exhibit Raman or florescence. Raman measurements have been problematic if the glass fiber also exhibits Raman[53]. The main problems with today's current options for remote optical chemical analysis is that either the probes are not truly remote, or that they don't give enough information, i.e. not broadband, or/and that the data from the probes are not analyzed to give meaningful results.

Current Analysis Techniques

Even though the broadband optical systems have the most potential for quantitative chemical analysis, the data analysis techniques are not sufficient. There are

many types of analysis techniques in the literature [46, 49-51, 53, 55, 56, 58-65], but they all seem to fall short. Each particular technique has its faults.

One of the most common techniques is to use a Beer's Law type of analysis, while assuming that the signal to background is transmission in an optical sense. This is extremely simple, and is the same analysis recommended for ATR by FTIR instruments manufacturers. The same problem with shifting peaks occurs.

Others get more elaborate, realizing that the light does not actually transmitted through the material and they try to analyze the spectra as losses by the evanescent wave. Measurements taken with the probe discussed in this chapter are often referred to as fiber evanescent wave spectroscopy or FEWS. Evanescent waves are electromagnetic waves that travel along an interface when total internal reflection occurs. The use of the term evanescent wave spectroscopy in the context of fiber probes is incorrect. The evanescent wave is an imaginary component of the mathematical solution to total internal reflections traveling along the interface. Only when total internal reflection occurs will the evanescent wave mathematically appear, and as such only when both the core and cladding material,(or sample) has no imaginary component to its index of refraction, or does not absorb. When this specialized condition is met, the evanescent wave carries no power and is not absorbed by the cladding. The typical analysis of those claiming to perform FEWS is either the length of the fiber is the thickness of their sample or the use of an effective path length based upon the depth of penetration vs. incident angle. Each method is an attempt to simplify the results for ease of comparison with direct transmission spectra. In both cases the end result is a Beer's Law type analysis of quasi-

absorption from transmission through a sample. The problems of shifting peaks are not addressed.

Others, who also realize the deficiencies of the above two methods, have based their analysis on reflectivity, but fall short of explaining the shifting peaks. Still more explain shifting peaks by changes is chemical distribution about the fiber with concentrations. Much of the incorrect analysis is based upon previous work that was based upon assumptions and simplifications that are not valid. As such the inaccurate and non-scientifically based analysis is pervasive in the literature.

Experiment

The Fiber Probe

This experiment was conducted in the Laboratoire des Verres et Céramiques, University of Rennes, Rennes France, in the research group of Dr. Jaques Lucas. A chalcogen glass of composition $Te_2As_3Se_5$, was prepared and the fiber probe was pulled by the Lucas group in their standard fashion[66]. The glass is prepared at a high purity level of 99.999% starting elements and distilled to further remove impurities. The mixed components are sealed in a silica tube and homogenized in a rocking furnace(700 C). The glass is then slow cooled to close to its glass transition temperature (127 C) and annealed before slow cooling to room temperature. The glass was then drawn into a fiber with a diameter of approximately 400 microns and clad with a protective polymer coating. During the drawing process a length of the fiber of approximately 8 cm was tapered to a diameter of approximately 140 microns by momentarily accelerating the drawing and thus reducing the fiber diameter for a short section. The diameter of the fiber is monitored online. Due to the hand pulling of the

fiber, the diameter is not consistently 140 microns, but 140 microns was the smallest diameter. The variation in the diameter over the sensing zone of the fiber was not reported. The reduced diameter allows for a more flexible sensing region, while the larger diameter of the rest of the fiber allows easier coupling of the infrared light to the fiber and is less fragile. Additionally the reduced diameter increases the optical sensitivity of the fiber[61, 64, 67]. After cooling and remaining on a large spool for over two days, the fiber was cut to an overall length of 2 meters. The section of reduced diameter was striped of its polymer coating by an acid etch. The resultant fiber is schematically shown in Figure 7.2.

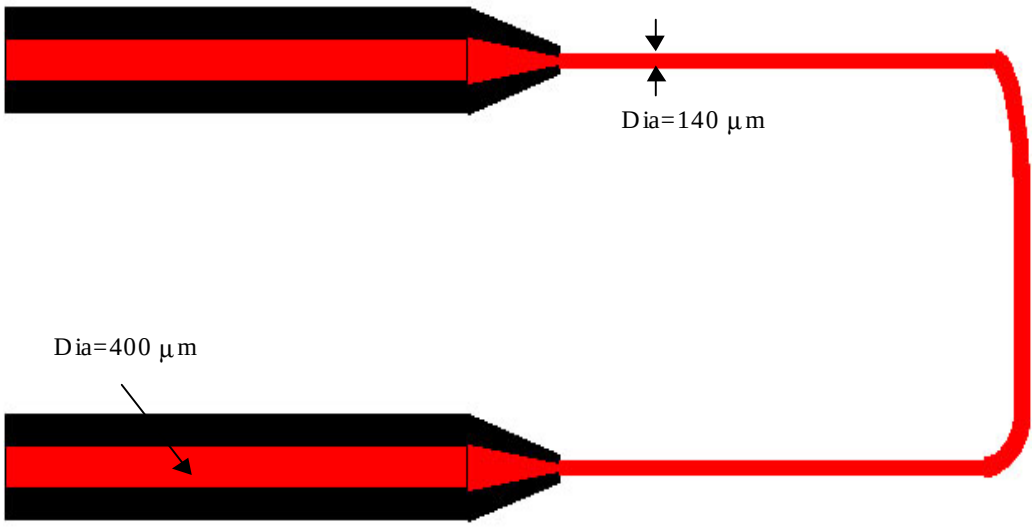

Figure 7.2 Schematic diagram of fiber optic probe.

Chemical Preparation

Solutions of ethyl alcohol, de-ionized water and mixtures of 20%, 40%, 60%, and 80% ethyl alcohol, with the balance being de-ionized water were prepared. Six 50ml

Pyrex beakers were cleaned and rinsed with 99.9% pure ethyl alcohol. They were wiped dry with a clean paper towel. A pipette with 1ml markings was used to measure out 2,4,6 and 8 ml of de-ionized water and put into 4 of the six clean beakers. The pipette was rinsed 2 times with ethyl alcohol and was used to measure out 2,4,6 and 8 ml of ethyl alcohol, adding the appropriate volume to make four 10 ml solutions of varying concentration.

Measurements

The fiber probe was placed in an FTIR spectrometer assembly with a external mercury-cadmium telluride infrared detector as shown in Figure 7.3. The coupling of the fiber to the spectrometer was done with two micro-positioning systems, one to couple the fiber to the source and one to couple the fiber to the detector. The fiber was adjusted to produce the maximum signal on the detector. The sensing zone of the fiber was placed in a glass sampling boat with a contact length between the fiber and sample of 5 cm. A background signal was taken without a sample, in laboratory air, in a sampling boat. The chemical solutions were alternately placed in the sampling boat. Between measurements the sampling boat was rinsed with ethyl alcohol and allowed to dry. All infrared spectra were recorded with a resolution of 2 cm^{-1} over the spectral range from 600 to 6000 cm^{-1}.

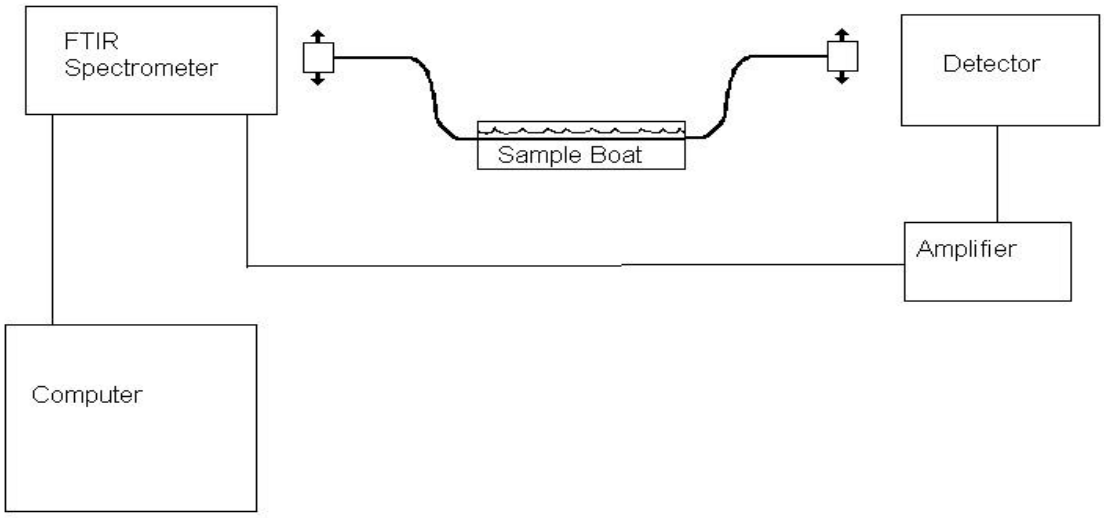

Figure 7.3 Schematic of experimental apparatus.

Results

The measured spectra are shown in Figure 7.4 a-g and Figure 7.5 shows a compilation of all measurements of the chemicals. All of the separate plots of Figure 7.4 are shown on the same scale. Figure 7.6 show the measurements plotted as absorbance, vs. wavenumber.

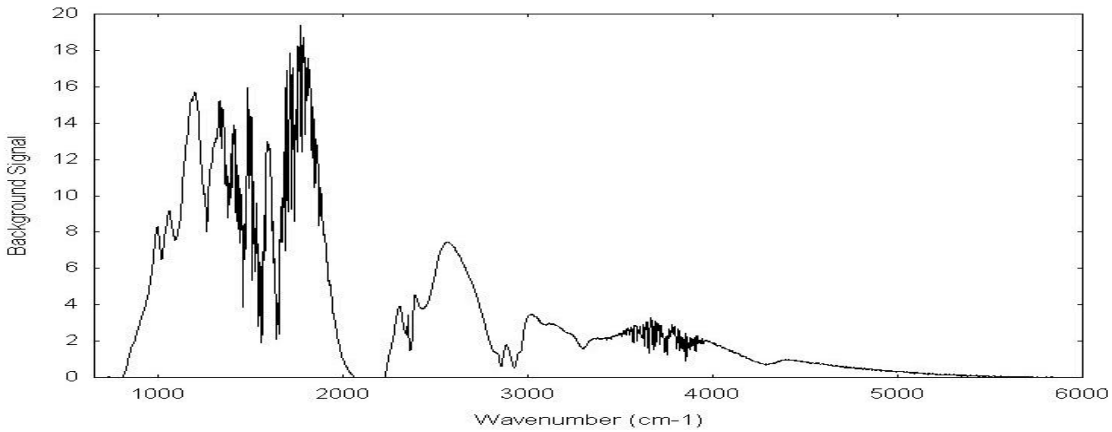

Figure 7.4a Measured background signal

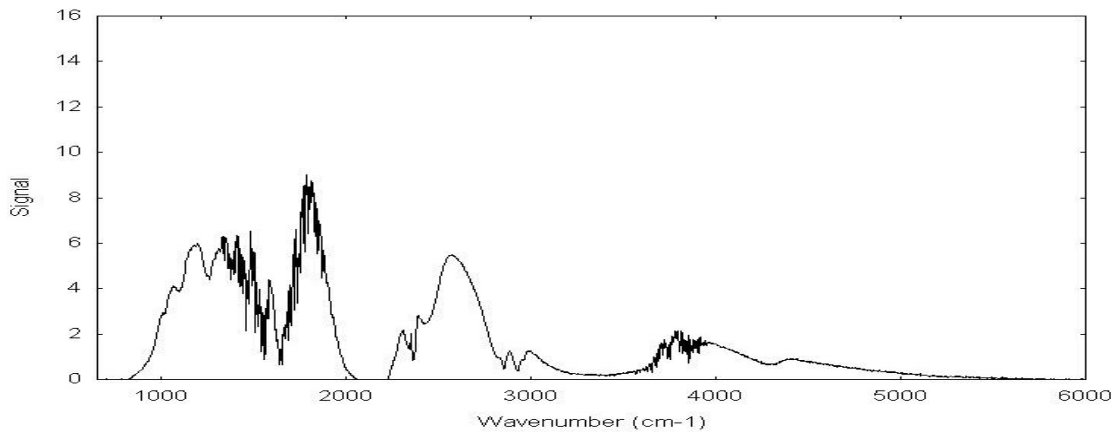

Figure 7.4b Measured signal for DI water

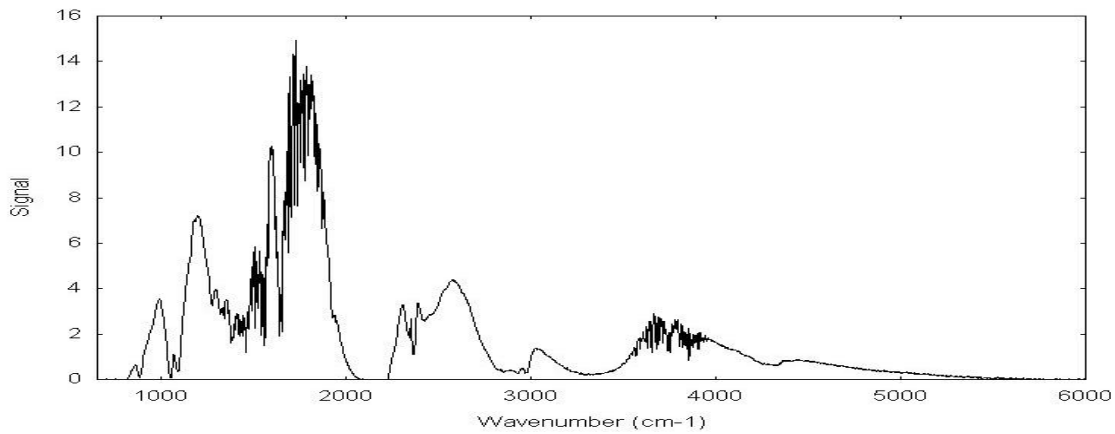

Figure 7.4c Measured signal for ethyl alcohol

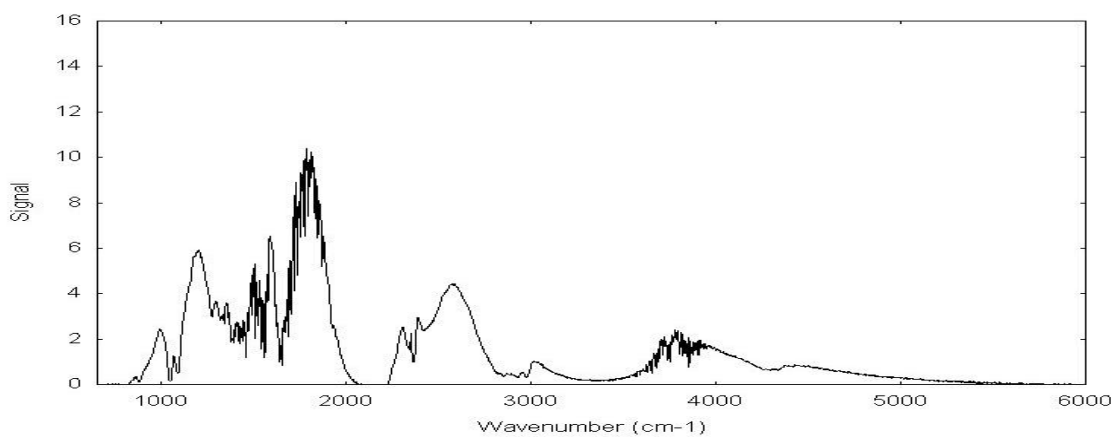

Figure 7.4d Measured signal for 80% ethyl alcohol- 20% DI water

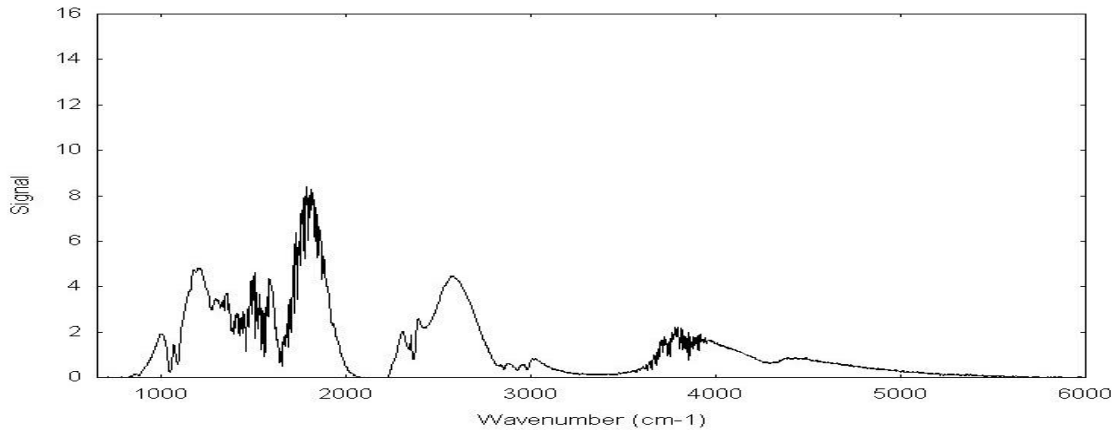

Figure 7.4e Measured signal for 60% ethyl alcohol- 40% DI water

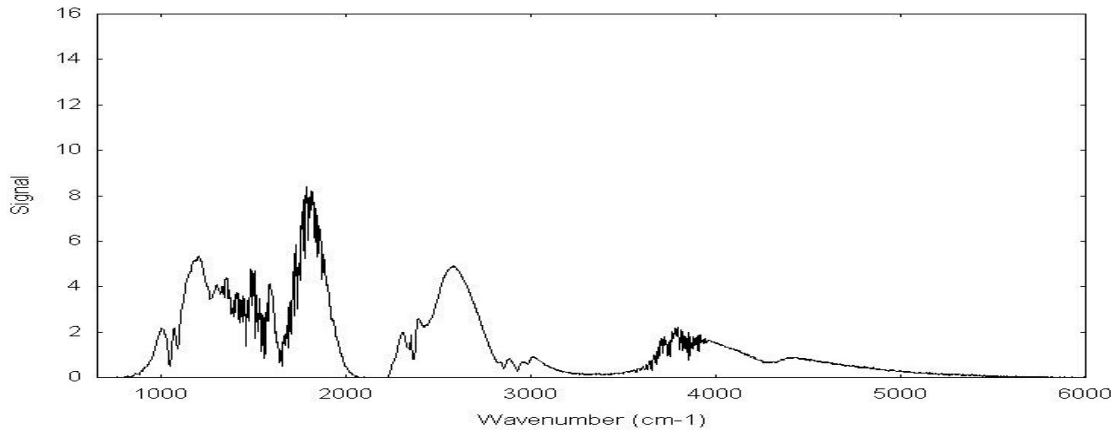

Figure 7.4f Measured signal for 40% ethyl alcohol- 60% DI water

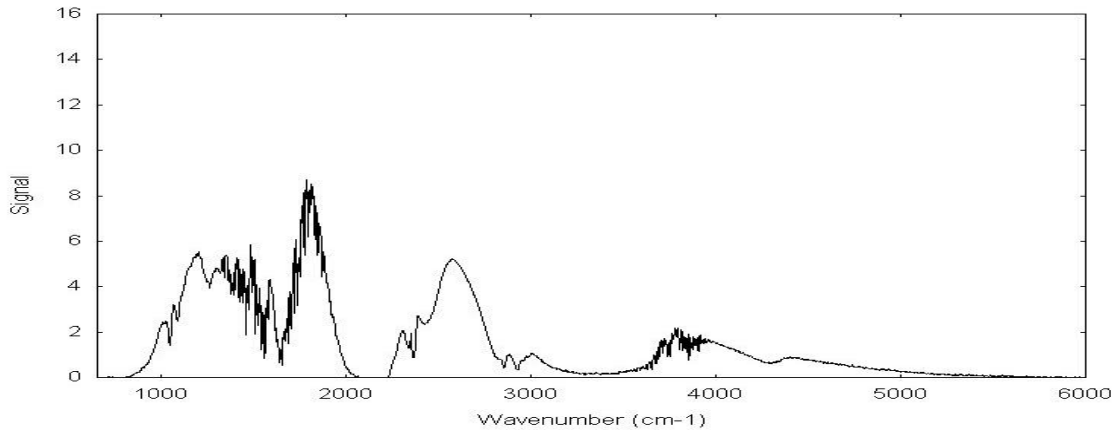

Figure 7.4g Measured signal for 20% ethyl alcohol- 80% DI water

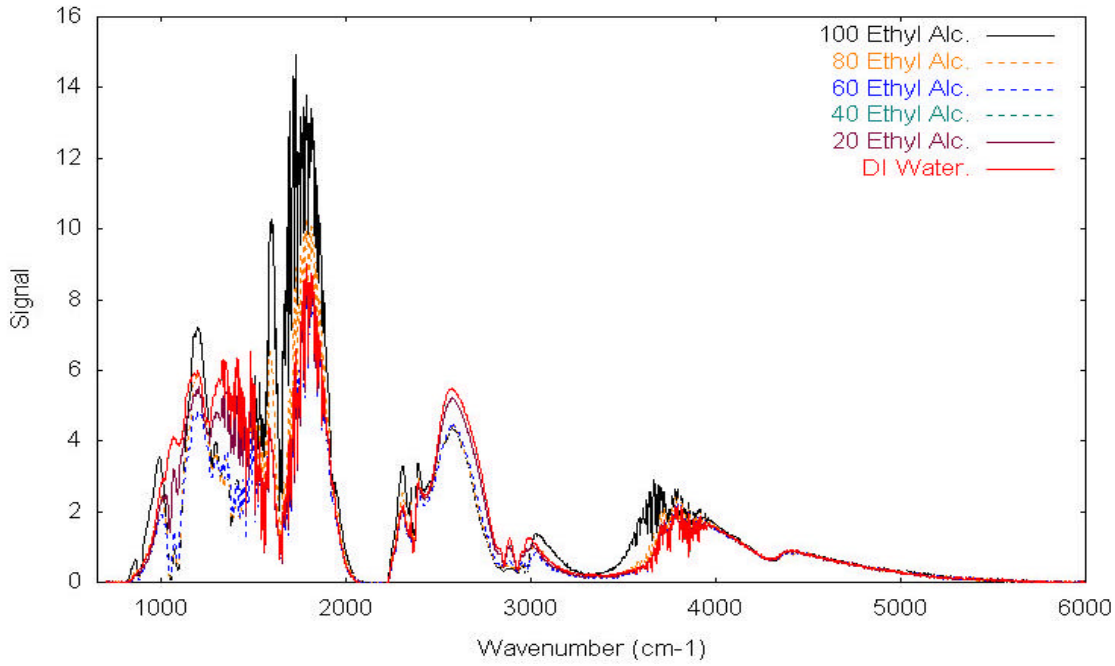

Figure 7.5 Measured signals for ethyl alcohol-DI water system

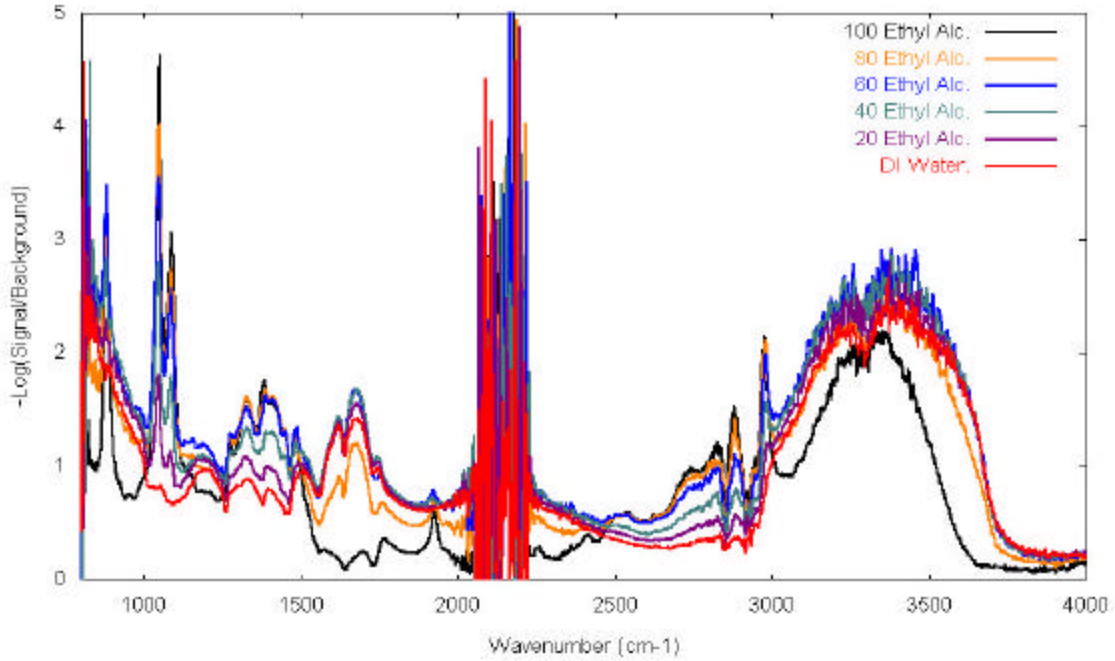

Figure 7.6 Absorbance vs. wavenumber for ethyl alcohol-DI water system.

Discussion of Results and Analysis

The results of the fiber probe for the different concentrations of ethyl alcohol and water are similar to that of the liquid ATR cell measurements in Chapter 5 and measurements of other investigators[47, 61, 63, 66, 68]. The background shown in Figure 7.3a shows that at some wavelengths there is no transmission through the fiber probe. This, as well as the many sharp contours of the background, is due to absorbance bands of both the fiber and of the polymer cladding. The region between 2000 and 2300 cm^{-1} is due to the absorbance of the Si-H bonds from hydrogen impurities in the $Te_2As_3Se_5$ glass, as mentioned in Chapter 6.

One of the typical analyses for these measurements is to look at the absorbance of individual peaks and to plot the amplitude vs. concentration, or to perform a Beers law type of analysis. The peaks chosen for analysis are typically the doublet peaks in the 1040 to 1100 cm^{-1} region. These peaks are generally used due to the flat absorbance in the surrounding spectral region. Figure 7.7 shows absorbance vs. wavenumber for these peaks, and Figure 7.8 is a plot of the peak amplitudes vs. concentration. These plots are consistent with other experiments of this type, the exception is the actual values of absorbance, which change with the investigator and physical setup. With increasing concentration, the absorbance values increase as shown in Figure 7.8. The increase is approximately linear with concentration. The near linear behavior of the absorption peaks makes this type of analysis attractive.

The difficulties with this type of analysis are that the absorbance values change from one experiment to the next, and the peak positions move. Both peaks drift to higher wave numbers. Additionally, with more complicated mixtures it may be impossible to choose a spectral region without overlapping peaks from different chemical species.

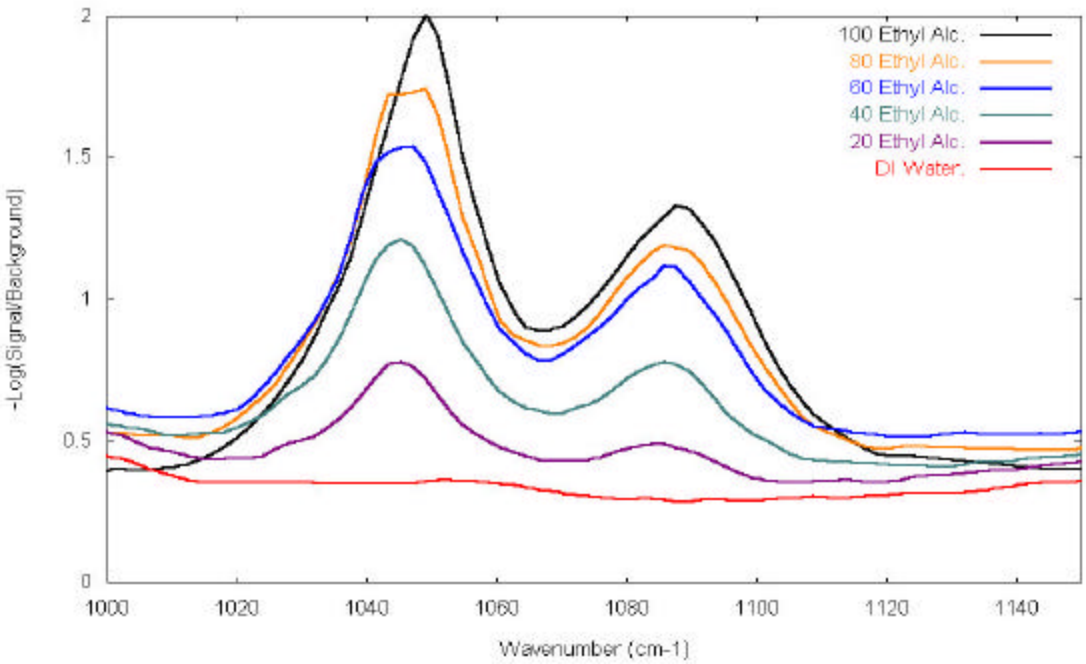

Figure 7.7 Absorbance vs. Concentration of ethyl alcohol in 1000 to 1150 cm^{-1} spectral region.

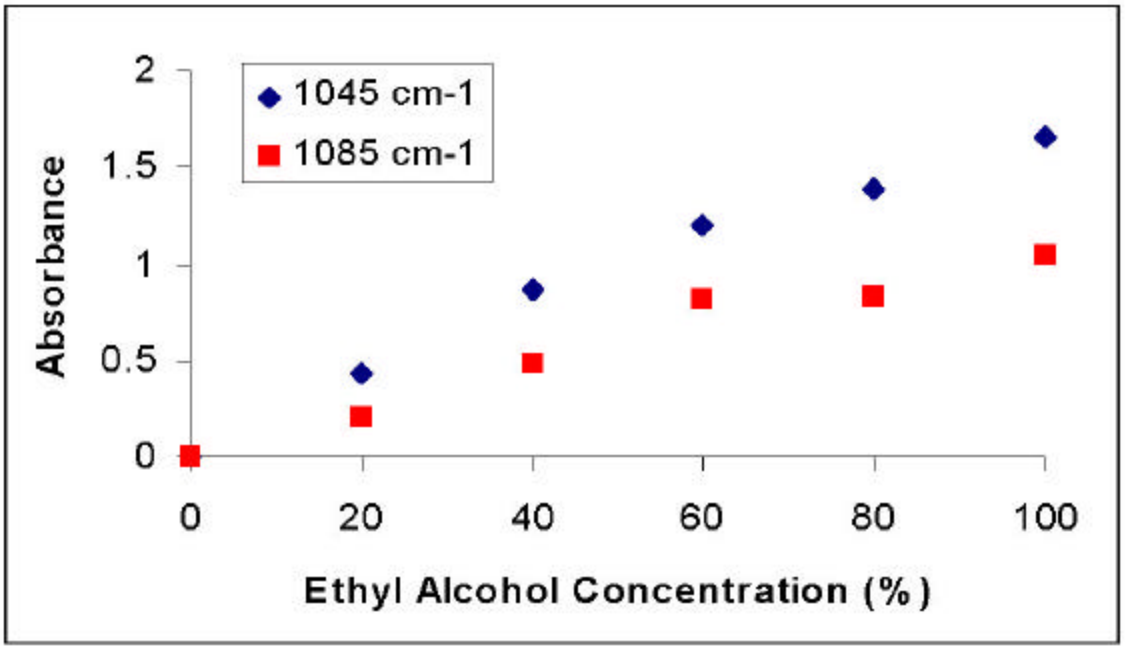

Figure 7.8 Peak Absorbance vs. Concentration of ethyl alcohol for 1045 and 1085 cm^{-1} peaks.

These difficulties may not seem important, and may be manageable in simple cases like the ethyl alcohol water system, but these problems, as in ATR, do not allow for analysis of more complicated systems and thus restricts this potentially powerful chemical sensor to limited systems.

Theory

Introduction

By determining the optical properties of the chemical system, the difficulties discussed above, can be overcome. The fundamental optical properties of a particular chemical or mixture should be consistent from one measurement to the next regardless of investigator or physical apparatus. In mixtures, the dielectric function is the sum of the individual components dielectric functions, added in proportion to the molar concentration. This type of approach is based upon fundament optical theory and allows for the changes in amplitude and peak position with concentration and also allows for overlap of peaks from the different chemicals in a mixture. In order to determine the base optical properties it is important to understand the fiber's response to an absorbing medium

Theory Applicable to Fiber Optic Probe

In fiber optics, or dielectric optical waveguides, the goal is to transmit light from one end of the fiber to the other with low loss in intensity. This is accomplished by carefully selecting the fiber's core and cladding and operating wavelength. The cladding must have a lower index of refraction at the operating wavelength in order to allow total internal reflection to take place between the core and cladding. Additionally, the core and cladding must have low, or non-existent, absorption at the operating wavelength. This effectively confines and guides the light in a non-absorbing medium.

Applicable Optical Equations

Maxwell's equations are the starting point for the study of electromagnetic phenomena and are applicable to the study light propagation in an optical fiber**[69-72]**.

Maxwell's equations are:

$$\nabla \times E = -\frac{dB}{dt} \tag{51}$$

$$\nabla \times H = J + \frac{dD}{dt} \tag{52}$$

$$\nabla \cdot D = \rho_v \tag{53}$$

$$\nabla \cdot B = 0 \tag{54}$$

with E being the electric field strength in units of [V/m], H, the magnetic field strength in units of [A/m], B, magnetic induction in units of [Webers/m^2], D, the electric displacement in units of [C/ m^2], J, the volume current density in units of [A/m^2], and ρ_v, the volume charge density. Other pertinent equations relating the above terms are:

$$D = \varepsilon E = \varepsilon_0 E + P \tag{55}$$

with ε being the permittivity of the medium in units of [F/m], ε_0, permittivity of free space, equal to 8.85 x 10^{-12} [F/m], and P being the polarization density field, or dipole moment per unit volume in units of [C/ m^2],

$$P = \varepsilon_0 \chi_e E \tag{56}$$

$$D = \varepsilon_0 \varepsilon_r E \tag{57}$$

$$e_r = 1 + c_e \tag{58}$$

$$n = \sqrt{e_r} \tag{59}$$

with χ_e being the electric susceptibility , ε_r being the dielectric constant, n being the index of refraction, all of which are unit less and

$$B = mH = m_r m_0 H \tag{60}$$

$$J = sE \tag{61}$$

for which μ is the permeability[H/m], $\mu 0$, the permeability of free space[4π x10^{-7} H/m], μr, the relative permeability [unitless] and σ the conductivity [A/V].

For materials that are sourceless: conductivity and volume charge density equaling zero; homogenous, linear and isotropic, the equations simplify significantly. The Hemholtz equations

$$\nabla^2 E + k^2 E = 0 \tag{62}$$

$$\nabla^2 H + k^2 H = 0 \tag{63}$$

with

$$k \equiv w\sqrt{me} \tag{64}$$

ω, being the radian frequency. Just as Maxwell's equations are the governing equations for electromagnetic phenomenon, Hemholtz's equations are the governing equations for optical waveguides.

Optical fibers are technologically important because they are able to transmit light over long distances with low losses. In order for this to occur, both the fiber core and its cladding must have low losses at the operating wavelength. Additionally, total internal reflection (TIR) must occur at the interface of the cladding and the core to confine the electromagnetic wave. For TIR the following condition must be met.

$$\boldsymbol{q} \geq \boldsymbol{q}_c = Sin^{-1}(\frac{n_2}{n_1}) \tag{65}$$

where n_1 is the index of refraction of the core material, n_2 the index of refraction for the cladding material, θ_c , the critical angle, from normal, for TIR, and θ is the angle of incidence from normal. This condition for TIR is applicable to any situation, but addition constraints occur in a fiber. In order for waves to propagate along the fiber, i.e. not de-constructively interfere with each other, each reflection must be in phase with other reflected waves. During TIR the phase shifts,δ, upon a reflection as a function of angle according to:

$$\boldsymbol{d}_{TE} = 2Tan^{-1}\left(\frac{\sqrt{n^2 \sin^2(\boldsymbol{q}) - 1}}{n \sin^2(\boldsymbol{q})}\right) \tag{66}$$

and

$$\boldsymbol{d}_{TM} = 2Tan^{-1}\left(\frac{\sqrt{n^2 \sin^2(\boldsymbol{q}) - 1}}{\sin^2(\boldsymbol{q})}\right) \tag{67}$$

again with TE representing Transverse Electric, meaning the electric vector is parallel to the interface and TM representing the magnetic vector parallel to the surface.

The phase shift upon reflection and the phase shift from propagating in the medium must be equal for the waves to be in phase. Only certain angles of incidence, will meet this condition, resulting in modes of propagation for a particular wavelength. Furthermore, when the incident angle is greater than the critical angle, the solution of the wave equations leads to an imaginary wave vector along the core/cladding interface, called an evanescent wave, which propagates along the interface of the core and cladding and decays exponentially into the cladding material.

For a cylindrical fiber of radius a, index of refraction of n_1, and n_2, for the core and cladding, the solution to the propagation constants and modal equations has been performed by an number of authors, with the propagation constant, β, being bound as

$$n_2 k \le \boldsymbol{b} \le n_1 k \tag{68}$$

with

$$k = \frac{2\boldsymbol{p}}{\boldsymbol{l}} \tag{69}$$

k, being the free space propagation constant. The propagation constant is the phase shift per unit distance measured along the fiber axis. From β, the direction that a plane wave is traveling in the fiber can be determined. The modes,ν=0,1,2..., are generally solved numerically or graphically from the following equation.

$$(J_v + K_v)(k_1^2 J_v + k_2^2 K_v) = \left(\frac{\boldsymbol{bn}}{a}\right)^2 \left(\frac{1}{u^2} + \frac{1}{w^2}\right)^2 \tag{70}$$

with

$$k_x = n_x k \tag{71}$$

$$u^2 = k_1^2 - b^2 \tag{72}$$

$$w^2 = b^2 - k_2^2 \tag{73}$$

$$J_v = \frac{J_v^{'}(ua)}{uJ_v(ua)} \tag{74}$$

and

$$K_v = \frac{K_v^{'}(wa)}{wK_v(wa)} \tag{75}$$

J_v and J_v' functions represent the Bessel functions of the first kind, and K_v and K_v' represent the Modified Bessel functions. The propagation constant, β, for each mode at each different wavelength describes the direction of travel for that particular mode.

Theoretical Predictions

Introduction

The complete solution of light interaction along the fiber probe involves the following. 1) Entrance conditions of the infrared beam and losses associated with it. 2) Interaction and attenuation along the clad section, and the setting up of the propagation modes or angles as described by Equation 70. 3) The transition of these modes during the taper to the sensing zone. 4) The attenuation of the signal as it propagates through the unclad region. 5) The transition back to the larger diameter clad section. 6) Exit of the

beam from the fiber and detection. 7) Additional factors in the propagation are bends in the fiber and surface roughness along the fiber.

Model

A model of the fiber optic probe's response is presented to aid in predictions. Others have developed models for the propagation and interaction for FEWS. The ability to predict the response with changing fiber diameters and sensing lengths is desirable [47, 49, 50, 53, 55, 58-64, 66, 68] . Many of the factors involved in the complete solution can be removed by a background spectrum, and due to the complexity some plausible assumptions are made to simplify calculations. With diameters of 100 microns and larger the fibers are considered multi-mode, and the solution to Equation 70 is omitted. The complexity by adding the solution to Equation 70 is considerable and it is thought that since the number of modes is large that a continuum of angles per wavelength is present and an integration, or summation, over all angles will be a sufficient first approximation. It is also assumed that each angle carries equivalent power. Additionally the effects of the cladding should be removed by the use of a background. The exception will be at wavelengths where the attenuation due to the cladding is large enough to reduce the intensity of the beam to zero. Thus the only area to be considered is the section of fiber in contact with the sample. Additionally only meridian rays are considered, that is the rays that travel through the center of the core. Non meridian rays are expected to cancel out.

The number of reflections over length L of a fiber with a diameter of d is dependent upon the following:

$$N(q,d,L) = L * \frac{\tan(90-q)}{d} \tag{76}$$

With θ, being the angle of incidence from normal. Assuming equal components of polarization the angle dependent reflectance is with R_{TM} and R_{TE} being defined by Equations 43 an 44 in Chapter 5 and ε_i and ε_t again being defined by the complex dielectric functions, ε_t for the fiber and ε_i for the sample.

$$R(q,e_i,e_t) = 0.5 * R_{TM}(q,e_i,e_t) + 0.5 * R_{TE}(q,e_i,e_t) \tag{77}$$

The transmission of signal over length L, at angle θ, would be

$$T_L(L,q,e_i,e_t) = R(q,e_i,e_t)^{N(q,d,L)} \tag{78}$$

Assuming that the number of modes is large and continuous, the total signal for a given wavelength with a summation from 0 to 90 degrees is

$$T_L(e_i,e_t) = \sum_{q=0}^{90} T_L(L,q,e_i,e_t)\,. \tag{79}$$

The signal to background is then calculated from

$$\frac{Signal}{Background} = \frac{T_L(e_{sample},e_{fiber})}{T_L(e_{air},e_{fiber})} \tag{80}$$

This model differs significantly from other models developed in that it is based upon the reflection instead of absorbance.

Calculations

The model developed was tested against the measured data. The combination of this model with Gaussian dispersion analysis could be used, but due to uncertainty of the model and assumptions of it, the implementation uses the dielectric function of the materials and mixtures.

The signal to background was calculated with the values of ε_{sample} being a mixture of the dielectric functions calculated for water and ethyl alcohol in Chapter 5, proportional to the mixture concentration, ε_{air} being 1 + 0i, and ε_{fiber} being the dielectric function of the fiber as determined in Chapter 6. Additionally different values of diameter and sensing length were substituted into the model to see if the predictions follow the trends of experimental measurements.

The calculations for a diameter of 140 μm, and a sensing length of 5 cm are shown in Figures 7.9-7.15. The calculated spectrum has the same general shape as that of the measured spectrum, but it appears that the model assumes a larger sensitivity than the actual measurements. Coupled with the higher sensitivity, is the uncertainty of the dielectric functions for both water and ethyl alcohol, as they were determined in Chapter 5, and the apparent effects from the cladding. There are some sharp peaks that correlate with spikes in the background spectrum and did not cancel out. Figure 7.15 and 7.16 are plots of calculated spectra for less sensitive fibers that better fit the measured data for water and 100% ethyl alcohol. The calculations correspond to a diameter of 140 μm and a sensing length of 1 cm.

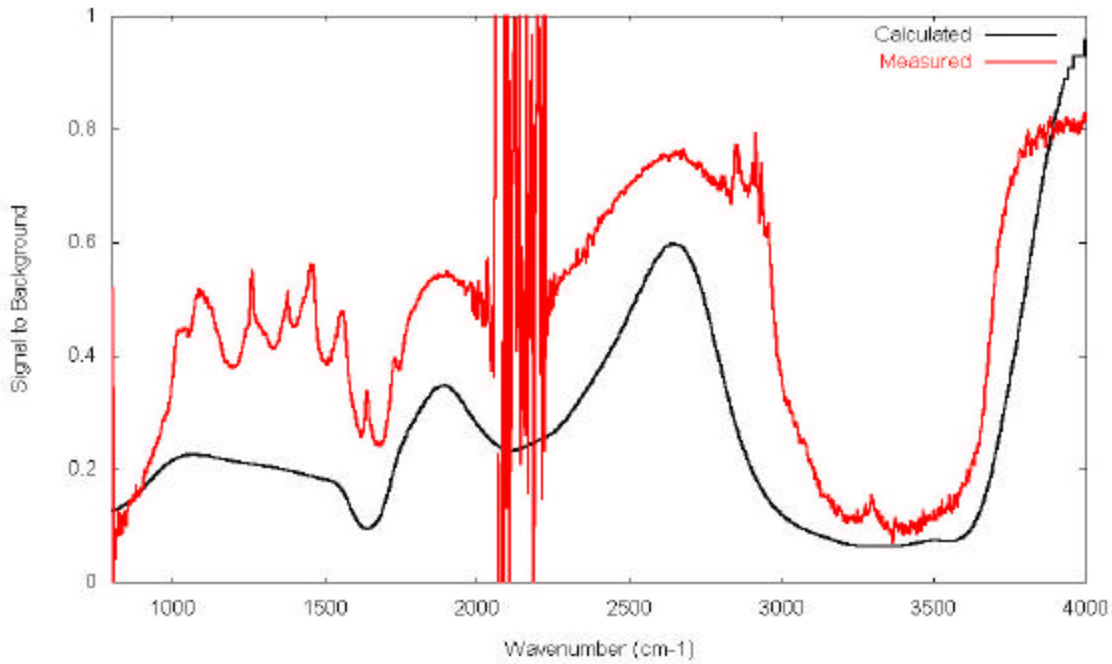

Figure 7.9 Measured Fiber Spectrum for water compared to calculated by developed model.

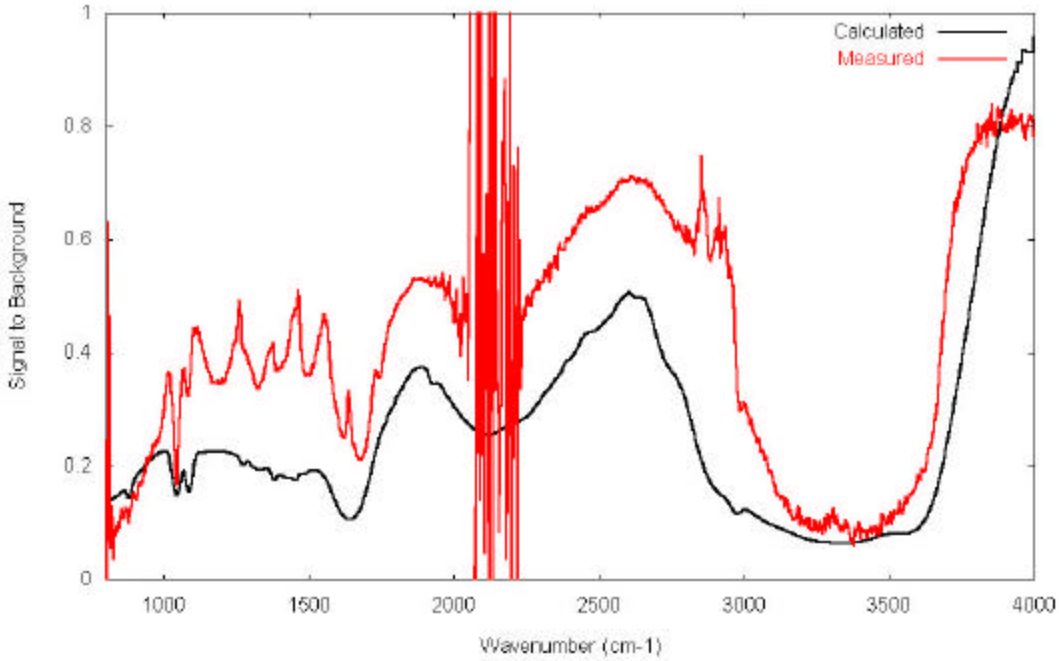

Figure 7.10 Measured Fiber Spectrum for 20% ethyl alcohol compared to calculated by developed model.

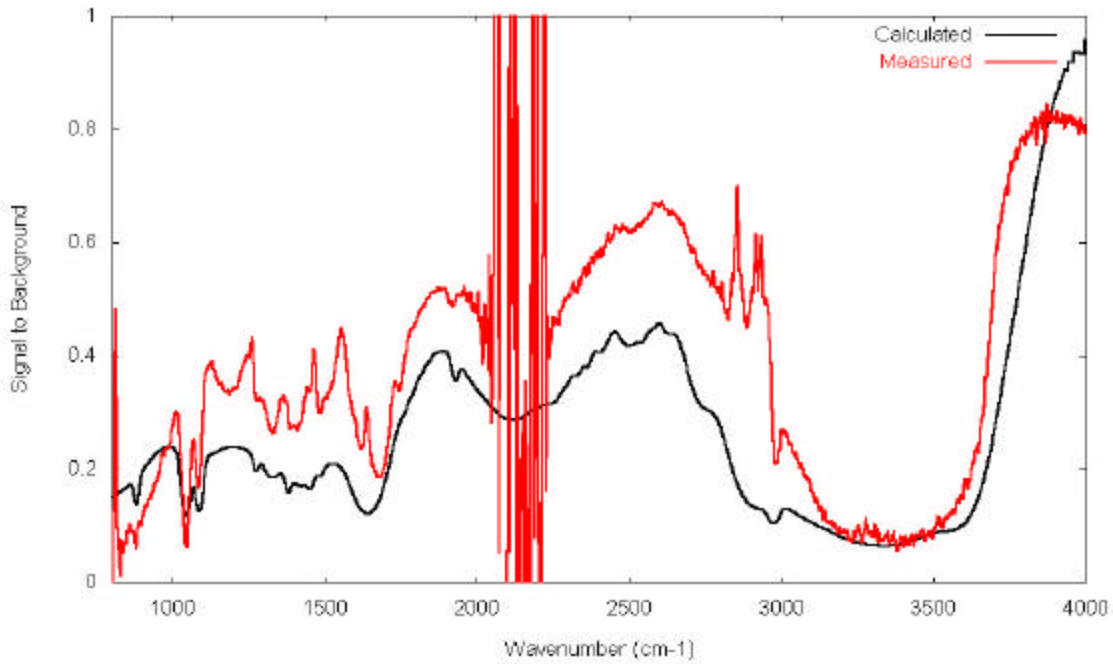

Figure 7.11 Measured Fiber Spectrum for 40% ethyl alcohol compared to calculated by developed model.

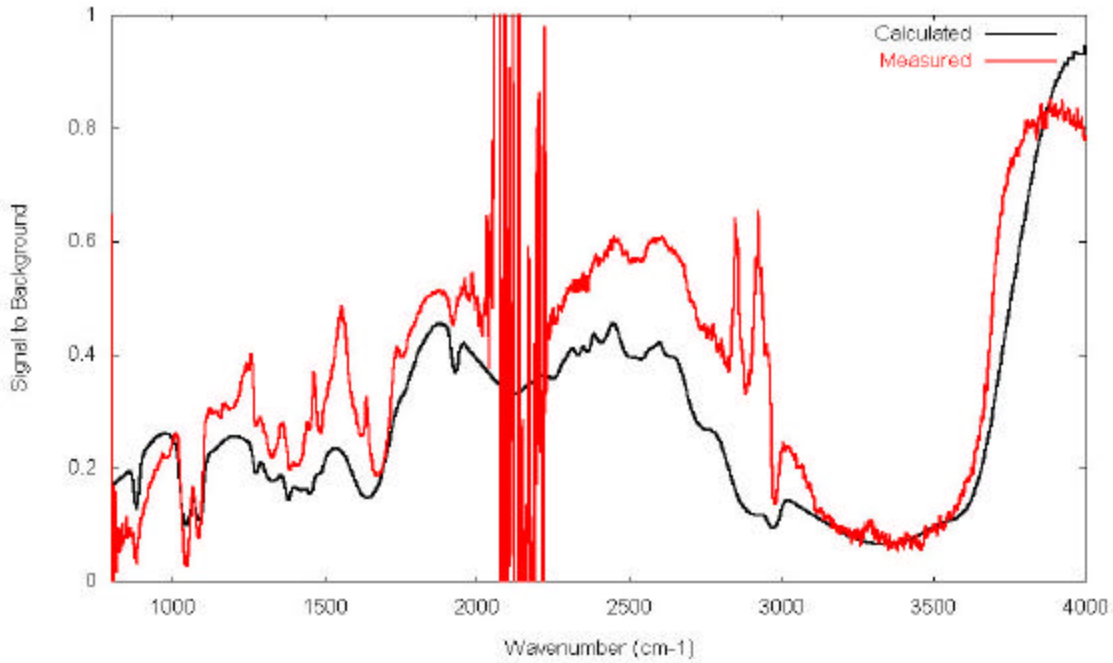

Figure 7.12 Measured Fiber Spectrum for 60% ethyl alcohol compared to calculated by developed model.

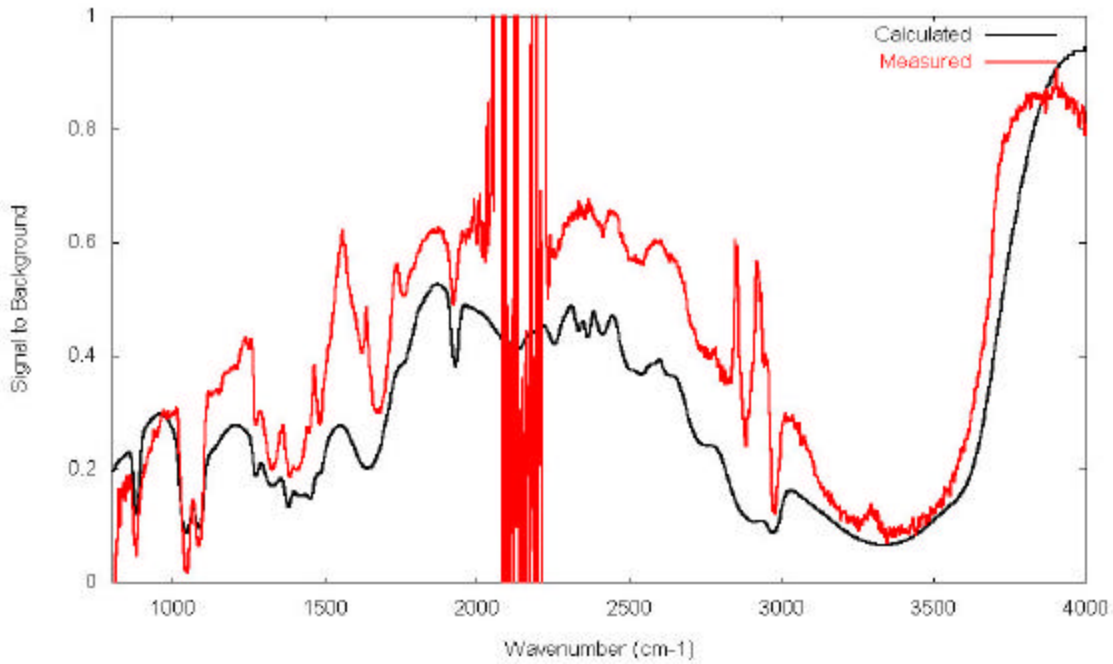

Figure 7.13 Measured Fiber Spectrum for 80% ethyl alcohol compared to calculated by developed model.

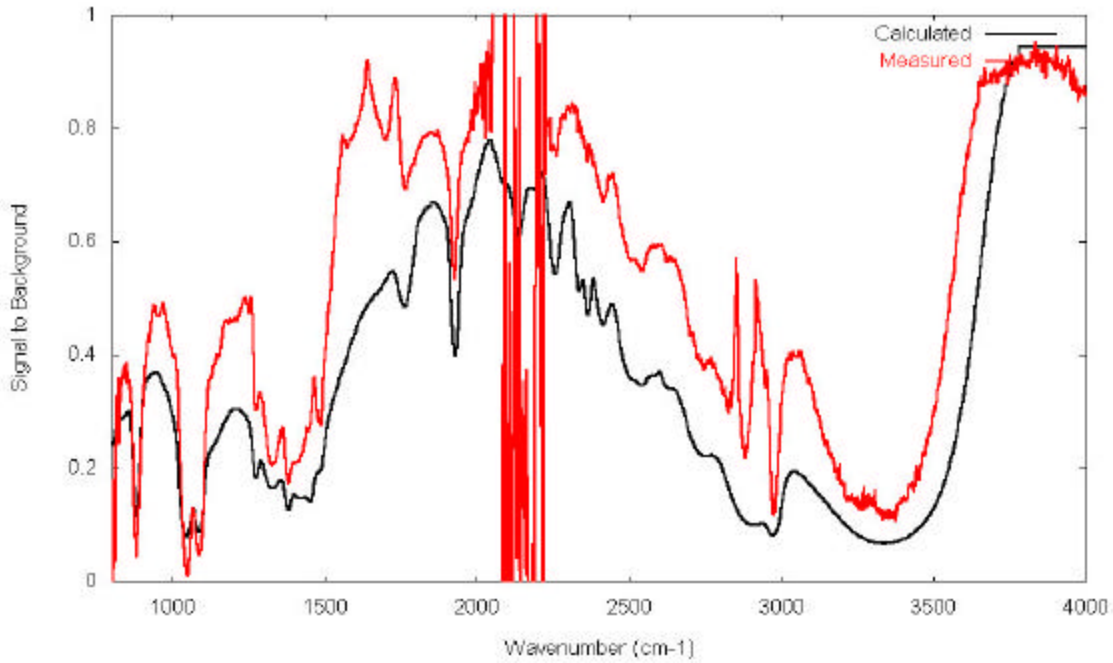

Figure 7.14 Measured Fiber Spectrum for 100% ethyl alcohol compared to calculated by developed model.

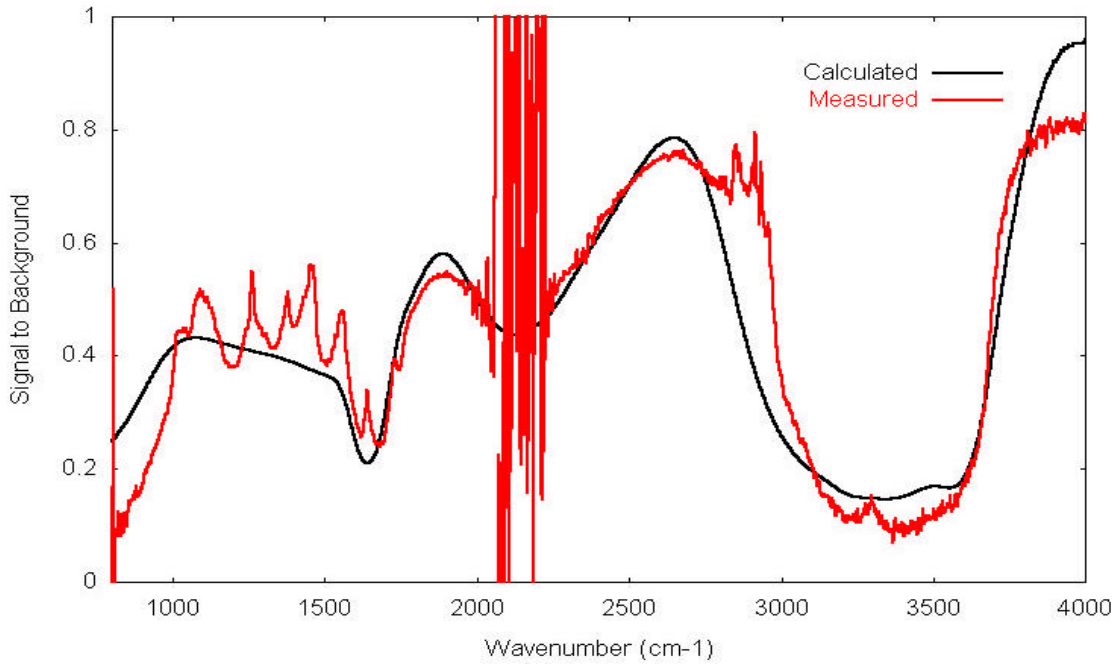

Figure 7.15 Measured Fiber Spectrum for water compared to calculated by model with diameter of 140 microns and immersion length of 1 cm.

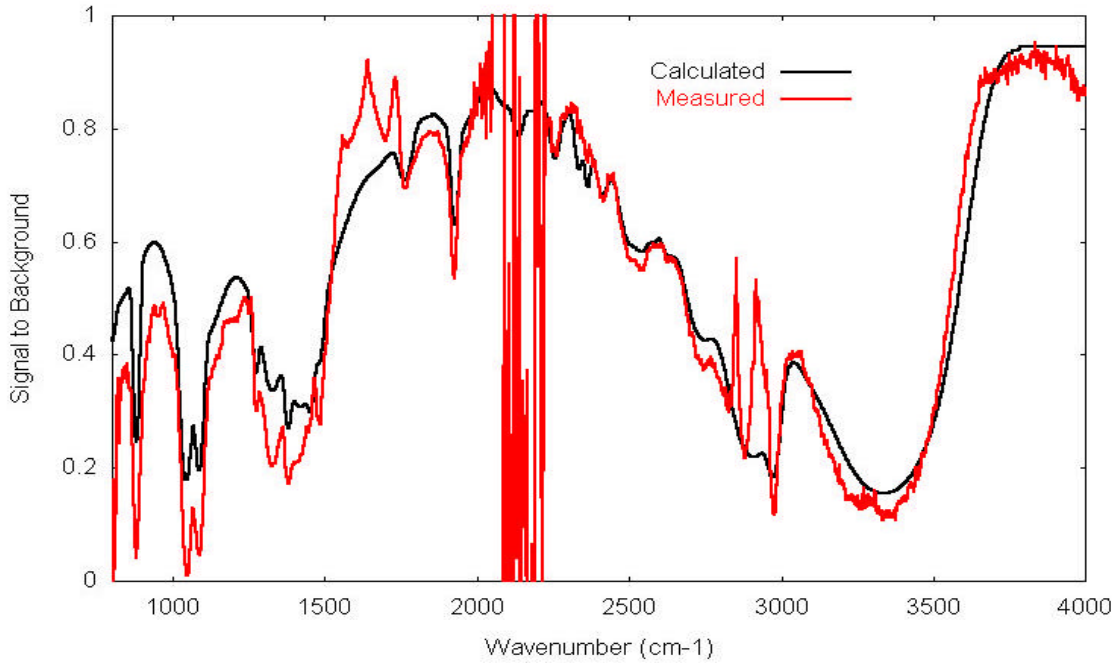

Figure 7.16 Measured Fiber Spectrum for water compared to calculated by model with diameter of 140 microns and immersion length of 1 cm.

The response of the model to varying diameters and lengths is straight forward, as these parameters only change the number, N, to which the reflection coefficient is raised to at each angle. Thus, as the length increases, N increases linearly. The effects on the diameter are similar, as the diameter decreases the number of reflections increases by 1/d. In the actual operation of the fiber, particularly as the diameter is reduced, the assumed continuum of angles may not be valid and the sensitivity at each angle may increase but with less overall signal. These trends, for both diameter and length, follow what other investigators have found [47, 53, 55, 58, 60, 61].

Conclusions and Future Work

Current technology is not sufficient to allow quantitative measurements to be made from the fiber sensors described in this chapter. Previous analysis applied to the fiber's optical response was based upon many different theories. Such theories were based on the direct transmission through the media, evanescent wave propagation, effective path lengths in the sample media, and some upon reflectivity. Of those who realize that the interaction along the fiber is a reflection process between the fiber and sample, no analysis technique concentrates upon determining the dielectric function in order to allow concentrations to be determined. Attempts to quantify the measurements have been frustrated by the shifting and overlapping of peaks

There are many difficulties to be overcome before remote quantitative analysis by a fiber probe will become a reality. The fiber probes themselves need to be made to tighter tolerances, as the unknown variation of the diameter along the probe is impossible to account for. The fiber materials, both the core and cladding, need to be fully optically characterized. An attempt was made to determine the optical properties of the glass

material in Chapter 6, but this needs to be confirmed and improved upon. Furthermore, the model presented here should be expanded to include solutions of the modal equations for the clad section, possible scattering due to surface roughness, and the effects of the tapering zone.

APPENDIX
COMPUTER PROGRAMS USED FOR DATA ANALYSIS

Computer programs where used extensively in the analysis of data. The programming language PYTHON was used, as it was freely available and simple to use. The programs used are broken were collected into different modules, each with its own file. The modules refer to each other's programs.

Module Atrtest:

```
"""This program will run the analizefile function given the input
paramiter file"""

def ATR(paramfile,average,low,high):
        x=Filefunctions.inparam(paramfile)
        sig=[]
        Filefunctions.openreadreflectancefile(x[0],sig)
        sig.sort()
        sig=Filefunctions.average(sig,average)                    #Average out data
        h=Filefunctions.find(sig,high,0)                    #High data element number

        l=Filefunctions.find(sig,low,0)                     #Low data element number
        sig=sig[l:h]                    #Truncate from Low to High Data
        w= Filefunctions.getcol(sig,0)                              #
        s= Filefunctions.getcol(sig,1)
        Vars=x[2]
        Vars,
Error=LEVENBERGMARQUARDT.main( w,s,Opticalfunctions.ATRsample,x[2],x[3],-
1,1,5)
        print Vars
        y=[]
        y.append(x[0])
        y.append(x[1])
        y.append(Vars)
        y.append(x[3])
        Filefunctions.outparam(paramfile,y)
        R,er,ei=Opticalfunctions.ATRsample(Vars,w)
        d=Filefunctions.diff(R,s)
        out=map(None,w,s,R,d,er,ei)
        Filefunctions.writearraytofile(x[1],out)
```

```
def main():                                    #Main program

        paramfile='d:\\........prm'
        average=1
        low=655
        high=2500
        ATR(paramfile,average,low,high)

if (__name__=="__main__"): main()
```

Module CalculateOscillator

```
import Filefunctions
import cmath
import umath
import Opticalfunctions
import UniversalFitter
import LevenbergMarquardt
LM=LevenbergMarquardt
Ff=Filefunctions
Of=Opticalfunctions
fname="c:\\......"
vars=[2.25,.91,50.0,10.0,4.9,200,60]


def calculateR(param,w):
        ecomp=Opticalfunctions.ecomplexgauss(param,w)
        ecomp=map(Opticalfunctions.ncomplex,ecomp)
        r=map(Opticalfunctions.R1,ncomp)
        out=map(None,w,r)
        return w

def calculatefile(param,w,filename):
        ecomp=Opticalfunctions.EComplexGauss(param,w)
        ei=map(lambda x:x.imag,ecomp)
        er=map(lambda x:x.real,ecomp)
        ncomp=map(Opticalfunctions.ncomplex,ecomp)
        n=map(lambda x:x.real,ncomp)
        k=map(lambda x:x.imag,ncomp)
        r=map(Opticalfunctions.R1,ncomp)
        xarray=map(None,w,r,n,k,er,ei)
        Filefunctions.writearraytofile(filename,xarray)

def calculate_e_file(param,w,filename):
```

```
        ecomp=Opticalfunctions.EComplexGauss(param,w)
        ei=map(lambda x:x.imag,ecomp)
        er=map(lambda x:x.real,ecomp)
        xarray=map(None,w,er,ei)
        Filefunctions.writearraytofile(filename,xarray)

def calculate_alpha_file(param,w,filename):
        ecomp=Opticalfunctions.EComplexGauss(param,w)
        a=[]
        for i in range(len(ecomp)):
                nt= pow(ecomp[i],0.5)
                a.append(Opticalfunctions.Alpha(nt,w[i]))
        xarray=map(None,w,a)
        Filefunctions.writearraytofile(filename,xarray)

def outputfilecomparison(w,r,fnameout,param):
        ecomp=Opticalfunctions.EComplexGauss(param,w)                    # calculate
ecomplex from given variables
        ei=map(lambda x:x.imag,ecomp)                    # e2
        er=map(lambda x:x.real,ecomp)                    # e1
        ncomp=map(Opticalfunctions.ncomplex,ecomp)                       # n*
        n=map(lambda x:x.real,ncomp)                     # n
        k=map(lambda x:x.imag,ncomp)                     # k
        rcal=map(Opticalfunctions.R1,ncomp)                              # Calculated
Reflectivity
        res=Filefunctions.diffsq(rcal,r)                         # Difference Between
Calculated and Experimnetal R
        out= map(None,w,r,rcal,res,n,k,er,ei)
        Filefunctions.writearraytofile(fnameout,out)


def main():                                     #Main program
        w=map(float,range(1,2000,1))
        calculatefile(vars,w,fname)

if (__name__=="__main__"): main()
```

Module fiberfunctions

```
import Opticalfunctions,Filefunctions,Numeric
OF=Opticalfunctions
FF=Filefunctions
def NperLavsd(angle_deg_range,dia_range):
#Number of Reflections per angle
#dependant only on length of Fiber section, Diameter and Angle
        numbang=len(angle_deg_range)
```

```
        numbdia=len(dia_range)
        NperL=Numeric.zeros((numbang,numbdia),'f')
        for a in range(numbang):
                angle_rad=((90-angle_deg_range[a])*Numeric.pi/180)
                tan=Numeric.tan(angle_rad)
                for d in range(numbdia):
                        NperL[a,d]=tan/dia_range[d]
#returns An Array with dia as one axis, Angle as the 2nd axis the number of Refelctions
as the Data
        return  NperL
def RperA(e_fiber,e_sample,angle_deg_range,numbang):
# The reflection Coefficient for each angle for the dielectrics at specific Wavenumber
#The Reflection Coefficient Assumes as 50-50% mixture of TE & TM light
        rpar=OPTICALFUNCTIONS.Rll(angle_deg_range,e_fiber,e_sample)
        rperp=OPTICALFUNCTIONS.R_l_(angle_deg_range,e_fiber,e_sample)
        R=Numeric.zeros(numbang,'f')
        for a in range(numbang):
                R[a]=(.5*rperp[a]+.5*rpar[a])
#returns an Array with angle as the only axis, the Data being the Reflection coefficient
        return R
```

def RtoNsumrangeofdia(angle_deg_range,wavenumber_range,e_fiber_range,e_sample_range,length,dia_range,mb):

```
        numbang=len(angle_deg_range)            # number of Angles assumed
        numbdia=len(dia_range)                          # number of Diameters calculated
        numbcm=len(wavenumber_range)            # number of Wavenumbers
        N=NperLavsd(angle_deg_range,dia_range)*length  # Array of Reflections per
angle per dia for lenght considered
        RNsRNb=Numeric.zeros((numbcm,numbdia+1),'f')
        RNs=Numeric.zeros((numbcm,numbdia+1),'f')
        RNb=Numeric.zeros((numbcm,numbdia+1),'f')
        Abs=Numeric.zeros((numbcm,numbdia+1),'f')
        RNsum_back=Numeric.zeros((numbcm,numbdia+1),'f')
        RNsum_sample=Numeric.zeros((numbcm,numbdia+1),'f')
        StoBtrue=Numeric.zeros((numbcm,numbdia+1),'f')
        abstrue=Numeric.zeros((numbcm,numbdia+1),'f')


        for i in range(numbcm):
        #Considers the Spectra Wavenumber by Wavenumber
                StoBtrue[i,0]=wavenumber_range[i]
                abstrue[i,0]=wavenumber_range[i]
                RNsum_back[i,0]=wavenumber_range[i]
                RNsum_sample[i,0]=wavenumber_range[i]
                RNsRNb[i,0]=wavenumber_range[i]
```

```
            Abs[i,0]=wavenumber_range[i]
            e_air=1.0+0.0j
        # Air is assumed to be equal to a vacume
            e_fiber=e_fiber_range[i]
            e_sample=e_sample_range[i]
            Rback=RperA(e_fiber,e_air,angle_deg_range,numbang)
        #Reflection Coef. per angle for Wavenumber for Air dielectric & Fiber Dielectric
            Rsample=RperA(e_fiber,e_sample,angle_deg_range,numbang)
        #Reflection Coef. per angle for Wavenumber for sample Dielectric & Fiber
Dielectric
            for d in range(numbdia):
        #Considers Each Diameter
                RNs_sum=0
                RNb_sum=0
                for a in range(numbang):
        # Considers each angle
                    RNs=pow(Rsample[a],N[a,d])
        # Refl. coef. raised to number of reflections for Sample
                    RNb=pow(Rback[a],N[a,d])
        # Refl. coef. raised to number of reflections for Air(background)
                    RNs_sum=RNs_sum+RNs
                    RNb_sum=RNb_sum+RNb
        #Sum over all angles
                RNsum_sample[i,d+1]=RNs_sum/numbang
                RNsum_back[i,d+1]=RNb_sum/numbang
        #Corrects for sumation
                RNsRNb[i,d+1]=RNs_sum/RNb_sum
        #Signal div Background
                Abs[i,d+1]=-1*Numeric.log10(RNs_sum/RNb_sum)
        # Calculate Conventional Absorbance
        for i in range(numbcm):
            for d in range(numbdia):
                temp=RNsRNb[i,d+1]*mb[i]
                StoBtrue[i,d+1]=temp
                if temp < 0.00001:
                    temp=.00001
                abstrue[i,d+1]=-1*Numeric.log10(temp)
#Conversion to list for output
        StoB=RNsRNb.tolist()
        StoBt=StoBtrue.tolist()
        #signal to background
        Absorbance=Abs.tolist()
        Absorbancet=abstrue.tolist()
        #Absorbance
        RNssum=RNsum_sample.tolist()
        #raw signal
```

```
        RNbsum=RNsum_back.tolist()
        #raw background
        #Absorbancet,
        return StoB,StoBt,Absorbance,Absorbancet,RNssum,RNbsum
```

Module FiberTest

```
import Opticalfunctions,Filefunctions,Numeric,Fiberfunctions
dir="d:\\....
Mbf="d:\\....background.txt"
Percent=1.0                     #percent ethyl alcohol for sample
                                #balance water
ethyl=[]
h2o=[]
fiber=[]
MBa=[]
FILEFUNCTIONS.openreadreflectancefile(Mbf,MBa)
MBb=FILEFUNCTIONS.getcol(MBa,1)
FILEFUNCTIONS.openreadreflectancefile(dir+'start\\e_ethylalc_atr.txt',ethyl)
FILEFUNCTIONS.openreadreflectancefile(dir+'start\\e_h2o_atr.txt',h2o)
FILEFUNCTIONS.openreadreflectancefile(dir+'start\\e_fiber.txt',fiber)
wavenumber_range=FILEFUNCTIONS.getcol(h2o,0)
e_h2o_range=[]
e_ethyl_range=[]
e_fiber_range=[]
e_sample_range=[]
#sample Dielectric
for i in range(len(wavenumber_range)):
        e_h2o=h2o[i][1]+h2o[i][2]*1j
        e_ethyl=ethyl[i][1]+ethyl[i][2]*1j
        e_h2o_range.append(e_h2o)
        e_ethyl_range.append(e_ethyl)
        #Water Dielctric
        e_fiber_range.append(fiber[i][1]+fiber[i][2]*1j)
        #fiber dielectric
        e_sample_range.append(Percent*e_ethyl+(1-Percent)*e_h2o)
angle_deg_range=Numeric.arange(1.0,90.0,1.0)# from normal
length=.01                      #meters
dia_range=Numeric.arange(0.000140,0.000150,.00001)              #meters
sb,sbt,A,At,s,b= Fiber.RtoNsumrangeofdia(angle_deg_range,
wavenumber_range,e_fiber_range,e_sample_range,length,dia_range,MBb)
#dia_range_microns=dia_range*1000000
#print e_h2o_range
dir="d:\\........"
FILEFUNCTIONS.writearraytofile(dir+"stob_probesection.txt",sb)
FILEFUNCTIONS.writearraytofile(dir+"stob_total.txt",sbt)
FILEFUNCTIONS.writearraytofile(dir+"b_probesection.txt",b)
```

```
FILEFUNCTIONS.writearraytofile(dir+"Absorbance_probesection.txt",A)
FILEFUNCTIONS.writearraytofile(dir+"Absorbance_Total.txt",At)
FILEFUNCTIONS.writearraytofile(dir+"s_probesection.txt",s)
```

Module Filefunctions

```
import string,types,Numeric,os,glob

def converttodecimal(file):
	reflect=[]
	openreadreflectancefile(file,reflect)
	reflect=multiply(reflect,1,.01)
	writearraytofile(file,reflect)

def inparam(filename):
	l=openreadtextfile(filename)
	infile=string.strip(l[0])
	outfile=string.strip(l[1])
	v=[]
	f=[]
	for i in l[2:]:
		if i[0]== "F" :
			f.append(0)
			v.append(string.atof(i[1:]))
		else:
			f.append(1)
			v.append(string.atof(i))
	return (infile,outfile,v,f)


def outparam(filename,list):
	f=open(filename,'w')
	f.write("%s\n" % list[0])
	f.write("%s\n" % list[1])
	for i in range(len(list[2])):
		if list[3][i]==0:
			outstring="F"+str(list[2][i])
			f.write("%s\n" % outstring )
		else:
			f.write("%s\n" % str(list[2][i]))
	f.close()

def writearraytofile(filename,xarray):
	f=open(filename,'w')
	for i in xarray:
		if type(i) in (types.TupleType, types.ListType):
```

```
                for j in i[:-1]:
                        if j==None:j=0
                        f.write("%8.4f\t" % j)
                i=i[-1]
        if i==None:i=0
        f.write("%6.4f\n" % i)
    f.close()

def openreadtextfile(filename):
    print "This text file is currently being read: ", filename
    f=open(filename)
    farray=f.readlines()
    f.close
    flist=[]
    for i in farray:
        i=string.strip(i)
        flist.append(i)
    return flist

def openreadreflectancefile(filename,xlist):
    print "This reflectance file is currently being read: ",filename
    f=open(filename)
    farray= f.readlines()
    f.close()
    for i in farray:
        if i[0]=='#':continue
        i= string.split(i)
        x=len(i)
        z=0
        hold=[]
        while z<x:
            hold.append(string.atof(i[z]))
            z=z+1
        xlist.append(hold)

def convertcsvtotsv(directory):
    pat=os.path.join(directory,'*.csv')# all files with csv extention
    files=glob.glob(pat)
    #print files
    for file in files:
        outname=os.path.splitext(file)[0]+'.txt'
        #print outname
        if not os.path.isfile(outname):
            #print file
            f=open(file)
            o=open(outname,'w')
```

```
                for line in f.readlines():
                        x=string.split(line,',')
                        x[0]=str(string.atof(x[0]))
                        x[1]=str(string.atof(x[1])*.01)
                        o.write(string.join(x,'\t')+'\n')
                f.close

##########################################################################
#####################################
def runallcalc(listfileofparams,avg):
        direct=openreadtextfile(listfileofparams)
        for dl in direct:
                if dl[0]=="#":continue
                d=string.strip(dl)
                x=inparam(d)
                CalculateOscillator.AnalizeFile(x[0],x[1],x[2],avg)


##########################################################################
#####################################
def combineparams(keyfile,outfile):
        flist=openreadtextfile(keyfile)
        x=len(flist)
        cx=0
        cz=0
        temp=[]
        while cx<x:
                temp.append(inparam(flist[cx]))
                cx=cx+1
        z= len(temp)
        y= len(temp[0][2])
        outar=Numeric.zeros((y,z),Numeric.Float)
        while cz<z:
                cy=0
                while cy<y:
                        outar[cy,cz]= temp[cz][2][cy]
                        cy=cy+1
                cz=cz+1
        out=outar.tolist()
        f=open(outfile,'w')
        for i in out:
                if type(i) in (types.TupleType, types.ListType):
                        for j in i[:-1]:
                                j=str(j)
                                f.write("%s\t" % j)
                        i=str(i[-1])
```

```
            f.write("%s\n" % i)
        f.close()

def Harvest(keyfile,outfile,col=0):
        flist=openreadtextfile(keyfile)
        x=len(flist)
        c=0
        y=0
        temp=[]
        out=[]
        while c<x:
                openreadreflectancefile(flist[c],temp)
                l=len(temp)
                if y<l:y=l
                if c==0:
                        h=getcol(temp,0)
                        out.append(h)
                h=getcol(temp,col)
                temp=[]
                out.append(h)
                c=c+1
        arout=listtoarray(out)
        arout=Numeric.transpose(arout)
        out=arout.tolist()
        writearraytofile(outfile,out)


def find(array,val,col=0):
        z=len(array)-1
        v=0
        if val < array[0][col]: return 0
        if val > array[z][col]: return z
        while v<z:
                if array[v][col]<=val:
                        v=v+1
                else:
                        break
        return v-1

def average(list,av=2):
        c=0
        out=[]
        w=len(list[0])
        holder=Numeric.zeros((w),Numeric.Float)
        for i in list:
                x=0
```

```
            while x < w:
                holder[x]=holder[x]+i[x]
                x=x+1
            c=c+1
            if c%av==0:
                aver=holder/av
                out.append((aver[0],aver[1]))
                holder[0]=0
                holder[1]=0
        return out

def multiply(list,col,fact=1):
        out=[]
        for i in list:
            temp=[]
            for j in i:
                if j==i[col]:
                    temp.append(j*fact)
                else:
                    temp.append(j)
            out.append((temp))
        return out

def divid(list1,list2):
        l=len(list1)
        x=0
        out=[]
        while x<l:
            if list2[x]<0.0001:
                f=list1[x]/0.0001
            else:
                f=list1[x]/list2[x]

            out.append(f)
            x=x+1
        return out

def diff(list1,list2):
        l=len(list1)
        x=0
        out=[]
        while x<l:
            out.append(list1[x]-list2[x])
            x=x+1
        return out
def diffsq(list1,list2):
```

```
        l=len(list1)
        x=0
        out=[]
        while x<l:
                out.append(pow((list1[x]-list2[x]),2.0))
                x=x+1
        return out
def getcol(list,col):
        out=[]
        for i in list:
                out.append(i[col])
        return out

##########################################################################
#########################

def ltoarrayoned(list):
        x=len(list)
        z=Numeric.zeros(x)
        c=0
        while c < x:
                z[c]=list[c]
                c=c+1
        return z

def listtoarray(list,d=2):
        if d==1:
                z=ltoarrayoned(list)
        else:
                y=len(list)
                c=0
                x=0
                while c<y:
                        h=len(list[c])
                        if x<h:
                                x=h
                        c=c+1
                z=Numeric.zeros((y,x),Numeric.Float)
                x=0
                y=0
                for i in list:
                        for j in i:
                                z[y,x]=j
                                x=x+1
                        x=0
                        y=y+1
```

```
        return z
```

Module KKreflectanalysis

```
import Filefunctions,KKtheta
KK=KKtheta
Ff=Filefunctions

#Data Files
datafile="
#datafile="c.......txt"
fnamein="d:\\......txt"
fnameout="d:\\......kkx"
low=400
high=2000
outl=400                                        #output starting wavenumber
outh=2000                                       #output ending wavenumber



def AnalizeFile(fnamein):
        reflect=[]                              #Reflection List
        Filefunctions.openreadreflectancefile(fnamein,reflect)      #Read exp. data into
list (w,r)
        reflect=Filefunctions.average(reflect,5)
        h=Filefunctions.find(reflect,high,0)                #high data element number

        l=Filefunctions.find(reflect,low,0)                 #low data element number
        Reflect=reflect[l:h]                    #new data set from low to high
        l=Filefunctions.find(Reflect,outl,0)
        h=Filefunctions.find(Reflect,outh,0)
        Reflectshort=Reflect[l:h]               #Data range for output
        return KK.KramersKronig(Reflect,Reflectshort)
#######################################################################
#######################
#                                               Main Program
#######################################################################
#######################

def main():
        if datafile<>":
                files=Filefunctions.openreadtextfile(datafile)
                l=len(files)
                for i in files:
```

```
                        if i[0]<>'#':
                                print i
                                outname=i[:-3]+'kkx'
                                Filefunctions.writearraytofile(outname,AnalizeFile(i))
                                print outname
        else:
                Filefunctions.writearraytofile(fnameout,AnalizeFile(fnamein))

if (__name__=="__main__"): main()
```

Module Kktheta

```
import umath, Opticalfunctions, Numeric
pi=umath.pi
ln=umath.log
Of=Opticalfunctions

lrlnw2=[]
srlnw2=[]

def F(v,f):
        global lrlnw2,srlnw2
        if srlnw2[f][0]==lrlnw2[v][0]:
                return 0
        else:
                return (lrlnw2[v][1]-srlnw2[f][1])/(srlnw2[f][0]-lrlnw2[v][0])

def SimpApprox(Range,f):
        Lr=len(Range)
        v=0
        Th=0.0
        while v<=Lr-3:
                aw=Range[v][0]
                cw=Range[v+2][0]
                Th=Th+(cw-aw)*(1.0/6.0)*(F(v,f)+4.0*F(v+1,f)+F(v+2,f))
                v=v+2
        return Th

def TrapApprox(Range,f):
        Lr=len(Range)
        v=0
        Th=0.0
        while v<=Lr-2:
                aw=Range[v][0]
                bw=Range[v+1][0]
```

```
            Th= Th + (bw-aw)*(.5)*(F(v,f)+F(v+1,f))
            v=v+1
        return Th


def KramersKronig(Long,Short):
        z=[]
        ws=Long[-1][0]
        LR=len(Long)
        SR=len(Short)
        global lrlnw2,srlnw2
        lrlnw2=[]
        srlnw2=[]
        for w,r in Long:
            if r==0: r=.0001
            lrlnw2.append((w**2,ln(r)))
        for w,r in Short:
            if r==0: r=.0001
            srlnw2.append((w**2,ln(r)))
        f=0
        Theta=0
        while f < SR-1:# f is the index of the wavenumber in Range
            fw=Short[f][0]          #Current Wavenumber value
            fr=Short[f][1]
            if fr==0:fr=.0001
            if f%10==0:   print fw
            if ws<>fw:
                Theta=(0.5/pi)*(lrlnw2[-1][1]-ln(fr))*(ln((ws-fw)/(ws+fw)))
        #First value in array for wavenumber v is the upper wing aproximation
            else: Theta=0
            Theta=Theta + (fw/pi)*SimpApprox(Long,f)
            n=Opticalfunctions.n1(fr,Theta)
            k=Opticalfunctions.k1(fr,Theta)
            e1=Opticalfunctions.ereal(n,k)
            e2=Opticalfunctions.eimag(n,k)
            rcal=Opticalfunctions.R2(n,k)
            z.append((fw,fr,n,k,e1,e2,Theta))
            f=f+1
        return z
```

Module LevenburgMarquardt

```
import Numeric,LinearAlgebra,string,Filefunctions
LA=LinearAlgebra

def writeprogfile(Parameters, filename='d:\\steve\\data\\atr\\path.txt'):
        pathfile = open(filename, 'w')
```

```
class ParamLog:
	def __init__(self, filename):
		self.file = open(filename, 'w')
	def addline(self, Parameters):
		format = ["%f"]*len(Parameters)
		format = string.join(format, "\t") + "\n"
		self.file.write(format % tuple(Parameters))
	def close(self):
		if self.file is not None:
			self.file.close()
			self.file = None
	def __del__(self):
		self.close()



def
Detoffit(MeasuredDataX,MeasuredDataY,Sigma,Ndatapoints,Function,Parameters,N_Pa
rameters,Fixed,N_Fit):
	Alpha=Numeric.zeros((N_Fit,N_Fit))*1.0
	Beta=Numeric.zeros(N_Fit)*1.0
	CalculatedY,DyDa =Function(Parameters,MeasuredDataX,Fixed)
	Chi_Sqr=0
	for i in range(Ndatapoints):
		dy= MeasuredDataY[i]- CalculatedY[i]
		sig2i=1/pow(Sigma[i],2.0)
		#Chi_Sqr= Chi_Sqr+pow((dy/MeasuredDataY[i]),2.0)/sig2i
		Chi_Sqr= Chi_Sqr+pow((dy),2.0)/sig2i
		dyda=DyDa[i]
		j=-1
		for l in range(N_Fit):
			j=j+1
			wt=dyda[l]*sig2i
			k=-1
			for m in range(l+1):
				k=k+1
				Alpha[j,k]= Alpha[j,k]+dyda[m]*wt
			Beta[j]=Beta[j]+wt*dy
	for j in range(N_Fit):
		for k in range(j):
			Alpha[k,j]=Alpha[j,k]
	return CalculatedY,Chi_Sqr,Alpha,Beta

def
main(MeasuredDataX,MeasuredDataY,Function,Parameters,Fixed,Lamda,Print=0,Updat
```

```
e=10,Sigma=[]):
#Fixed = 0 for fixed, 1 for variable
        Updatecounter=1
        Ndatapoints=len(MeasuredDataX)
        if Sigma==[]:
                Sigma=Numeric.ones(Ndatapoints)
        N_Parameters=len(Parameters)
        N_Fit=Numeric.sum(Fixed)
        pathlog = ParamLog('d:\\steve\\data\\atr\\path.txt')
        while 1:
                if Lamda < 0:
                        Lamda=.00001
                        CalDataY,Chi_Sqr, Alpha,
Beta=Detoffit(MeasuredDataX,MeasuredDataY,Sigma,Ndatapoints,Function,Parameters,
N_Parameters,Fixed,N_Fit)
                        OldChi_Sqr= Chi_Sqr
                        StartingX2=Chi_Sqr
                        TryParameters=[]
                        for i in range(N_Parameters):
                                TryParameters.append(Parameters[i])
                        LamdaLoopLimit=0
                Identity=Numeric.identity(N_Fit)*1.0
                Covar=Alpha*Identity*(1.0+Lamda)
                Da=Beta
                Delta=LA.solve_linear_equations(pow(Covar,2),Da)
                for i in range(len(Delta)):
                        if Delta[i]>5:Delta[i]=5
                        if Delta[i]<-5:Delta[i]=-5
                        if Delta[i]<.01 and Delta[i]>0:
                                Delta[i]=0
                        if Delta[i]>-.01 and Delta[i]<0:
                                Delta[i]=0
                j=-1
                for i in range(N_Parameters):
                        if Fixed[i]==0:
                                TryParameters[i]=Parameters[i]
                        else:
                                j=j+1
                                TryParameters[i]=Parameters[i]+Delta[j]
                                while TryParameters[i]<0.01:
                                        TryParameters[i]=TryParameters[i]-Delta[j]*.1
                                while TryParameters[i]>10000:
                                        TryParameters[i]=TryParameters[i]-Delta[j]*.1


        CalDataY,Chi_Sqr,Alpha,Beta=Detoffit(MeasuredDataX,MeasuredDataY,Sigma,
```

```
Ndatapoints,Function,TryParameters,N_Parameters,Fixed,N_Fit)
                if Print==1:

                        print "Old CHi_Sqr", OldChi_Sqr
                        print "trial Chi_Sqr: ",Chi_Sqr
                if Chi_Sqr < OldChi_Sqr:

                        for i in range(N_Parameters):
                                Parameters[i]=TryParameters[i]
                        #print Parameters
                        pathlog.addline(Parameters)
                        if Print==1:
                                print "improvement in Chi_SQr:", OldChi_Sqr-Chi_Sqr
                                if Updatecounter%Update==0:

        t=map(None,MeasuredDataX,MeasuredDataY,CalDataY)
                                        Filefunctions.writearraytofile("d:\\temp\\test.txt",t)
                        Updatecounter=Updatecounter+1
                        Average_Chi_Sqr=Chi_Sqr/Ndatapoints
                        if Print==1:print "Improvement has been made"
                        #if (OldChi_Sqr-Chi_Sqr)< .000001:
                                #if Print==1:print "end due to small changes"
                                #break
                        if Average_Chi_Sqr< .00001:
                                print "Average_Chi_Sqr: ",Average_Chi_Sqr
                                if Print==1:print "end due to low avergeX2"
                                break
                        OldChi_Sqr=Chi_Sqr
                        Alpha=Covar
                        Beta=Da
                        Lamda=Lamda/10.0
                        LamdaLoopLimit=0
                else:
                        Chi_Sqr = OldChi_Sqr
                        d=1
                        if LamdaLoopLimit==20 :
                                if Print==1:print "Looped out"
                                break
                        else:
                                LamdaLoopLimit=LamdaLoopLimit+1
                                if Print==1:print "Increase Lamda"
                                #print "Lamda loop counter= ",LamdaLoopLimit
                                Lamda=Lamda*10.0
        Average_Chi_Sqr=Chi_Sqr/Ndatapoints
        #print "Starting Chi_Sqr: ",StartingX2
        #print "final Chi_Sqr: ",
```

```
        #print "Average_Chi_Sqr",Average_Chi_Sqr
        return Parameters,Chi_Sqr
```

Module MixxedATR

```
"""This program will run the analizefile function given the input
parameter file"""

import Filefunctions,CalculateOscillator, Numeric
import Opticalfunctions

Of=Opticalfunctions
Ff=Filefunctions
co=CalculateOscillator

def mixxedATR(Ph2o,datafile1,datafile2,outputfile):
        h2o=[]
        eth=[]
        Filefunctions.openreadreflectancefile(datafile1,h2o)
        Filefunctions.openreadreflectancefile(datafile2,eth)
        ratioll=0.5
        angle_deg=45
        R=[]
        re=[]
        I=[]
        w= Filefunctions.getcol(h2o,0)
        eth1=Filefunctions.getcol(eth,4)
        eth2=Filefunctions.getcol(eth,5)
        h2o1=Filefunctions.getcol(h2o,4)
        h2o2=Filefunctions.getcol(h2o,5)
        for i in range(len(w)):
                r= Ph2o*h2o1[i]+(1-Ph2o)*(eth1[i])
                im=Ph2o*h2o2[i]+(1-Ph2o)*(eth2[i])
                c=r+im*1j
                re.append(r)
                I.append(im)
                R.append(Opticalfunctions.ATRfunction(ratioll,angle_deg,w[i],c))
        out=map(None,w,R,re,I)
        Filefunctions.writearraytofile(outputfile,out)
def main():                                     #Main program
        p=1.1
        while p<1:
                t=str(p*100)
                file='calmix1'+t[:2]+'.txt'
                print file
                p=p+.05
```

```
            mixxedATR(p,file)
        datafile1='d:\\Steve\\Data\\atr\\apr27\\c\\h2opf.cal'
        datafile2='d:\\Steve\\Data\\atr\\apr27\\c\\ethylalc.cal'
        mix='mixpf'
        outputfile='d:\\steve\\data\\atr\\apr27\\'+mix+'\\mix2575.cal'
        percentdf1=0.75
        mixxedATR(percentdf1,datafile1,datafile2,outputfile)

        outputfile='d:\\steve\\data\\atr\\apr27\\'+mix+'\\mix5050.cal'
        percentdf1=0.5
        mixxedATR(percentdf1,datafile1,datafile2,outputfile)

        outputfile='d:\\steve\\data\\atr\\apr27\\'+mix+'\\mix7525.cal'
        percentdf1=0.25
        mixxedATR(percentdf1,datafile1,datafile2,outputfile)
        #mixxedATR(.75,'cal3mix75.txt')
        #mixxedATR(.25,'cal3mix25.txt')

if (__name__=="__main__"): main()
```

Module Opticalfunctions

```
import umath,Numeric,cephes
##############################################################################
#########################################
def ncomplex(e):
        return umath.sqrt(e)
def R1(ncomp):
        r=(ncomp-1)/(ncomp+1)
        R= r*umath.conjugate(r)
        if type(R) == type(1j):
            return R.real
        else: return R
def R2(n,k):
        return ((n-1)**2+k**2)/((n+1)**2+k**2)
def R3(e):
        ncomp=ncomplex(e)
        return R1(ncomp)
def n1(R,Theta):
        r=umath.sqrt(R)
        return (1-R)/(1-2*r*umath.cos(Theta)+R)
def k1(R,Theta):
        r=umath.sqrt(R)
        return 2*r*umath.sin(Theta)/(1-2*r*umath.cos(Theta)+R)
def n2(er,ei):
        return (.5*((er**2+ei**2)**.5+er))**.5
```

```
def k2(er,ei):
        return (.5*((er**2+ei**2)**.5-er))**.5
def ereal(n,k):
        return pow(n,2)-pow(k,2)
def eimag(n,k):
        return 2*n*k
def Ecomplex(n,k):
        return ereal(n,k) +eimag(n,k)*j
def Theta1(ncomp):
        k=ncomp.imag
        n=ncomp.real
        return umath.arctan((2*k)/(pow(n,2)+pow(k,2)-1))
##########################################################################
##############################################
def lorent((a0,a1,a2),w):
        return a0/(1.0+((w-a1*1.0)/a2*1.0)**2)
def Lorentziancomplex((os,wo,gamma),w):
        return os/(wo**2-w**2-1j*gamma*w)
def Lorentziandispertion((gamma,wo,os),w):
        return os*(wo**2-w**2)/((wo**2-w**2)**2+gamma**2*w**2)
def Lorentzian((gamma,wo,os),w):
        return os*gamma*w/((wo**2-w**2)**2+gamma**2*w**2)
def ecomplexlorentzian(Parameters,w):
        e0=Parameters[0]
        e=0
        Parameters=Parameters[1:]
        while Parameters:
                oscparam = Parameters[:3]
                e=e+map(lambda
x,oscparam=oscparam:Lorentziancomplex(oscparam,x),w)
                Parameters=Parameters[3:]
        Ecomplex=map(lambda x,e0=e0:e0+x,e)
        return Ecomplex

def GaussArea((a0,a1,a2),x,GetDerivatives=[0,0,0]):
        if a0==0:a0=1e-10
        if a1==0:a1=1e-10
        if a2==0:a2=1e-10
        p=pow(2,0.5)/2
        o=1/(Numeric.pi*a2)
        z=pow(((x-a1)/a2),2)
        ex=umath.exp(-.5*z)
        value=p*o*ex*a0
        d=[]
        if GetDerivatives[0]==1:d.append(value/a0)
        if GetDerivatives[1]==1:d.append(p*o*a2/a1*(ex*(z-1)))
```

```
        if GetDerivatives[2]==1:d.append(p*o*ex*(x-a1)*a2/pow(a1,2))
        return value,d

def GaussAmp((a0,a1,a2),x,GetDerivatives=[0,0,0]):
        if a0==0:a0=1e-10
        if a1==0:a1=1e-10
        if a2==0:a2=1e-10
        z=pow(((x-a1)/a2),2)
        ex=umath.exp(-.5*z)
        value=ex*a0
        d=[]
        if GetDerivatives[0]==1:d.append(ex)
        if GetDerivatives[1]==1:d.append(value*(x-a1)/pow(a2,2))
        if GetDerivatives[2]==1:d.append(value*z/a2)
        return value,d

def GaussAmpDispertion((a0,a1,a2),x,GetDerivatives=[0,0,0]):
        if a0==0:
                print a0,a1,a2
                a0=1e-10
        if a1==0:
                print a0,a1,a2
                a1=1e-10
        if a2==0:
                print a0,a1,a2
                a2=1e-10
        j=pow(2,0.5)*a2
        z1=(x-a1)/j
        z2=(x+a1)/j
        p=2.0/pow(Numeric.pi,0.5)
        dawz1=cephes.dawsn(z1)
        dawz2=cephes.dawsn(z2)
        value=a0*p*(dawz2-dawz1)
        d=[]
        if GetDerivatives[0]==1:d.append(p*(dawz2-dawz1))
        if
GetDerivatives[1]==1:d.append((p*a0/a2)*(x*pow(2,0.5)/a2+2*pow(z2,2)*dawz2+2*po
w(z1,2)*dawz1))
        if GetDerivatives[2]==1:d.append(-p*a0*pow(2,0.5)/a2*(z1*dawz1+z2*dawz2))
        return value,d
##########################################################################
#####################################
def ERealGauss(Parameters,Wavenumber,GetDerivatives=[]):
        d=[]
        value=Parameters[0]
        if GetDerivatives==[]:
```

```
            GetDerivatives= Numeric.zeros(len(Parameters))
        if GetDerivatives[0]==1: d.append(1)
        Parameters=Parameters[1:]
        GetDerivatives=GetDerivatives[1:]
        while Parameters:

        eh,dh=GaussAmpDispertion(Parameters[:3],Wavenumber,GetDerivatives[:3])
            value=value+eh
            for i in dh:
                d.append(i)
            Parameters=Parameters[3:]
            GetDerivatives=GetDerivatives[3:]
        return value,d

def EImagGauss(Parameters,Wavenumber,GetDerivatives):
        value=0.0
        d=[]
        if GetDerivatives[0]==1:
            d.append(0)
        Parameters=Parameters[1:]
        GetDerivatives=GetDerivatives[1:]
        while Parameters:
            eh,dh=GaussAmp(Parameters[:3],Wavenumber,GetDerivatives[:3])
            value=value+eh
            for i in dh:
                d.append(i)
            Parameters=Parameters[3:]
            GetDerivatives=GetDerivatives[3:]
        return value,d

def EComplexGauss(Parameters,WavenumberList,GetDerivatives=[]):
        Ecomplex=[]
        dErList=[]
        dEiList=[]
        if GetDerivatives==[]:
            GetDerivatives= Numeric.zeros(len(Parameters))
        for i in WavenumberList:
            Er,dEr=ERealGauss(Parameters,i,GetDerivatives)
            Ei,dEi=EImagGauss(Parameters,i,GetDerivatives)
            Ecomplex.append(complex(Er,Ei))
            dErList.append(dEr)
            dEiList.append(dEi)
        if Numeric.sum(GetDerivatives)<>0:
            return Ecomplex,dErList,dEiList
        else: return Ecomplex
##########################################################################
```

```
#####################################
def Rderivative(er,ei,der,dei):
        k= pow(pow(er,2)+pow(ei,2),0.5)
        k_er_srt=pow(k+er,0.5)
        sqr_2=pow(2,0.5)
        denom=  pow(k+(k_er_srt)*sqr_2+1,2)*(k_er_srt*k)
        numer=-sqr_2*(-er*k+pow(ei,2)+er-pow(er,2)+k)
        numei=sqr_2*ei*(k-1+2*er)
        drdv=[]
        for i in range(len(der)):
                if denom==0:
                        drdv.append(1000000)
                else:
                        drdv.append((der[i]*numer+dei[i]*numei)/denom)
        return drdv

def Rparm(Parameters,WavenumberList,GetDerivatives=[]):
        if GetDerivatives==[]:
                GetDerivatives=Numeric.zeros(len(Parameters))
        Ecomplex,der,dei=EComplexGauss(Parameters,WavenumberList,GetDerivatives)
# calculate ecomplex from given variables
        ei=map(lambda x:x.imag,Ecomplex)                # e2
        er=map(lambda x:x.real,Ecomplex)                # e1
        ncomp=map(ncomplex,Ecomplex)                            # n*
        #n=map(lambda x:x.real,ncomp)                           # n
        #k=map(lambda x:x.imag,ncomp)                           # k
        rcal=map(R1,ncomp)
        drdv=[]
        for j in range(len(ei)):
                for i in GetDerivatives:
                        if i==1:
                                drdv.append(Rderivative(er[j],ei[j],der[j],dei[j]))

        return rcal,drdv
def TRparm(Parameters,WavenumberList): #returns T and R for materials that transmit
        thickness=Parameters[0]
        Sigmarms=Parameters[1]
        Parameters=Parameters[2:]
        Ecomplex=EComplexGauss(Parameters,WavenumberList)
        ei=map(lambda x:x.imag,Ecomplex)                # e2
        er=map(lambda x:x.real,Ecomplex)                # e1
        ncomp=map(ncomplex,Ecomplex)                            # n*
        rcal=map(R1,ncomp)
        RFlist=roughnessfactor(Sigmarms,WavenumberList)
        T=[]
        R=[]
```

```
        nr=[]
        ni=[]
        alph=[]
        for i in range(len(WavenumberList)):
                rc=rcal[i]*RFlist[i]
                alpha=Alpha(ncomp[i],WavenumberList[i])
                loss=Numeric.exp(-1.0*alpha*thickness)
                n=pow(1-rc,2)*loss
                d=1-rc*rc*Numeric.exp(-2.0*alpha*thickness)
                t=n/d
                T.append(t)
                nr.append(ncomp[i].real)
                ni.append(ncomp[i].imag)
                alph.append(alpha)
                r=rc*(1+t*loss)
                R.append(r)
        return T,R,nr,ni,alph,er,ei


def Rll(angle_deg,et,ei):#Electric field parallel to interface or TE
        angle_rad=angle_deg*Numeric.pi/180
        Cos_angle=Numeric.cos(angle_rad)
        Sin_angle=Numeric.sin(angle_rad)
        e=ei/et
        a=e*Cos_angle
        b=pow(e-pow(Sin_angle,2.0+0j),0.5)
        r=(a-b)/(a+b)
        return Numeric.absolute(pow(r,2))
def R_l_(angle_deg,et,ei):#Electric field perpendicular to interface or TM
        angle_rad=angle_deg*Numeric.pi/180
        Cos_angle=Numeric.cos(angle_rad)
        Sin_angle_sqr=pow(Numeric.sin(angle_rad),2)
        e=ei/et
        a=Cos_angle
        z= e-Sin_angle_sqr
        b=pow(z,0.5)
        r=(a-b)/(a+b)
        return Numeric.absolute(pow(r,2))
def T_l_(angle_deg,nt,ni):
        return (1-R_l_(angle_deg,nt,ni))
def Tll(angle_deg,nt,ni):
        return (1-Rll(angle_deg,nt,ni))
def Alpha(nt,wavenumber):
        #Alpha is returned in units of 1/cm
        k=nt.imag
        return 4.0*Numeric.pi*k*wavenumber
```

```
def Absorptance(Alpha,t):
        # Absorbance is the ratio if Inensity out/ Intensity in
        # it Does not account for reflectance
        return 1-Numeric.exp(-1.0*Alpha*t)
def Transmition(n,w,x):
        alpha=Alpha(n,w)
        r=R1(n)
        n=Numeric.exp(-1.0*alpha*x)*(pow(1-r,2))
        d=1-r*r*Numeric.exp(-2.0*alpha*x)
        return(n/d)


##########################################################################
#############################################
#angle_deg is the angle of incidence (from nornal) in degrees
#nt is index of refraction for medium that the light is transmitting through
#ni is index of refraction for medium that the light is incedent on
#wavenumber is the Wavenumber in units of 1/cm
#t is the thickness of the sample in cm
def ZnSe(w):# return the index of refraction for ZnSe using the Salmyer(sp?) coeficients
        a0=4.2980149
        a1=0.192063
        a2=0.62776557
        a3=0.3787826
        a4=2.8955633
        a5=46.994595
        l=10000.0/w
        l_sqr=pow(l,2.0)
        f0=a0*l_sqr/(l_sqr-pow(a1,2.0))
        f1=a2*l_sqr/(l_sqr-pow(a3,2.0))
        f2=a4*l_sqr/(l_sqr-pow(a5,2.0))
        return pow(1+f0+f1+f2,0.5)
##########################################################################
#############################################
def ATRsample(Parameters,WavenumberList,GetDerivatives=[]):# assumes 50:50
polarization
        if GetDerivatives==[]:
                GetDerivatives=Numeric.zeros(len(Parameters))
        ATR=[]
        angle_deg= Parameters[0]
        angle_rad=angle_deg*Numeric.pi/180.0
        Cos_angle=Numeric.cos(angle_rad)
        Sin_angle=Numeric.sin(angle_rad)
        Sin_angle_sqr=pow(Sin_angle,2.0)
        Parameters=Parameters[1:]
        GetDerivatives=GetDerivatives[1:]
```

```
        ratioll=0.5
        if Numeric.sum(GetDerivatives)<>0:

        Ecomplex,der,dei=EComplexGauss(Parameters,WavenumberList,GetDerivatives)
                eznse=map(lambda x:pow(ZnSe(x),2.0),WavenumberList)
                dfdv=[]
                for i in range(len(Ecomplex)):
                        esr=Ecomplex[i].real
                        esi=Ecomplex[i].imag

        f,df=funcATR(ratioll,esr,esi,eznse[i],Cos_angle,Sin_angle_sqr,der[i],dei[i],GetDe
rivatives)
                        ATR.append(f)
                        dfdv.append(df)
                return ATR,dfdv
        else:
                Ecomplex=EComplexGauss(Parameters,WavenumberList)
                ei=[]
                er=[]
                for i in range(len(Ecomplex)):

        ATR.append(ATRfunction(0.5,angle_deg,WavenumberList[i],Ecomplex[i]))
                        ei.append(Ecomplex[i].imag)
                        er.append(Ecomplex[i].real)
                return ATR,er,ei
def sign(x):
        if x<0:return -1.0
        return 1.0
def funcfg(esr,esi,eznse,Cos_angle,GetDerivatives=[]):
        arg=Cos_angle/eznse
        f=esr*arg
        g=esi*arg
        return f,g
def funcb(esr,eznse,Sin_angle_sqr):
        b= esr/eznse-Sin_angle_sqr
        return b
def funcd(esi,eznse):
        d=esi/eznse
        return d
def funcnm(b,d):
        halfphi= Numeric.arctan2(d,b)*0.5
        h=pow(b*b+d*d,0.25)
        n=h*Numeric.cos(halfphi)
        m=h*Numeric.sin(halfphi)
        return n,m
def funcdndm(d,b,n,m,db,dd):
```

```
        h1=b*db+d*dd/(2*(pow(b,2)+pow(d,2)))
        h2=(dd/b+d*db/pow(b,2))/(2*(1+pow(d/b,2)))
        dn=n*h1-m*h2
        dm=m*h1+m*h2
        return dn,dm
def funcATRderivative(ratioll,a,b,d,n,m,f,g,eznse,Cos_angle,R_l_,Rll,value,desr,desi):
        dvar=desr+desi
        db=desr/eznse
        dd=desi/eznse
        dn,dm=funcdndm(d,b,n,m,db,dd)
        df,dg=funcfg(desr,desi,eznse,Cos_angle)#same function as f,g
        denom_l_=pow(a+n,2.0)+pow(m,2.0)
        h1=-2.0*((a-n)*dn+m*dm)/denom_l_
        h2=(R_l_)*2.0*((a+n)*dn+m*dm)/denom_l_
        dR_l_=h1-h2
        denomll=(pow(f+n,2.0)+pow(g+m,2.0))
        h3=2*((f-n)*(df-dn)+(g-m)*(dg-dm))/denomll
        h4=Rll/denomll*2.0*((f+n)*(df+dn)+(g+m)*(dg+dm))
        dRll=h3-h4
        df=10.0*pow(((1-ratioll)*R_l_+ratioll*Rll),9.0)*(ratioll*dRll+(1-ratioll)*dR_l_)
        return df

def
funcATR(ratioll,esr,esi,eznse,Cos_angle,Sin_angle_sqr,desr=[],desi=[],GetDerivatives=[
]):
        f,g=funcfg(esr,esi,eznse,Cos_angle)
        a=Cos_angle
        b=funcb(esr,eznse,Sin_angle_sqr)
        d=funcd(esi,eznse)
        n,m=funcnm(b,d)
        R_l_= (pow(a-n,2.0)+pow(m,2.0))/((pow(a+n,2.0)+pow(m,2.0)))
        Rll= (pow(f-n,2.0)+pow(g-m,2.0))/(pow(f+n,2.0)+pow(g+m,2.0))
        value=(pow(ratioll*Rll+(1.0-ratioll)*R_l_,10.0))
        dvaldvar=[]
        if Numeric.sum(GetDerivatives)<>0:
                x=0
                for i in GetDerivatives:
                        if i==1:

        dvaldvar.append(funcATRderivative(ratioll,a,b,d,n,m,f,g,eznse,Cos_angle,R_l_,R
ll,value,desr[x],desi[x]))
                                x=x+1
                return value,dvaldvar
        else:return value

def ATRfunction(ratioll,angle_deg,w,esample):
```

```
        et=pow(ZnSe(w),2.0)
        Rpar=Rll(angle_deg,et,esample)
        Rperp=R_l_(angle_deg,et,esample)
        value=(pow(ratioll*Rpar+(1.0-ratioll)*Rperp,10.0))
        return value
##########################################################################
##########################################
def roughnessfactor(sig,wavenumberlist):

        #sig is rms value of roughness in units of nm
        sigcm=0.0000001*sig
        pi=Numeric.pi
        temp=4*pi*sigcm
        r=[]
        for i in wavenumberlist:
                r.append(Numeric.exp(-pow(temp*i,2)))
        return r
```

Module Runfitonparamfile

```
"""This program will run the analizefile function given the input
paramiter file"""

import Filefunctions,CalculateOscillator, Numeric
import Opticalfunctions
import UniversalFitter
UF=UniversalFitter
Of=Opticalfunctions
import LevenbergMarquardt
LM=LevenbergMarquardt
Ff=Filefunctions
co=CalculateOscillator

def analparamfilepupdate(paramfile,average,low,high):
        x=Filefunctions.inparam(paramfile)
        reflect=[]
        Filefunctions.openreadreflectancefile(x[0],reflect)
        reflect.sort()
        reflect=Filefunctions.average(reflect,average)                    #Average out
data
        h=Filefunctions.find(reflect,high,0)                #High data element number

        l=Filefunctions.find(reflect,low,0)                 #Low data element number
        reflect=reflect[l:h]                    #Truncate from Low to High Data
        w= Filefunctions.getcol(reflect,0)                          #
        r= Filefunctions.getcol(reflect,1)
```

```
        N_param=len(x[3])
        print x[2]
        Vars=x[2]
        #Vars,
Error=LEVENBERGMARQUARDT.main(w,r,Opticalfunctions.Rparm,x[2],x[3],-1,1)
        #y=[]
        #y.append(x[0])
        #y.append(x[1])
        #y.append(Vars)
        #y.append(x[3])
        #Filefunctions.outparam(paramfile,y)
        CalculateOscillator.outputfilecomparison(w,r,x[1],Vars)

def main():                                     #Main program
        paramfile="d:\\............."
        average=5
        low=400
        high=4000
        analparamfilepupdate(paramfile,average,low,high)

if (__name__=="__main__"): main()
```

Module Roughness

```
import Numeric,Filefunctions,string, Opticalfunctions
Ff=Filefunctions
def a(file,sig,average=1):
        reflect=[]
        Filefunctions.openreadreflectancefile(file,reflect)
        reflect=Filefunctions.average(reflect,average)
        w= Filefunctions.getcol(reflect,0)
        r= Filefunctions.getcol(reflect,1)
        roufac=Opticalfunctions.roughnessfactor(sig,w)
        R=[]
        for i in range(len(r)):
                if roufac[i]==0: R.append(r[i])
                else:R.append(r[i]/roufac[i])
        return map(None,w,r,R)

def absRefwrough(paramfile):
        l=Filefunctions.openreadtextfile(paramfile)
        infile=string.strip(l[0])
        outfile=string.strip(l[1])
        rms=string.atof(l[2])
        average=string.atof(l[3])
        Filefunctions.writearraytofile(outfile,a(infile,rms,average))
```

```
def main():                                     #Main program
        x=1
        if x==1:
                paramfile='D:\\..........'
                absRefwrough(paramfile)
        else:
                keyfile='D:\\.............'
                flist=Filefunctions.openreadtextfile(keyfile)
                x=len(flist)
                c=0
                while c<x:
                        paramfile= flist[c]
                        absRefwrough(paramfile)
                        c=c+1

if (__name__=="__main__"): main()
```

Module RunATRFIT

```
"""This program will run the analizefile function given the input
parameter file"""

import Filefunctions,CalculateOscillator, Numeric
import Opticalfunctions
import UniversalFitter
UF=UniversalFitter
Of=Opticalfunctions
import LevenbergMarquardt
LM=LevenbergMarquardt
Ff=Filefunctions
co=CalculateOscillator

def ATR(paramfile,average,low,high):
        x=Filefunctions.inparam(paramfile)
        sig=[]
        Filefunctions.openreadreflectancefile(x[0],sig)
        sig.sort()
        sig=Filefunctions.average(sig,average)                  #Average out data
        h=Filefunctions.find(sig,high,0)                #High data element number

        l=Filefunctions.find(sig,low,0)                 #Low data element number
        sig=sig[l:h]                    #Truncate from Low to High Data
        w= Filefunctions.getcol(sig,0)                          #
        s= Filefunctions.getcol(sig,1)
        Vars=x[2]
        #for a in Vars:
```

```
        fix= x[3]
        #for i in range(len(fix)):
        #       fix[i]=0
        #for i in range(len(fix)):
        #       if i>1:
        #               fix[i]=1
        #               print fix
        #Vars,
Error=LEVENBERGMARQUARDT.main(w,s,Opticalfunctions.ATRsample,x[2],fix,-
1,1,5)
        #               fix[i]=0
        print Vars
        y=[]
        y.append(x[0])
        y.append(x[1])
        y.append(Vars)
        y.append(x[3])
        Filefunctions.outparam(paramfile,y)
        #print Error
        R,er,ei=Opticalfunctions.ATRsample(Vars,w)
        diff=Filefunctions.diff(s,R)
        perdiff=Filefunctions.divid(diff,s)
        out=map(None,w,s,R,diff,perdiff,er,ei)
        Filefunctions.writearraytofile(x[1],out)



def main():                                     #Main program
        paramfile='c:\\.....'
        average=5
        low=650
        high=4000
        ATR(paramfile,average,low,high)
```

LIST OF REFERENCES

1. Potts, L.W., *Quantitative Analysis: Theory and Practice*. 1987, New York: Harper & Row Publishers.
2. Ewing, G.W., *Instrumental Methods of Chemical Analysis*. 1975, New York: McGraw-Hill Book Company.
3. Nazarewicz, W., *et al.*, *Abac Chart for Fast Calculation of the Absorption and Reflection Coefficients.* Applied Optics, 1962. **1**(3): p. 369.
4. Andermann, G., A. Caron, and D.A. Dows, *Kramers-Kronig Dispersion Analysis of Infrared Reflectacne Bands.* Journal of the Optical Society of America, 1965. **55**(10): p. 1210-1216.
5. Adiga, R., A.A. Barkatt, and D.E. Clark, *Leach Behavior of a Defense Waste Glass Under Static and Dynamic Conditions*, in *Advances in Ceramics.* 1986. p. 487-494.
6. Bunker, B.C., G.W. Arnold, and E.K. Beauchamp, *MECHANISMS FOR ALKALI LEACHING IN MIXED-Na-K SILICATE GLASSES.* Journal of Non-Crystalline Solids, 1983. **58**: p. 295-322.
7. Bunker, B.C., *et al.*, *EFFECT OF MOLECULAR STRUCTURE ON BOROSILICATE GLASS LEACHING.* Journal of Non-Crystalline Solids, 1986. **87**: p. 226-253.
8. Bunker, B.C., *Molecular mechanisms for corrosion of silica and silicate glasses.* Journal of Non-Crystalline Solids, 1994. **179**: p. 300-308.
9. Christensen, H., *et al.*, *Leaching of Simulated Nuclear Waste Glass under Dynamic Conditions*, in *Advances in Ceramics*. 1986. p. 475-485.
10. Clark, D.E. and E.L. Yen-Bower, *Corrosion of Glass Surfaces.* Surface Science, 1980. **100**((1980)): p. 53-70.
11. Dieold, F.E. and J.K. Bates, *Glass- Water Vapor Interaction*, in *Advances in Ceramics*. 1986. p. 515-522.
12. Houser, C.A., I.S.T. Tsong, and W.B. White, *ION-BEAM DEPTH-PROFILING STUDIES OF LEACHED GLASSES.* RADIATION EFFECTS, 1982. **64**: p. 103-108.
13. Sprenger, D., *et al.*, *XPS Study of leached glass surfaces.* Journal of Non-Crystalline Solids, 1990. **126**: p. 111-129.

14. Sprenger, D., *et al.*, *Discrete bond Model (DBM) of sodium silicate glasses derived from XPS, Raman and NMR measurements.* Journal of Non-Crystalline Solids, 1993. **159**: p. 187-203.
15. Clark, D.E., *et al.*, *Quantitative analysis of corroded glass using infrared frequency shifts.* Glass Technology, 1977. **18**(4): p. 121-124.
16. Salem, A.A., R. Kellner, and M. Grasserbauer, *Study of corrosion processes in glass by a multitechnique approach. Part 2. Infrared spectroscopy.* Glass Technology, 1994. **35**(3): p. 135-140.
17. Sanders, D.M., W.B. Person, and L.L. Hench, *New Methods Studying Glass Corrosion Kinetics.* Aplied Spectroscopy, 1972. **26**(5): p. 530-536.
18. Sanders, D.M., W.B. Person, and L.L. Hench, *Quantitative Analysis of Glass Structure with the Use of Infrared Reflection Spectra.* Applied Spectroscopy, 1974. **28**(3): p. 247-255.
19. Zellmer, L.A. and W.B. White, *Characterization of Hydrated Surface Layers on Nuclear Waste Glasses by Infrared Reflectance Spectroscopy.* Material Research Society Symposium Proceedings, 1985. **44**: p. 74-80.
20. Burns, A., H.P. Brack, and W.M.J. Risen, *Dielectric and infrared reflectance studies of inorganic oxide glasses.* Journal of Non-Crystalline Solids, 1991. **131-133**: p. 994-1000.
21. Efimov, A.M. and E.G. Makarova, *Dispersion Equation For The Complex Dielectric Constant Of Vitreous Materials And The Dispersion Analysis Of Their Reflection Spectra.* Fizika i Khimiya Stek-la, 1985. **11**(4): p. 385-401.
22. Gervais, F., *et al.*, *Infrared Reflectivity spectroscopy of silicate glasses.* Journal of Non-Crystalline Solids, 1987. **89**: p. 384-401.
23. White, G.S., D.C. Greenspan, and S.W. Freiman, *Corrosion and Crack Growth in 33% Na2O-67% SiO2 and 33% Li2o-67% Sio2 Glasses.* Journal of the American Ceramics Society, 1986. **69**(1): p. 38-44.
24. Galeener, F.L., A.J. Leadbetter, and M.W. Stringfellow, *Comparison of the neutron, Raman, and Infrared vibrational spectra of vitreous SiO2, GeO2 and BeF2.* Physical Review B, 1983. **27**(2): p. 1052-1078.
25. Husung, R.S. and R.H. Doremus, *The infrared transmission of four silicate glasses before and after exposure to water.* Journal of Material Research, 1990. **5**(10, Oct 1990): p. 2209-2217.
26. Philipp, H.R., *Silicon Dioxide (SiO2)(Glass)*, in *Handbook of Optical Constants.* 1985, Academic Press Inc. p. 749-763.
27. Poerteus, J.O., *Relation between the Height Distribution of a Rough Surface and the Reflectance at Normal Incidence.* Journal of the Optical Society of America, 1963. **53**(12): p. 1394-1402.
28. Matson, D.W., S.K. Sharma, and J.A. Philpotts, *The Structure of High-Silica Alkali-Silicate Glasses. A Raman Spectroscopic investigation.* Journal of Non-Crystalline Solids, 1983. **58**: p. 323-352.
29. Philipp, H.R., *Silicon Dioxide (SiO2) Type a(Crystalline)*, in *Handbook of Optical Constants.* 1985, Academic Press Inc. p. 719-747.
30. Varshneya, A.K., *Fundamentals of Organic Glasses*, . 1994, Academic Press, Inc. p. 99-104.

31. Merzbacher, C.I. and W.B. White, *The structure of alkaline earth alumionosilicate glasses as determined by vibrational spectroscopy*. Journal of Non-Crystalline Solids, 1991. **130**: p. 18-34.
32. Almeida, R.M., T.A. Guiton, and C.G. Pantano, *Characterization of Silica gels By Infrared Reflection Spectroscopy.* Journal of Non-Crystalline Solids, 1990. **121**: p. 193-197.
33. Wallace, S., J.K. West, and L.L. Hench, *Interactions of Water with Trisiloxane rings. I. Experimental analysis.* Journal of Non-Crystalline Solids, 1993. **152**: p. 101-108.
34. Furukawa, T., K.E. Fox, and W.B. White, *Raman spectroscopic investigation of the structure of silicate glasses. III. Raman intensities and structural units in sodium silicate glasses.* Journal of Chem. Phys., 1981. **75**(7): p. 3326-3237.
35. Darby, G., D. Clark, and J. Simmons, *FT-IRRS Analysis of Surface Reactions in Alkali Silicate Glasses*, in *Proceedings of American Ceramics Society 1999 Cocoa Beach Meeting*. 2000. p. 141-151.
36. Glebov, L.B., *et al.*, *Effects of Leaching on the Reflection and Luminescence Spectra of Na2O-3SiO2 Glass in the Fundamental Absorption Region.* Fizika i Khimiya Stekla, 1985. **11**(3): p. 363-368.
37. Bennett, H.E. and J.O. Porteus, *Relation Between Surface Roughness and Specular Reflectance at Normal Incidence.* J. of the Optical Society of America, 1960. **51**(2): p. 123.
38. Bennett, *Specular Reflectance of Aluminized Ground Glass and the Heigh Distribution of Surface Irregularities.* Journal of the Optical Society of America, 1963. **53**(12): p. 1389-1394.
39. Ohlidal, I., *Expression for reflectance of randomly rough surfaces derived with Fresnel approximation.* Applied Optics, 1980. **19**(11): p. 1804.
40. Heitmann, D. and V. Permien, *Determination of Surface Roughness from Light Scattering Measurements.* Optics Communications, 1977. **23**(1): p. 131-134.
41. Schey, J.A., *Introduction to Manufacturing Processes*. 1987, New York: McGraw-Hill Book Company.
42. Baulsir, C.F., *Multiple Reflection versus Single Reflection ATR Accessories*, , Spectra-Tech, Inc: Shelton, CT.
43. Querry, M., D.M. Wieliczka, and D.J. Segelstein , *Water(H2O)*, in *Handbook of Optical Constants of Solids II*. 1991, Academic Press. p. 1059.
44. Ward, L., *Zinc Selenide(ZnSe)/Zinc Telluride(ZnTe)*, in *Handbook of Optical Constants of Solids II*. 1991, Academic Press: New York, NY. p. 745.
45. Yamamoto, K. and H. Ishida, *Optical Theory applied to infrared spectroscopy.* Vibrational Spectroscopy, 1994. **8**: p. 1-36.
46. Muller, G., K. Abraham, and M. Schaldach, *Quantitative ATR spectroscopy: some basic considerations.* Applied Optics, 1981. **20**(7): p. 1182.
47. Hocde, S., *et al. Remote Analysis using IR glass fibers*. in *SPIE*. 1999. Boston, MA.
48. Zhang, X.H., *et al.*, *Low loss fibers of the tellurium halide-based glasses, the TeX glasses.* Journal of Non-Crystalline Solids, 1993. **161**: p. 327-330.

49. Tai, H., H. Tanaka, and T. Yashino, *Fiber-optic evanescent wave methane-gas sensor using optical absorption for the 3.392 -mm line of a He-Ne laser.* Optical Letters, 1987. **12**(6): p. 437.
50. Paul, P. and G. Kychakoff, *Fiber-optic evanescent field absorption sensors.* Appl. Phys. Lett., 1987. **51**(1): p. 12.
51. Gobel, R., *et al.*, *Performance studies of an IR fiber optic sensor for chlorinated hydrocarbons in water.* Fresenius J. Anal Chem, 1994: p. 514.
52. Driver, R.D., G.M. Leskowitz, and L.E. Curtiss, *Fiber-optic chemical sensing with infrared transmitting optical fiber*, in *Chemical, Biochemical and Environmental Sensors*. 1989, SPIE. p. 60.
53. Newby, K., *et al.*, *Remote spectroscopic sensing of chemical adsorption using a single multi-mode optical fiber.* Applied Optics, 1984. **23**(11): p. 1812.
54. Merschman, S.A. and D.C. Tilotta, *Fiber-optics Sensor for Aromatic Compounds in Water Based on Solid-Phase Microextraction and Ultraviolet Evanescent Wave Absorption Spectroscopy.* Applied Spectroscopy, 1998. **52**(10): p. 106.
55. Ruddy, V., B.D. MacCraith, and J.A. Murphy, *Evanescent wave absorption spectroscopy using multimode fibers.* J. Appl. Phys., 1990. **67**(10): p. 6070.
56. Potyrailo, R.A., V.P. Ruddy, and G.M. Hieftje, *Kramers-Kronig analysis of molecular evanescent-wave absorption spectra obtained by multimode step-index optical fibers.* Applied Optics, 1996. **35**(21): p. 4102.
57. Dankner, Y. and A. Katzir, *Evanescent wave spectroscopy for the determination of the optical constants of thin Silver films deposited on a silver-halide fiber.* Applied Optics, 1997. **36**(4): p. 873.
58. Messica, A., A. Greenstein, and A. Katzir, *Theory of fiber-optic, evanescent-wave spectroscopy and sensors.* Applied Optics, 1996. **35**(13): p. 2274.
59. Simhony, S., E.M. Kosower, and A. Katzir, *Novel attenuated total internal reflectance spectroscopy cell using infrared fiber for aqueous solutions.* Appl. Phys. Lett., 1986. **49**(5): p. 253.
60. Simhony, S., *et al.*, *Evanescent wave infrared spectroscopy of liquids using silver halide optical fibers.* J. Appl. Phys, 1988. **64**(7): p. 3732.
61. Brunimovich, D. and A. Katzir, *Infrared Fiberoptic Evanescent Wave Spectroscopy using Flattened Optical Fibers*, 2000, Unpublished.
62. Sanghera, J.S., *et al.*, *Infrared evanescent-absorption spectroscopy with chalcogenide glass fibers.* Applied Optics, 1994. **33**(27): p. 6315-6322.
63. Heo, J., *et al.*, *Remote fiber-optic chemical sensing using evanescent-wave interactions in chalcogenide glass fibers.* Applied Optics, 1991. **30**(27): p. 3944.
64. Mignani, A.G., R. Falcial, and L. Ciaccheri, *Evanescent Wave Absorption Spectroscopy by Means of Bi- Tapered Multimode Optical Fibers.* Applied Spectroscopy, 1998. **52**(4): p. 546.
65. Burck, J., J.P. Conzen , and H.J. Ache, *A fiber optic evanescent field absorption sensor for monitoring organic contaminants in water.* Fresenius J. Anal Chem, 1992: p. 394.
66. Hocde, S., *et al.*, *Chalcogen based glasses for IR fiber chemical sensors*, . 2000.
67. Lucas Research Group, Rennes, France, Personal Communication with, 2000.
68. Hocde, S., *et al. Recent Developments in chemical sensing using infrared glass fibers.* in *Journal of Non-Crystalline Solids*. 1999. Tucson AZ.

69. Marcuse, D., *Theory of Dielectric Optical Waveguides*. 1991, Boston: Academic Press, Inc.
70. Keiser, G., *Optical Fiber Communications*. 1983, New York: McGraw-Hill, Inc.
71. Buck, A., *Fundamentals of Optical Fibers*. 1995, New York: John Wiley and Sons, Inc.
72. Diament, P., *Wave Transmission and Fiber Optics*. 1990, New York: Macmillian Publishing Company.